



Hydrodynamic processes and the stability of intertidal mussel beds in the Dutch Wadden Sea

Jasper Donker

Hydrodynamic processes and the stability of intertidal mussel beds in the Dutch Wadden Sea

Hydrodynamische processen en de stabiliteit van litorale mosselbanken in de
Nederlandse Waddenzee

(met een samenvatting in het Nederlands)

PROEFSCHRIFT

ter verkrijging van de graad van doctor aan de Universiteit Utrecht
op gezag van de rector magnificus, prof. dr. G. J. van der Zwaan,
ingevolge het besluit van het college voor promoties in het openbaar te verdedigen

op woensdag 20 mei 2015 des ochtends te 10.30 uur

door

Jasper Jan Adriaan Donker

geboren op 10 september 1986 te Zaltbommel

Promotor:

Prof. dr. P. Hoekstra

Copromotor:

Dr. M.van der Vegt

Hydrodynamic processes and the stability of intertidal mussel beds in the Dutch Wadden Sea

Utrecht Studies in Earth Sciences

Local Editors

Prof. dr. S. M. de Jong

Dr. M. J. J. G. Rossen

Prof. dr. C. G. Langereis

Drs. J. W. de Blok

ISSN 2211-4335

Utrecht Studies in Earth Sciences 83

Hydrodynamic processes and the stability of intertidal mussel beds in the Dutch Wadden Sea

Jasper Donker

Utrecht 2015

Department Physical Geography
Faculty of Geosciences - Utrecht University

Promotor:

Prof. dr. P. Hoekstra

Copromotor:

Dr. M. van der Vegt

Examination committee

Prof. dr. Peter M. J. Herman, Koninklijk Nederlands Instituut voor Onderzoek der Zee

Prof. dr. Morten Pejrup, University of Copenhagen, Denmark

Prof. dr. Ad J. H. M. Reniers, Delft University of Technology

Prof. dr. Huib E. de Swart, Utrecht University

Dr. Katja J. M. Philippart, Koninklijk Nederlands Instituut voor Onderzoek der Zee

This work was financially supported by het Waddenfonds, Rijkswaterstaat and the provinces of Fryslân and North-Holland.

ISBN 978-90-6266-395-8

Copyright © Jasper Donker c/o Faculty of Geosciences, Utrecht University, 2015.

Cover: Mussels in an intertidal mussel bed. Photograph by Jantien Rutten, design by Margot Stoete.

Niets uit deze uitgave mag worden vermenigvuldigd en/of openbaar gemaakt door middel van druk, fotokopie of op welke andere wijze dan ook zonder voorafgaande schriftelijke toestemming van de uitgevers.

All rights reserved. No part of this publication may be reproduced in any form, by print or photo print, microfilm or any other means, without written permission by the publishers.

Printed in the Netherlands by CPI Wöhrmann Print Service, Zutphen

Zeg ken jij de mosselman

Dutch children's song

Contents

1	Introduction	13
1.1	Background	13
1.2	Intertidal mussel beds	16
1.3	Hydrodynamic processes and mussel beds	17
1.3.1	Currents and pattern formation	17
1.3.2	Wave influence on mussel beds	18
1.3.3	Ice and mussel beds	19
1.4	Research questions	20
1.5	Approach and outline	21
2	Hydrodynamic forcing over an intertidal mussel bed	23
2.1	Introduction	23
2.2	Theory	25
2.2.1	Physical roughness estimation from turbulent energy dissipation	25
2.2.2	Physical roughness estimation from wave attenuation	26
2.2.3	Bed shear stress	28
2.3	Materials and Methods	28
2.3.1	Field site	28
2.3.2	Deployment	29
2.3.3	Data collection and processing	30
2.3.4	Elevation and coverage	31
2.3.5	Data Selection	31
2.4	Results	33
2.4.1	Environmental conditions	33
2.4.2	Physical roughness	34
2.4.3	Forcing	37
2.4.4	Wave model	37
2.4.5	Observations of coverage	43
2.5	Discussion	44
2.5.1	Roughness	44
2.5.2	Forcing	45
2.5.3	Implications for mussel bed survival	45
2.6	Summary and Conclusions	46
3	How mussel hummocks influence flow patterns and food uptake in intertidal mussel beds	47
3.1	Introduction	47
3.2	Materials and Methods	50
3.2.1	Field experiment	50

3.2.2	Model Simulations	53
3.2.3	Advection-diffusion model with explicit food uptake	53
3.2.4	Simulations Overview	55
3.3	Results: field observations	56
3.4	Results: model simulations	60
3.4.1	Influence of hummock on flow behavior	60
3.4.2	Effects of water levels and geometry on flow patterns	61
3.4.3	Influence of hummock on food uptake	63
3.4.4	Effect of hummock geometry on uptake	65
3.5	Discussion	68
3.6	Summary and conclusions	70
4	Implications of an ice action event for the long-term persistence of an intertidal mussel bed	71
4.1	Introduction	72
4.2	Materials and Methods	74
4.2.1	Field location	74
4.2.2	Observations and processing	74
4.3	Results	77
4.3.1	Changes in mussel covered area	77
4.3.2	Change in mussel bed coverage	77
4.3.3	Change in mussel bed topography	79
4.3.4	Mechanism of ice action	81
4.4	Discussion and implications	83
4.4.1	Synergistic action of eroding agents	83
4.4.2	Implications for the persistence of intertidal mussel beds in the Dutch Wadden Sea	84
4.5	Conclusions	85
5	Wave forcing in the Dutch Wadden Sea and the effects on mussel habitats	87
5.1	Introduction	88
5.2	Materials and Methods	89
5.2.1	Study area	89
5.2.2	Data collection	90
5.2.3	Mussel bed contours	91
5.2.4	Model	91
5.3	Wind climate and fetch	94
5.3.1	Wind climate	94
5.3.2	Water level variations	94
5.4	Results	96
5.4.1	Near-bed wave orbital velocities in the Wadden Sea	96
5.4.2	Wave exposure per basin	98
5.4.3	Wave exposure at the 12 focus beds	102
5.4.4	Mussel bed exposure	102

5.5	Discussion	104
5.6	Summary and conclusions	107
6	Conclusions and Perspectives	109
6.1	Introduction	109
6.2	Summary of main findings	109
6.2.1	Hydrodynamic forcing over an intertidal mussel bed (Chapter 2) . .	109
6.2.2	Effects of flow patterns over high relief mussel beds on food avail- ability (Chapter 3)	110
6.2.3	Impact of erosion by ice scour on the long term development of an intertidal mussel bed (Chapter 4)	110
6.2.4	Spatial trends in wave forcing in the Dutch Wadden Sea and the implication for mussel habitat suitability (Chapter 5)	111
6.3	Perspectives	112
6.3.1	Main conclusions	112
6.3.2	Creating a new mussel bed	113
6.3.3	Mussel bed restoration	114
6.3.4	Stimulation of natural settlement	115
	Bibliography	117
	Summary	125
	Samenvatting	127
	Dankwoord	129
	Curriculum Vitae	131
	List of publications	133

1 Introduction

1.1 Background

Mussel beds are a striking feature on the intertidal flats of the Dutch Wadden Sea (Figure 1.1). These beds are aggregations of the blue mussel, *Mytilus edulis* L., a filter feeding shellfish species. Mussel beds occur on the intertidal flats, but also in the deeper subtidal areas, and form habitats that can extend over several kilometers (Commito and Dankers, 2001). When mussel beds cover a substantial area of the intertidal flats they have a strong impact on ecosystems as they increase biodiversity. Not only do they serve as a food source for birds (Nehls et al., 1997) and crabs (Jubb et al., 1983), but they also provide a habitat for many other species living in the Dutch Wadden Sea such as other shellfish species (van der Zee et al., 2012). Furthermore, they interact with suspended sediments in the water as they filter the water for food, thereby changing the sediment composition (Dame and Dankers, 1988; Widdows et al., 2002), promoting sediment deposition and preventing erosion by stabilizing sediments (Oost, 1995). Mussel beds are abundant in the Wadden Sea, in some tidal basins they occupy up to 6% of the intertidal area (Folmer et al., 2014). Mussels are, due to their high abundance and impact on both biotic and abiotic processes, considered to be a key species in the ecosystem of the Dutch Wadden Sea (Dankers and Zuidema, 1995).

The Wadden Sea, a system of interconnected back-barrier basins, is located along the northern coast of the Netherlands and extends along the German coast and the South Western coast of Denmark. This thesis focuses on the Dutch part of the Wadden Sea (Figure 1.2) which is approximately 150 km long and covers an area of 2250 km². It is sheltered from the North Sea by six large barrier islands, while dikes form the boundary on the mainland coast. The main inflow of freshwater comes from Lake IJssel in the west and the Ems estuary in the east. The basins are connected with the North Sea through six tidal inlets. The tidal drainage divide South of the island of Terschelling separates the Dutch Wadden Sea in an eastern and a western part. Astronomical tidal amplitude ranges from 1.10 m to 1.90 m with respect to N.A.P. (Dutch Ordinance Datum) in the Western Wadden Sea and 2.50 m to 3.60 m Eastern Wadden Sea. Additionally, water levels in the Wadden Sea decrease or increase as a result of strong winds in the North Sea, which can push water away or towards the Dutch coast. Waves in the Wadden Sea are locally generated, since the barrier islands and ebb-tidal deltas shelter the back barrier basin from high North Sea waves (Kaiser et al., 1994).

Mussel coverage in the Dutch Wadden Sea is nowadays monitored by mapping the contours of mussel beds. The mapping method is standardized in the TMAG protocol, which is described in de Vlas et al. (2004) and Herlyn (2005). It describes the definition of a mussel bed in terms of density and maximal gap size between individual patches. The first most extensive mapping of mussel bed habitats has been performed by Dijkema (1991). These maps were based on aerial photographs taken between 1969 and 1979.



Figure 1.1 Photographs of intertidal mussel beds in the Dutch Wadden Sea. In the top left panel an aerial photograph of a banded patterned mussel bed. The top right panel shows a mussel bed which is uniformly covered in the center and patchy at the edges. In the bottom left a photograph highlighting the height variations in a patchy mussel bed. The bottom right panel shows a mussel bed from up close showing aggregations of mussels and other bivalves that attach to the sediment bed. The photographs are taken by the author (1-3) and Jantien Rutten (4).

From these maps a total area of $4.1 \times 10^8 \text{ m}^2$ of mussel beds was estimated for the Dutch parts of the Wadden Sea. After 1980, the mussel area started to decline, caused by a combination of intense fishing and severe winters (1985-1987), during which ice floes removed part of the beds. In the late 1980s, the last beds were removed from the intertidal flats by fisheries. In response policies were introduced to promote recovery of intertidal mussel beds. These policies were in part successful as the mussel population started to increase again (Dankers et al., 2001, 2004). Modern day mussel population (Figure 1.3) peaked during the spring of 2002 at $3 \times 10^8 \text{ m}^2$. Mussel cover varies over the years as a result of (1) strong annual variations in recruitment; (2) variations in environmental pressure from predation, storms, ice and, prior to 1994, fisheries (Dankers et al., 2001). Differences in coverage are large between the eastern and western part of the Dutch Wadden Sea. The coverage of intertidal area with mussel beds is relatively low in the western part. Between 2000 and 2006 less than 10% of the intertidal mussel cover was located in the western part.

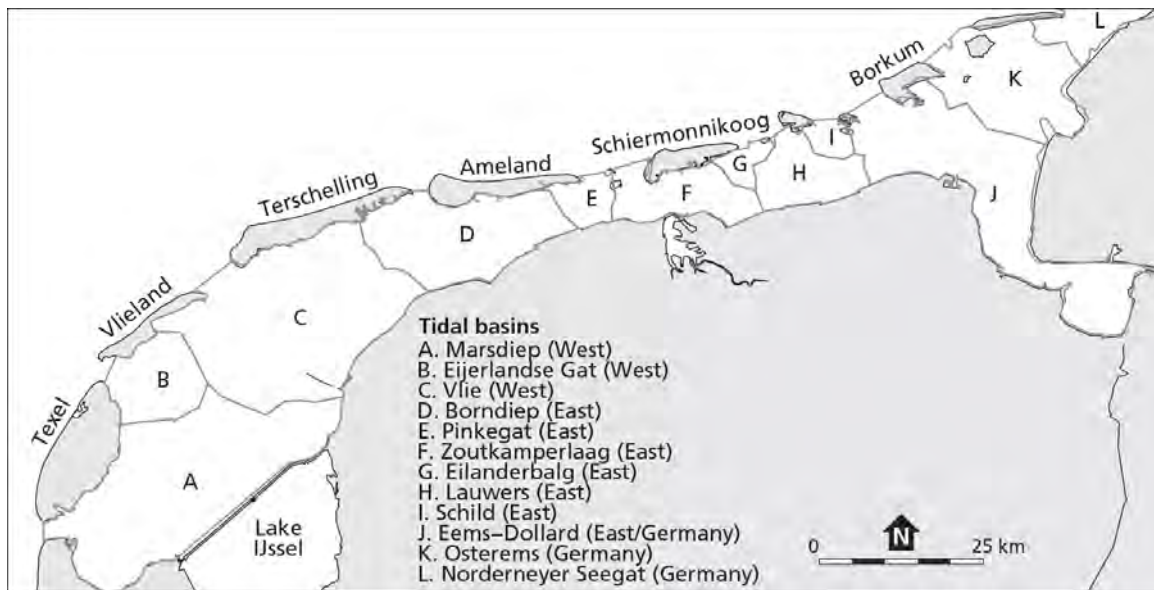


Figure 1.2 Map of the Dutch Wadden Sea, with names of the tidal basins and names of the inhabited islands.

In order to increase the mussel population in western parts of the Dutch Wadden Sea the restoration of intertidal mussel beds is considered. Habitat suitability maps, such as described in Brinkman et al. (2002), have been used to determine locations for restoration of intertidal mussel beds. The maps were mainly based on abiotic processes. This approach had little success, restoration efforts have been unsuccessful up to date (Dankers, 2014). Additional knowledge is required on the environmental/ecological factors and processes that determine the long term stability of mussel beds to increase the chance of a successful mussel bed restoration. Therefore project Mosselwad (www.mosselwad.nl) was initiated. Within the project several factors that influence the stability of intertidal mussel beds are investigated. These factors are predation (birds, crabs, starfish), attachment properties (sediment composition, substrate use, byssus strength), pattern development, population dynamics, food availability and hydrodynamic processes. The results presented in this thesis were obtained within the context of the Mosselwad project.

The main aim of this thesis is to determine the effects of hydrodynamic processes on the stability of intertidal mussel beds. Hydrodynamic processes interact with mussel beds generally in three ways. (1) Food is transported to mussel beds by the flows, which allows the mussels in the bed to grow and to reproduce (Seed and Suchanek, 1992). (2) Waves and currents are capable of eroding mussel beds, either by directly removing mussels from the bed or by eroding the underlying substrate they attach to (Seed and Suchanek, 1992; Dankers et al., 2004). (3) Hydrodynamic processes affect the composition and sediment balance of mussel beds (Oost, 1995).

In the following sections a brief introduction on the formation and development of intertidal mussel beds is given (Section 1.2). This is followed by a discussion of the relation between the main hydrodynamic processes and mussel beds (Section 1.3). Lastly, the

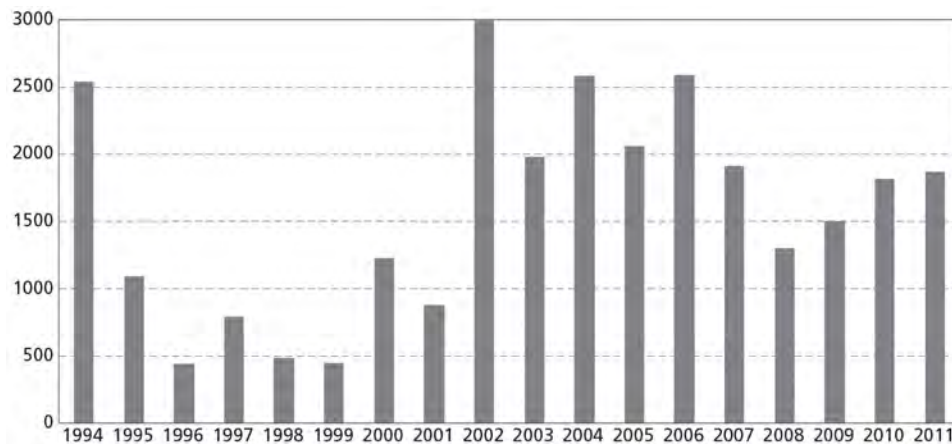


Figure 1.3 Intertidal mussel stock in the Dutch parts of the Wadden Sea between 1994 and 2011. Adapted from van den Ende et al. (2013).

research questions and give a brief outline of the thesis chapters is presented (Sections 1.4 and 1.5).

1.2 Intertidal mussel beds

Mussel beds form when mussel larvae settle on an intertidal flat, a process called spatfall. Only a small portion of the millions of larvae produced per individual will settle on a solid substrate (Brinkman et al., 2002). As mussel larvae are small and mussel spatfall occurrence is unpredictable (Pulfrich, 1995), little is known about the behavior of mussel larvae prior to settling. Mussels settle when they are large enough (0.5 - 2 mm) by attaching themselves to a suitable substrate at a location where at that time hydrodynamic forcing is low. Spatfall therefore often occurs near local watersheds where current velocities are small (Dankers et al., 2004). Probably, wave forcing is small as well in these areas, but this has not been studied yet. Solid substrates are widely available on rocky shores and mussels can survive as an individual. However, solid substrates are absent in soft-sediment intertidal areas such as the study area. Therefore mussels attach themselves to each other and to the sediment; they cannot survive as individuals. Mussel spat survival increases when the sediment contains shell material or when other shellfish reefs are present (wa Kangeri et al., 2014). The attachment to the substrate is formed by byssus threads which grow from the foot of the mussel. Depending on local conditions byssus threads vary in number and strength. Using their byssus attachment mussels are able to reallocate to optimize their location.

During the first year mussels grow rapidly and, when no erosion occurs, a juvenile mussel bed (mussels between 1 - 2 cm) is formed. In the first months after settlement, mussels adapt their attachment and reallocate themselves to form net like structures (van de Koppel et al., 2008). Also the first effects on local morphology become apparent. Mussel beds promote local deposition of suspended sediment by filtering the water column for food. As a result, the sediment around mussel beds contains more silt and

organic matter (Oost, 1995). Mussels are buried when local deposition is large. To survive, mussels have to relocate themselves on top of the sediment to regain their access to food. As mussels climb on top of the sediment, the underlying substrate is protected from erosion. This process results in a substantial accumulation of sediments inside mussel covered areas. Especially, when the mussels are young they can reposition themselves quickly, a height increase of 6 cm over the course of a day has been observed by Widdows et al. (2002). The underlying substrate also becomes more stable when fine grained material is consolidated (Grabowski et al., 2011). After the first months also more large-scale patterns become apparent as mussels continue to reposition to increase their survival chance. Studies by van de Koppel et al. (2005) and Liu et al. (2014a) suggest that these patterns are formed to optimize food uptake or to increase the resilience against low food conditions. Formation of patterns leads to a more heterogeneous mussel cover, which is reflected by structures such as bands and hummocks. Height differences in the bed often increase over time as accumulation continues in the mussel covered area. Height variations of 30-40 cm have been observed after the first half year (Dankers et al., 2004). These variations can reach up to 1 m.

A large portion of the newly settled mussel beds does not survive the first winter period (Dankers et al., 2004) due to storminess (Nehls and Thiel, 1993) and ice (Strasser et al., 2001). A mussel bed is considered stable after the bed survives its first winter. As mussels grow (>3 cm) their ability to relocate reduces and less sediment is accumulated. Thereby, the bed loses its ability to quickly adapt to the changing conditions. In this phase of the life cycle the initially formed patterns slowly break up and mussel cover often becomes more scattered as a result of losses by erosion. The chance to sustain damage by a major storm also increases with lifetime. Moreover, reduced food availability and suffocation due to sediment consolidation, can cause substantial annual mortality inside mature mussel beds. Also, older mussels ($10 > \text{yr}$) are more prone to mortality due to anaerobic conditions (Viarengo et al., 1989). Mussel beds that suffer little erosion can survive for a long period, mussel beds (and individual mussels) older than 10 years have been observed (McGrorty et al., 1990). For most beds, in order to ensure long-term survival of the bed, rejuvenation is required, for which the beds depend on the unpredictable processes of spatfall.

1.3 Hydrodynamic processes and mussel beds

In all stages of the life cycle hydrodynamic processes are important to the mussel bed. Currents transfer food towards the bed, while high shear stresses from waves and currents may erode mussels from the bed. Therefore, local hydrodynamic processes are important factors to understand the dynamics and persistence of intertidal mussel beds.

1.3.1 Currents and pattern formation

Food is transported towards the mussel bed by currents. Mussels feed themselves by filtering water in the bottom boundary layer (bbl) for small organisms. As filtration speeds are high with respect to the transport by the current and the food concentration the bbl is

rapidly depleted from food (Fréchette and Bourget, 1985). In order to replenish food in the bbl, vertical transport by means of turbulent mixing plays an important role (Wildish and Kristmanson, 1984). This rapid depletion results in variation in food availability over the mussel bed. Food availability is reflected in mussel health (Svane and Ompi, 1993). After settlement, mussels have little influence on large scale (> 1 km) flow patterns, which transport food towards the bed, but, on the small-scale they can enhance the vertical mixing by developing increased roughness inside the bed. The roughness the flow experiences is increased not only by the presence of mussels but also by their filter feeding activity (Van Duren et al., 2006). Present estimates for the current-related surface roughness are, however the results of laboratory flume experiments. In the field, surface roughness is more complex as patterns occur on a larger spatial scale than simulated in flume studies. Therefore, a more accurate determination of the bed roughness in the field is needed, to investigate the role of vertical mixing in transporting food towards the bed.

Sedimentation inside a patterned mussel bed has potentially substantial effects on local flow patterns. In mussel beds with small-scale heterogeneity (< 10 m), the resulting small-scale flow variations influence food transport. Studies for other biota, such as sea grass fields (Nepf, 1999; Zong and Nepf, 2010), coral structures (Hench and Rosman, 2013) and other epibenthic structures (Bouma et al., 2007) reveal that flow is accelerated over the elevated area. Furthermore, the flow can also be routed around the elevated area, suggesting reduced transport of food over the mussel covered area. These effects have not been studied before but can potentially have a substantial effect on mussel bed processes, development and long-term survival.

Vertical mixing may be affected by flow routing and acceleration around structures as well. The friction of the rough mussel bed increases at high flow velocities (Green et al., 1998). Along the edges, where both roughness and elevation changes, turbulent mixing is increased as flow has to adapt between flow regimes (Folkard and Gascoigne, 2009).

High relief within mussel beds leads to a change in transport, but simultaneously stimulates vertical exchange. Depending on the dominance of both processes, this could either result in an increase or a decrease in local food availability. The effects of these changes in transport and mixing on food availability have never been quantified. The effects of elevations within mussel beds with different patterns (small hummock, big hummock or banded mussel bed) on food uptake are therefore unknown. However, they may be important for the long term development of the bed.

1.3.2 Wave influence on mussel beds

Waves negatively affect mussel bed persistence. While wave forcing has been extensively researched for solid (rocky) substrates (Denny, 1987, 1995) few studies focus on the interaction between waves and mussel beds in soft substrates. A study by Brinkman et al. (2002) revealed, by combining wave model results with a statistical analysis of other abiotic factors, that wave forcing is the most important factor determining habitat suitability in the Dutch Wadden Sea. However, for the study only a wave model simulation of a single storm was used. By focusing on a single storm's potential effects of wind direction on mussel bed exposure to waves are ignored. Moreover, the potential role of

waves on settlement during larvae settlement and early mussel bed survival are not taken into account. The importance of waves for mussel bed persistence is further substantiated by the observed losses in mussel bed area after winter storms (Nehls and Thiel, 1993). Mussel erosion thresholds for soft-sediments and effects of mussel beds on wave behavior have not been determined. Yet, studies for other biota suggest a self-protecting effect (Möller et al., 1999).

Some of the results obtained in research for exposed rocky intertidal areas are applicable to sheltered mussel habitats on soft substrates as well. It was shown by (Witman and Suchanek, 1984) that the strength of its byssal attachment is of importance for the survival of the mussels. Mussels can adapt their attachment strength and strategy to the hydrodynamic exposure, by increasing or decreasing the formation of byssal threads Witman and Suchanek (1984); Young (1985); Moeser et al. (2006). Also, Denny (1987) shows that mussels do not erode as individuals but rather as patches or clumps. Important differences between the exposed rocky shores and the sheltered soft-sediment intertidal areas are the attachment strength and erodability of the underlying substrate. Firstly, on rocky shores a strong byssal attachment to the solid substrate is sufficient for survival. This is not the case on soft substrates, as the underlying substrate may erode. Mussels inside the bed are interconnected and thereby increase their resilience against erosion. An extensive flume study on the role of currents in eroding mussels and the effects of different substrates has been performed by Widdows et al. (2002). They showed that before the mussels were eroded from the substrate the sediment starts to erode. The erosion chance is thus also influenced by the erodability of the underlying substrate.

Secondly, the forces required to detach mussels from the substrate are larger in rocky shores than on soft sediments. Erosion on rocky shores only occurs at stresses which are associated with wave breaking (Helmuth and Denny, 2003). In the more sheltered soft-sediment intertidal areas waves are smaller, but, attachment to the bed is also weaker than in rocky intertidal areas (wa Kangeri et al., 2014). Wave breaking is commonly confined to a small area depending on local morphology, wave height and water depth (Helmuth and Denny, 2003). In contrast the forcing by bed friction is present in the whole intertidal area but varies in strength. Determining the relevant erosional process leading to mussel bed erosion is important to upscale model results. Bed friction is also increased due to presence of a mussel bed as an area covered with mussels is likely to be rougher than the uncovered area. As friction is larger, more wave energy will be dissipated, which results in smaller waves and reduced bed shear stresses in the direction of wave propagation on the mussel bed. The mussel bed could thereby protect areas deeper inside the bed from high wave exposure. Field estimates of the bed roughness are needed to quantify its effect on wave attenuation, study the self-protection effect.

1.3.3 Ice and mussel beds

Several studies state that after a cold winter, mussel cover is reduced (Dankers et al., 2001, 2004). Two physical processes related to ice formation are responsible for these losses. First, floes of drifting ice substantially affect the intertidal zone by moving sediments (Dionne, 1984; Pejrup and Andersen, 2000). Especially in the German and Danish part

of the Wadden Sea scour tracks have been observed in intertidal mussel beds (Strasser et al., 2001). Second, mussel bed erosion by ice occurs when water freezes on top of mussel covered areas. When the bed becomes submerged again the frozen-in mussels are extracted from the bed together with the ice by upward buoyant forcing (Denny et al., 2011). The role of both processes and relative importance of erosion by ice with respect to other eroding processes has not been studied.

1.4 Research questions

The main objective of this thesis is to increase the understanding of the mutual relations between local morphology, hydrodynamic processes and mussel bed stability in order to better predict the habitat suitability for intertidal mussel beds in the Dutch Wadden Sea. Therefore the research question of this thesis is:

What is the influence of hydrodynamic processes on the stability of intertidal mussel beds in the Dutch Wadden Sea?

Several sub-questions are formulated to answer the main research question. As discussed in Section 1.3, field observations on the behavior of hydrodynamic processes over intertidal mussel beds are lacking. In order to assess the effects of hydrodynamic processes on the large scale stability of an intertidal mussel bed the small-scale and short-term interactions between intertidal mussel beds and hydrodynamic processes need to be determined first. Erosion is caused when shear stresses that are exerted by waves and currents on to the mussel bed exceed the attachment strength of the mussels to the bed. In order to investigate the long-term stability knowledge is required on the hydrodynamic forcing exerted on to an intertidal mussel bed. Furthermore, as currents and wave orbital motions exert a shear stress on the mussel bed, hydrodynamic energy is lost. When wave energy is lost over the mussel bed the areas more inside are exposed to smaller wave induced bed shear stresses. The first research question this thesis aims to answer is:

(1) What is the relative contribution of waves and currents to the total bed shear stresses exerted on a uniformly covered mussel bed and how does a mussel bed influence the local current and wave patterns?

The spatial variation in hydrodynamic forcing caused by interaction with the mussel bed will also result in variations in food availability. This will especially occur in mussel beds with larger spatial heterogeneity in bed height. These height variations may be caused pattern formation inside mussel beds due to self-organization, but can also be the result of the breaking up of uniformly covered or banded mussel beds by erosion. The large spatial variations in mussel cover and bed height will affect advective food transport and vertical mixing, and thereby influence the long term development of the mussel bed. Therefore, the second research question of this thesis is:

(2) What are the effects of patterned mussel beds on flow patterns, vertical mixing and food availability?

The long term (> yr) effect of hydrodynamic processes on mussel bed erosion need to be established. Erosion has only been studied using changes of mussel bed contours, little is known on the exact eroding mechanism (storms or ice) and the spatial variation in erosion trends. Furthermore, the evolution of a mussel bed after an erosion event is unknown. This leads to the third research question:

(3) What is the impact of an erosion event on the mussel coverage and the topography of an intertidal mussel bed?

If wave erosion is an important factor in reducing the stability of an intertidal mussel bed, areas where wave forcing is high will be less suitable for mussel beds. Therefore the large-scale relation between wave exposure and the occurrence of mussel bed habitat needs to be further investigated. Differences in mussel cover between the Western and Eastern Wadden Sea may be related to differences in wave forcing. If this is the case, mussel beds will only be observed in regions which are exposed to small wave forcing. The suitability of areas to sustain stable mussel beds is investigated by the fourth research question:

(4) Is wave forcing limiting the formation of stable mussel beds in the Dutch Wadden Sea, which spatial patterns are observed?

1.5 Approach and outline

In order to answer the main research question, the four specific research questions are addressed in the different chapters of this thesis.

The first research question is addressed in **Chapter 2**, using a combination of field observations and model simulations. Field observations were obtained at a flat, uniformly covered mussel bed near de Cocksdorp, Texel. An Acoustic Doppler Velocimeter (ADV) was used to obtain wave- and current-induced bed shear stresses. Furthermore, using pressure sensors, the spatial variation in wave forcing was determined to test the self-protecting effect of the mussel bed. Moreover, and to determine the bed roughness. Subsequently, the spatial distribution in wave forcing was studied in more detail using SWAN (Booij et al., 1999), which is a wave model that solves the wave action balance. Field data was used to provide boundary conditions for the model study.

The second research question is addressed in **Chapter 3**, again a combination was used of field observations and model simulations. Flow observations over and around an elevated mussel patch (hummock) were gathered to study flow patterns and vertical

mixing. The observed flow patterns were further investigated based on flow simulations around an idealized mussel hummock. Simulations were performed using SWASH (Zijlema et al., 2011), a model which solves the non-hydrostatic shallow water equations. The effects of different hummock geometries, surface roughness and water levels on flow patterns and vertical mixing were investigated. The model was subsequently coupled to an advection-diffusion model for algae with explicit food uptake to study effects of relief in mussel beds on food availability.

In **Chapter 4** the third research question is investigated using the results of a long term monitoring campaign, which was performed on the intertidal mussel bed near de Cocksdorp, Texel. During the experiment the cover of the mussel bed was measured on a nearly daily basis using photographs from a rotating video camera system on top of a 10 m high camera pole. Additionally, morphologic changes were monitored using a combination of 3d terrestrial laser scans and dGPS measurements. Measurements of mussel coverage and morphology were analyzed to determine the impact of erosion events on an intertidal mussel bed.

The final research question forms the basis of **Chapter 5**, in which wave forcing for the entire Dutch Wadden Sea area was modeled. This was done using the wave model SWAN, which was also used in Chapter 2. SWAN simulations were performed to calculate the spatial distribution in the near-bed wave orbital velocity amplitude for 1480 scenarios of wind speed, wind direction and water level. By weighing these scenarios with their respective frequency of occurrence, both median and 95th percentile wave forcing were calculated at the intertidal areas. The role of wind-induced water level variations on wave forcing were studied. The spatial distribution of wave forcing was compared with the spatial distribution in mussel cover over a period of 17 years.

Chapter 6 synthesizes the main findings of this thesis and provides an outlook for future research on mussel bed stability, and presents recommendations for mussel bed restoration with respect to hydrodynamic processes.

2 Hydrodynamic forcing over an intertidal mussel bed

This chapter is based on:

DONKER, J. J. A., VAN DER VEGT, M., HOEKSTRA, P. (2013), Wave forcing over an intertidal mussel bed. *Journal of Sea Research* 82, 54–66.

Abstract

The Mosselwad project studies the stability and opportunities for restoration of mussel beds in the Wadden Sea. In this context predicting mussel bed stability with respect to hydrodynamic forcing is of key importance. To make accurate predictions of hydrodynamic exposure of mussel beds with models, field experiments are needed to determine relevant processes and to establish representative estimates for model parameters such as the physical roughness. To this goal a six week field campaign was carried out on a relatively young mussel bed in the Wadden Sea. During this period wave height, period, propagation velocity, dissipation and flow velocities were measured. From this data the total rate of energy dissipation and the rate of wave energy dissipation were determined. Results show a large increase in measured bed shear stress over the mussel bed compared with that over the uncovered parts of the intertidal flat. This is caused by the large roughness of the mussels. The turbulent kinetic energy was high above the covered parts of the bed. From the dissipation rate of TKE values for the corresponding bed shear stress and roughness length were calculated. Obtained values were subsequently applied to calibrate a wave model which was used to determine the spatial distribution of the wave forcing. Model results show that the bed shear stress decreases in shore ward direction over the mussel bed from a peak near the sea ward edge. Behind the bed the near bed orbital velocities increase again, when this area would be covered with mussels bed shear stress would have been higher than those on the shoreward parts of the present mussel bed. Furthermore, a model study of this area for the periode prior to the settlement of the mussel bed shows that a minimum in wave forcing on the bare flat coincides with the present seaward edge of the bed. This suggests that the bed is currently located at the optimal location with respect to wave forcing.

2.1 Introduction

Recently, an increase in shellfish restoration programs has led to a growing interest into the feedbacks between shellfish aggregations and hydrodynamic agents (currents, waves). The Mosselwad project, which comprehends the present study, studies the stability and opportunities for restoration of mussel beds in the Wadden Sea. The goal of this study is to determine the hydrodynamical forcing, in terms of the bed shear stress, on a mussel bed, and to quantify the physical roughness which can be used to model hydrodynamic

exposure of mussel beds. Mussel erosion chance is controlled by the byssus attachment strength to the bed and the forcing it is subjected to. It was demonstrated by Witman and Suchanek (1984) that the byssus attachment adapts itself to the amount of hydrodynamic agitation. This adaptation results in a large spatial variation in attachment strength related to wave exposure (Witman and Suchanek, 1984). Later, it was demonstrated that this ability to adapt itself was limited by energy availability, related to food availability and temperature, resulting in seasonal variation in attachment strength (Price, 1980, 1982; Carrington, 2002; Moeser et al., 2006).

The effect of wave forcing on mussels was investigated by Denny (1987, 1995), in the late eighties and early nineties. He did extensive research on the forces wave action exerts on shoreline organisms. He found that mussel erosion takes place by means of patch erosion instead of single mussel erosion (Denny, 1987) and defines three mechanisms (Denny, 1987) through which forces are exerted on mussels: form drag, acceleration reaction and lift. The relative importance of all these mechanisms is controlled by water level, morphology and mussel density. Lift is found to be the most important mechanism under breaking waves (Denny, 1987; Gaylord, 1999), while form drag is considered to be the main mechanism under non-breaking conditions. Acceleration reaction is only of importance near the mussel bed edge. Outside the viscous boundary layer these mechanisms lead to an increase in shear stresses that both the flow and wave orbital velocities experience (Garratt, 1994). The dominant variable for the wave forcing due to shear stresses under waves is the wave orbital velocity (Soulsby, 1997). The spatial variation of this parameter is controlled by the characteristics of the incoming wave field and its attenuation in the near-shore zone. The rate at which attenuation occurs is controlled by the water depth, and the amount of friction the wave is subjected to at the bed (Thornton and Guza, 1983). The spatial distribution of the wave forcing is thus controlled by the local morphology and the bed roughness.

The effects of currents on mussel bed stability were studied by Widdows et al. (2002), who showed that bed erosion by currents decreases the attachment strength of the mussel to the underlying substrate. Other studies showed the effects of currents over mussel beds in relation to sediment dynamics (Van Leeuwen et al., 2010) and turbulent mixing (Van Duren et al., 2006). Currents have, however, not directly been related to erosion of mussel aggregations. It was shown by Brinkman et al. (2002) and Hammond and Griffiths (2004) that there is an optimum in both wave orbital velocity and current velocity for which mussel bed abundance is the most common. The relation between the spatial distribution of mussel cover and hydrodynamical forcing on the scale of individual tidal flats has however never been investigated.

The main objective of the present study is to determine the spatial variation in bed shear stresses acting on an intertidal mussel bed. As a first step, field measurements were performed to quantify the physical roughness. This value was subsequently used to calculate the current and wave induced bed shear stresses. The magnitude of current and wave induced shear stress were compared to determine their contribution to the total bed shear stress. Next, the wave model SWAN (Booij et al., 1999) was applied to extrapolate the measured data to tidal flat scale. Finally, the results of this model study are related to the spatial distribution of mussel coverage. This chapter is organized as follows. First,

in Section 2.2 an overview is presented on methods to determine shear stresses acting on the bed. Next, the field experiment is described and methods for data processing are presented in Section 2.3. In Section 2.4 the results of both the field research and model study are shown. Subsequently, the results from the measurements and model study are integrated and discussed in Section 2.5. Finally, a summary of the results and the main conclusions are presented in Section 2.6 .

2.2 Theory

Here, the theoretical framework to determine the bed shear stress induced by waves and currents is presented. To determine the bed shear stress the physical roughness (or Nikuradse roughness) needs to be determined. Two methods are presented by which the physical roughness is estimated. First, a method is presented in which the physical roughness is calculated from the dissipation of turbulent kinetic energy. Second, a method is demonstrated that determines the physical roughness from wave attenuation. Finally, it is shown how these estimates of the physical roughness were used to estimate the bed shear stress.

2.2.1 Physical roughness estimation from turbulent energy dissipation

By means of high frequency velocity measurements the wave averaged current velocity \bar{u} , the wave orbital velocity u_b and the dissipation rate of turbulent kinetic energy (TKE), called ϵ , at the measurement height (z_m) are obtained. Observations of the dissipation rate of TKE the current friction velocity (U_{*c}) calculated by assuming a balance between turbulent energy production and dissipation.

$$U_{*c} = (\epsilon \kappa z)^{1/3}, \quad (2.1)$$

in which $\kappa = 0.4$ is the von Kármán constant and $z = z_m$. In the case of a fully developed boundary layer flow, the physical roughness (k_b), the current friction velocity (U_{*c}) and the average velocity at height z are related via the law of the wall ,

$$\bar{u}(z) = \frac{U_{*c}}{\kappa} \ln(30z/k_b), \quad (2.2)$$

Waves cause oscillating flows near the bed. The boundary layer has no time to develop properly as velocities change fast in both magnitude and direction, resulting in a much thinner boundary layer, typically in the order of centimeters above the bed. For combined wave and currents the effects of the wave boundary layer on the mean velocity profile outside the wave boundary layer can be modeled as an increase in surface roughness (Grant and Madsen, 1979). Inside the wave boundary layer the mean current velocities are reduced by wave induced turbulence, this effect is modeled by Grant and Madsen (1979) and Madsen (1994) as an increased eddy viscosity in the wave boundary layer. Adopting their approach results in two equations describing the vertical profile of the wave averaged current inside and outside the wave boundary layer:

$$\bar{u}(z) = \frac{U_{*c}^2}{\kappa U_{*cw}} \ln(30z/k_b) \quad z < \delta w, \quad (2.3)$$

$$\bar{u}(z) = \frac{U_{*c}}{\kappa} \ln(30z/k_{bc}) \quad z > \delta w. \quad (2.4)$$

Here, k_{bc} is the apparent roughness, δw is the height of the wave boundary layer and U_{*cw} is the maximum shear velocity inside the wave boundary layer induced by both the current and wave orbital motion. To determine the physical roughness first Equation 2.1 is used to obtain U_{*c} . Next, the apparent roughness (k_{bc}) is calculated by solving Equation 2.4 using the obtained value for U_{*c} . In the first Equation 2.3, however, two unknowns U_{*cw} and k_b remain. In order to find estimates for both unknowns the Grant and Madsen wave current interaction model (Madsen, 1994) is applied. This model predicts values for U_{*cw} , U_{*c} and k_{bc} from measurements of the mean current velocity, the wave orbital velocity u_b , the representative wave period and the angle between the wave and current direction, additionally, the model requires the physical roughness k_b . However, the latter is the quantity of interest. Using a first estimate of k_b the Grant and Madsen wave current interaction model is used to calculate U_{*c} and k_{bc} . Obtained values for U_{*c} and k_{bc} are subsequently compared with observations to improve the estimate of k_b . This procedure is repeated until convergence for k_b is achieved.

2.2.2 Physical roughness estimation from wave attenuation

In order to determine the physical roughness from wave attenuation several pressure sensors were placed around the mussel bed. By comparing the amount of wave energy that is transported past each pressure sensor per second, the wave energy flux (F), the loss in wave energy and the contribution of bed friction to this loss between two sensors was determined. Subsequently, the physical roughness was estimated from this wave energy loss by bed friction. To achieve this the pressure time series are converted into time series of sea surface elevation. From these time series, the wave energy (E) and the velocity by which it propagates, the group velocity (C_g), are calculated. Furthermore, the current velocity (u) also influences the velocity at which the wave energy is transported, for each pressure sensor the velocity of the most nearby velocity sensor was used. This allows calculation the wave energy flux,

$$F_x = E(C_{g,x} + u_x), \quad (2.5)$$

here x denotes the component along the line between two sensors. The wave energy is related to root mean squared wave height (H_{rms}) through

$$E = \frac{1}{8} \rho g H_{rms}^2. \quad (2.6)$$

Here, ρ is the density of water and g is the gravitational constant. The wave energy flux is only changed by production or dissipation e of wave energy. In shallow water production of wave energy is much smaller than dissipation of wave energy, therefore, production is neglected. In shallow water there are two dissipative mechanisms, wave breaking and bed friction. Under the assumption that sensors are perfectly aligned with respect to

the direction of wave propagation the change in wave energy flux can be determined through:

$$\frac{\delta F}{\delta x} = -e_b - e_f. \quad (2.7)$$

Here, e_b and e_f are the energy dissipation rates by wave breaking and bed friction respectively. By comparing the energy flux at two sensor locations ($F_{A,x}$ and $F_{B,x}$) under the assumption that the wave energy is constant in time, the transect averaged change in wave energy flux is determined,

$$\frac{\Delta F}{\Delta x} = \frac{F_{B,x} - F_{A,x}}{\Delta x}. \quad (2.8)$$

Several models have been developed to estimate the rates of dissipation from both mechanisms using common wave statistics. As the focus lies on the energy dissipation due to bed friction first the dissipation rate of wave breaking is subtracted from the total dissipation rate. The Thornton and Guza (1983) wave breaking model is used to estimate the dissipation rate of wave breaking,

$$e_b = \frac{3\sqrt{\pi}}{16} \frac{\rho g f_p}{\gamma^4 h^5} H_{rms}^7. \quad (2.9)$$

In this mode f_p is the peak frequency and h is the water depth. Other variables are the gravitational constant ($g=9.81 \text{ m}^2\text{s}^{-1}$), the critical breaking parameter ($\gamma = 0.42$). After subtraction of e_b from $\frac{\Delta F}{\Delta x}$ only the energy dissipation rate by bed friction remains. Following Lowe et al. (2005) the energy dissipation by bed friction, caused by the bed shear stress, is calculated through:

$$e_f = \frac{1}{4} \rho f_w \cos(\Theta) u_b^3. \quad (2.10)$$

Here, Θ is the phase lag between the near bed orbital velocity and the bed shear stress given by (Nielsen, 1992):

$$\Theta = \cos\left(33 - 6\log\left(\frac{u_b}{k_b 2\pi f_p}\right)\right). \quad (2.11)$$

in which k_b is the physical roughness. Furthermore, the wave friction factor can also be related to the physical roughness by the commonly used relation of Nielsen (1992) stating:

$$f_w = \exp\left(a_1 \left(\frac{u_b}{k_b 2\pi f_p}\right)^{a_2} + a_3\right) \quad (2.12)$$

with empirical coefficients a_1 , a_2 and a_3 , Madsen (1994) determined the following coefficients $a_1 = 7.02$, $a_2 = -0.078$, and $a_3 = -8.82$ for conditions which applied to the field experiments. By substituting Equation 2.11 and Equation 2.12 into Equation 2.10 the physical roughness of the mussel bed can be obtained from the wave friction dissipation rate. This method, however, assumes that the loss in wave energy by means of bed friction is constant for each frequency component. It has however been shown that roughness

damps waves with shorter periods more than waves with longer periods (Nielsen, 1992). A good overview of the modified version of the above presented equations for wave spectra is given by Lowe et al. (2005). The equations as presented in Lowe et al. (2005) are used with the only adaptation that the current velocity is taken into account when calculating the wave energy flux (see Equation 2.5).

2.2.3 Bed shear stress

To assess the relative importance of waves and currents to this bed shear stress the bed shear stresses were calculated for waves and currents from the observed wave and current characteristics. The bed shear stress from wave motion only (τ_w) can be calculated through:

$$\tau_w = \frac{1}{2} \rho f_w u_b^2. \quad (2.13)$$

Here, f_w follows from Equation 2.12. The bed shear stress for currents τ_c only is calculated by

$$\tau_c = \rho U_{*c}^2; \quad (2.14)$$

where U_{*c} is determined from the current velocity and the obtained value for the physical roughness by solving Equation 2.2. Finally, using the Madsen (1994) wave-current interaction model with the obtained value for k_b the bed shear stress from combined wave and current motion τ_{wc} is determined,

$$\tau_{wc} = \rho U_{*cw}^2. \quad (2.15)$$

By comparing the contribution of wave and current induced bed shear stresses to the total bed shear stress their relative importance can be determined.

2.3 Materials and Methods

2.3.1 Field site

The field experiment was conducted on a mussel bed in the Wadden Sea, eastward of the island of Texel (see Figure 2.1), which is one of the barrier islands in the North of the Netherlands (53°9'N, 4°53'O). The tidal flat, on which the investigated mussel bed is located, is sheltered from wind generated waves incident from the west, north east and south east due a limitation in fetch. The fetch is limited by both land on the west and by tidal flats to the north-east and the south-east of the bed. Moreover, for waves propagating from the North Sea into the Wadden Sea most energy dissipates over the ebb-tidal delta located in front of the inlet between the islands Texel and Vlieland. As a result, the site is mainly exposed to waves generated in the 6 km long tidal channel to the east of the site which has an average depth of 10 m below the average tidal level. The tidal flat in front of the mussel bed on the Wadden Sea side is sandy and is covered with long straight bed forms.

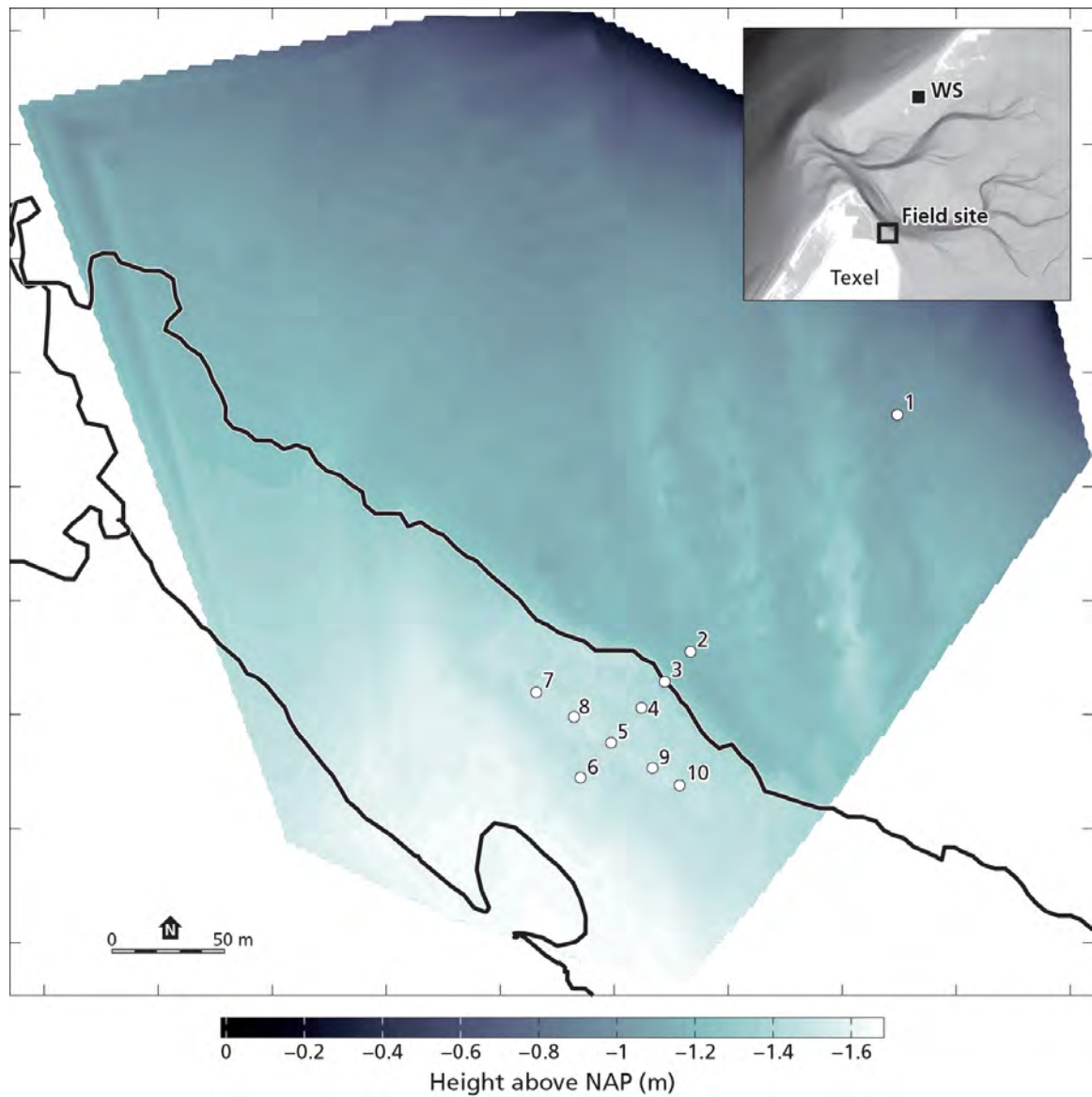


Figure 2.1 Contour plot of the local geometry surrounding the measurement array as derived from the DGPS measurements. The edge of the mussel bed is shown in black. The locations of the stations are numbered and given in white. The inset in the upper right corner shows the large scale morphology of the Wadden Sea and is based on soundings of Rijkswaterstaat (RWS), part of the Dutch Ministry of Infrastructure and the Environment (E&I). Both the location of the field site and weather station (WS) are marked in the inset.

2.3.2 Deployment

Measurement instruments used to determine wave and current characteristics were deployed from the 6th of October (Julian day 279) until the 22th of November (Julian day 326) during 2010. At ten locations pressure sensors type Ocean sensor systems OSS-010-003B Wave Gauge were used. The sensors were deployed in two perpendicular transects. The longest transect (216 m) was tilted 40 degrees to the east, and covers both the mussel

Sensor	Location	Height a.b. (m)	Height N.A.P. (m)	Frequency (Hz)	Orientation
Ossi 1	station 1	0.148	-0.11	10	down
Ossi 2	station 2	0.108	0.06	10	down
Ossi 3	station 3	0.093	0.023	10	down
Ossi 4	station 4	0.159	0.29	10	down
Ossi 5	station 5	0.030	0.29	10	down
Ossi 6	station 6	0.107	0.35	10	down
Ossi 7	station 7	0.079	0.31	10	down
Ossi 8	station 8	0.112	0.31	10	down
Ossi 9	station 9	0.128	0.35	10	down
Ossi 10	station 10	0.258	0.33	10	down
ADV 1	station 5	0.289	-0.08	32	326°
ADV 2	station 3	0.085	-0.07	32	80°
ADV 3	station 3	0.695	0.54	32	78°

Table 2.1 Overview of deployed sensors. The table shows the height above the bed (a.b.), the height with respect to the Dutch Ordnance Level (N.A.P.), the measurement frequency and the orientation of the sensors.

bed (4 stations) as well as the tidal flat (2 stations) on the Wadden Sea side of the bed. The perpendicular transect has a length of 75 m and contained 5 stations inside the mussel bed (including the common center station, see Figure 2.1). At the intersection point of the two transects a measurement frame was placed (station 5), a second measurement frame was located along the longest transect (station 1- station 6) at the transition point between the mussel bed and the bare tidal flat (station 3). The rest of the pressure sensors were attached to a single pole. To the measurement frame at the crossing point (station 5) a single Acoustic Doppler Velocimeter (ADV type Nortek Vector cabled version) was attached oriented in a direction opposite of the dominant flood current. At the 20th of October two additional ADVs were placed at station 3. An overview of deployed sensors at each station and their orientation, height and settings is given in table 2.1.

2.3.3 Data collection and processing

Velocity and pressure measurements were performed at 32 Hz by the 3 ADV beams and internal pressure sensor continuously throughout the measurement period. Time series collected by the 3 ADV beams were put in 10 minute records, the data was de-spiked and controlled using the guidelines proposed by Elgar et al. (2005) and Mori et al. (2007). Data series were rejected when more than 1% of the data did not pass the quality control, other time series were interpolated. Using the validated data set, current velocities were estimated from record averages. After which, the velocity power spectra were calculated and used to determine the wave directional spectrum as well as to determine the orbital velocities. The wave directional spectrum was averaged into log bands. Finally, dissipation of TKE is calculated from the power spectrum of the vertical velocity using the method from Feddersen et al. (2007). The power spectrum S_{ii} is calculated for all

3 velocity components of the ADV. Next, the turbulent rate of dissipation is calculated using the method from Feddersen et al. (2007) and adapted by Gerbi et al. (2009). The noise floor in both the horizontal as well as in the vertical direction were estimated from the velocity fluctuations at frequencies between 4 and 6 Hz. Only estimates for ϵ from the velocity component parallel to the sensor orientation passed both quality control checks. In this direction the measurement resolution is the highest, consequently, the noise is lower. Pressure time series were collected both by the ADV pressure sensors and OSSI pressure sensors at 32 Hz and 10 Hz respectively. Time series collected from all pressure sensors have been de-spiked and split into 10 minute records. Records during which the pressure sensor was covered by less than 10 cm of water were rejected, since the sensor may have been emerged shortly during measurements. Next, the records were corrected for air pressure and the Welch power spectrum $S_{p,j}$ is calculated using a 52s window with 50% overlap. Subsequently the pressure power spectrum was transformed into the surface height power spectrum using linear wave theory:

$$S_{w,j} = \left(\frac{\cosh(k_j h)}{\rho g \cosh(k_j (h - z))} \right)^2 S_{p,j} \quad (2.16)$$

From the surface height spectrum of these 10 minute records several wave characteristics were calculated following Lowe et al. (2005). Finally, the wave height spectrum was averaged into log bands.

2.3.4 Elevation and coverage

The local morphology was measured using a DGPS device (TRIMBLE GNSS ROVER). A local digital elevation map (DEM) was created from interpolation of the DGPS measurements. The DGPS device was also used to measure the heights of the measurement instruments. The contours of the whole mussel bed were determined by walking around the mussel bed carrying a GPS device (Garmin). More detailed information on mussel coverage and the degree of coverage was extracted from aerial photographs. These photographs were taken by a remote controlled UAV carrying a photo camera. Aerial photographs were taken just after the measurement period ended, half a year later and 10 months later.

2.3.5 Data Selection

Physical roughness estimation from turbulent dissipation

Estimates for dissipation which passed the quality control were used to estimate the physical roughness. The ebb current "collided" with the measurement frame, this resulted in increased turbulence, therefore all ebb current records were removed from the analysis. To prevent the use of records during which the tidal current reversed direction, and was affected by "collision" with the frame, also records with average flood current velocities smaller than 0.05 m s^{-1} were removed.

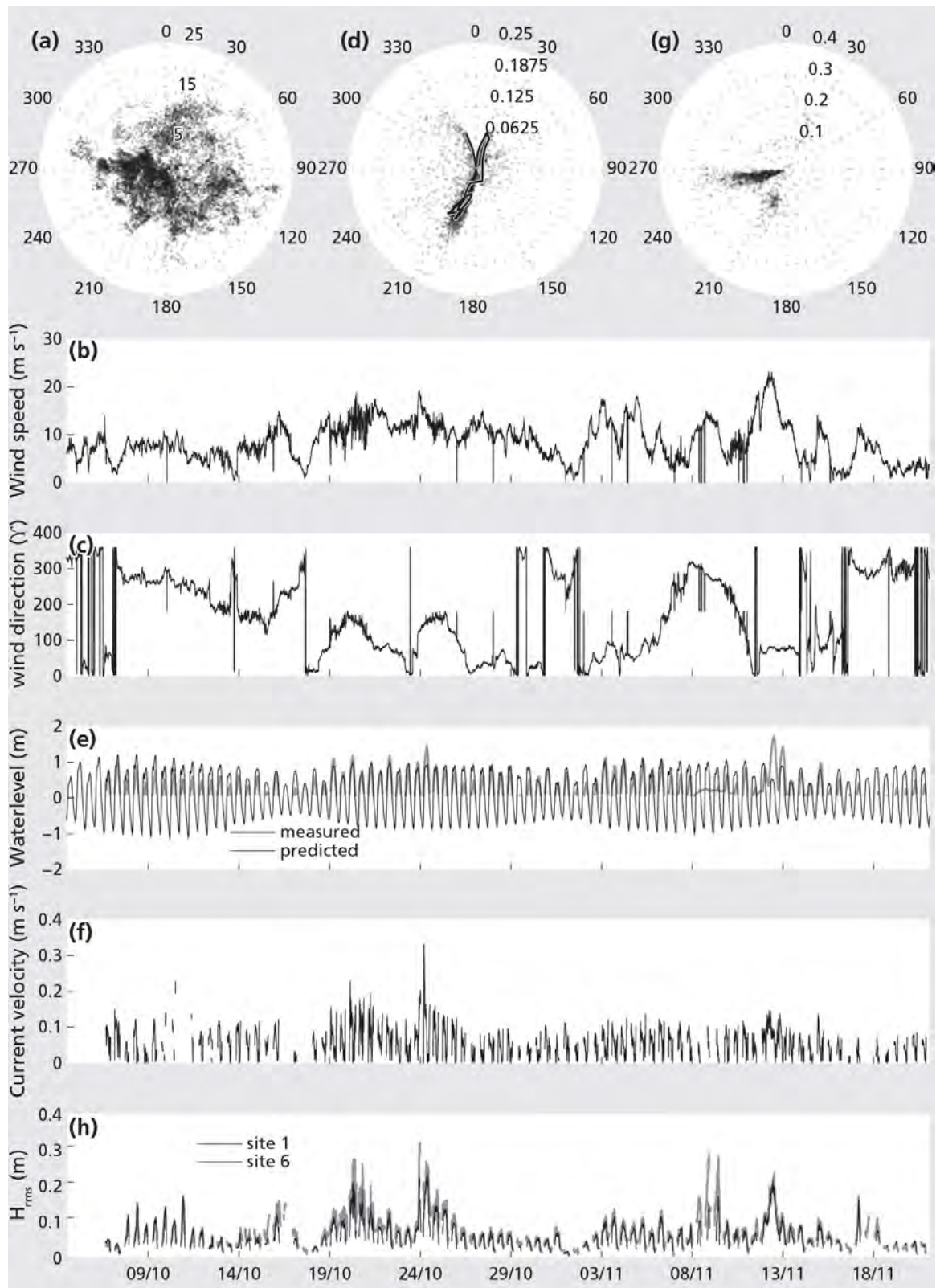


Figure 2.2 In panel a the wind speed is shown as a function of the angle of the wind. (Caption continues on next page)

Figure 2.2 (Continued) Panels b and c show time series of wind speed and direction respectively. In panel d the current velocity is shown as a function of current direction. In panel e two time series are shown; the first is of the astronomical tide for the tidal station Texel Noordzee and the second is of the measured water level at station 5. Panel f shows a time series of the current velocity. Panel g shows the wave height as a function of propagation direction. Finally, in panel h a time series of the wave height is shown.

Physical roughness estimation from wave attenuation

To ensure that estimates for the wave friction factor were as accurate as possible only records were taken into account if the dominant wave direction (measured at station 5) was parallel ($\pm 20^\circ$) to the transect between the considered pressure sensors. Additionally, only records for which relative wave height was sufficiently large ($H_{\text{rms}}/h > 0.18$) were included in the analysis, since for lower values the change in wave height between two stations was smaller than the measurement error. Additionally, records from periods during which breaking could have occurred ($H_{\text{rms}}/h < 0.3$) were excluded. Finally, only records were used during which the current velocity was smaller than 0.1 m s^{-1} and the near bed orbital velocity was larger than 0.2 m s^{-1} . This led to a substantial reduction in usable records (50 of a total of 5727 records were used for analysis between stations 5 and 7).

2.4 Results

2.4.1 Environmental conditions

Meteorological data was recorded by the nearby KNMI (Royal Dutch Meteorological Institute) weather station located on the island of Vlieland (see Figure 2.1). A compass plot of the measured wind speed as a function of wind direction throughout the measurement period is presented in Figure 2.2a. Time series of wind speed and direction are shown in Figure 2.2b and Figure 2.2c, respectively. A time series of the astronomical water level for the North Sea station is shown together with the locally measured water level at measurement station 1 in Figure 2.2e. Astronomical predictions on tidal conditions were calculated by Rijkswaterstaat, for a station located on the North Sea coast of Texel. Although the station is close to the measurement site there is a time lag, and possibly also a slight difference in the absolute height of the tidal wave. Time series of the tidal current-velocity and -direction, measured by the center ADV (station 5), are presented in Figure 2.2f and Figure 2.2d respectively. Maximal current velocities vary over a tidal cycle between 0.06 and 0.32 m s^{-1} . The tidal ellipses show 1 dominant flood direction while during ebb there are two dominant directions. Just after high water the ebb current is directed towards the gully next to the tidal flat while when the water level becomes lower the direction is shifted to the inlet. The wave climate is illustrated by a time series of the RMS wave height (at stations 1 and 6) in Figure 2.2f. In Figure 2.2g, a compass plot shows the wave height as a function of wave direction measured at station 5. The research area is subjected to waves from 2 dominant wave directions namely 80° and 15° . During the measurement period three meteorological events took place under which the

hydrodynamical forcing was increased due to an increase in wave height or due to set up. During one of these periods, namely the one around the 25th of October, this increased forcing led to erosion of mussels from the bed. During this period also the maximal wave height of 0.32 m for the most seaward station was observed, while the most shoreward station detected a maximum wave height of 0.23 m. Also, during this period the highest current velocity (0.33 m s^{-1}) was observed during flood. The other two stormy periods were observed between the 2nd and the 6th of November and around the 12th of November. The latter was a western storm which did not affect the local wave height on the mussel bed due to its sheltered position behind the island of Texel. However, the western storm led to a large set-up and slightly increased tidal currents at the measurement location as can be observed in Figure 2.2e. Throughout the measurement period wave heights varied under calm conditions between 0 and 0.15 m and were modulated by the tides.

2.4.2 Physical roughness

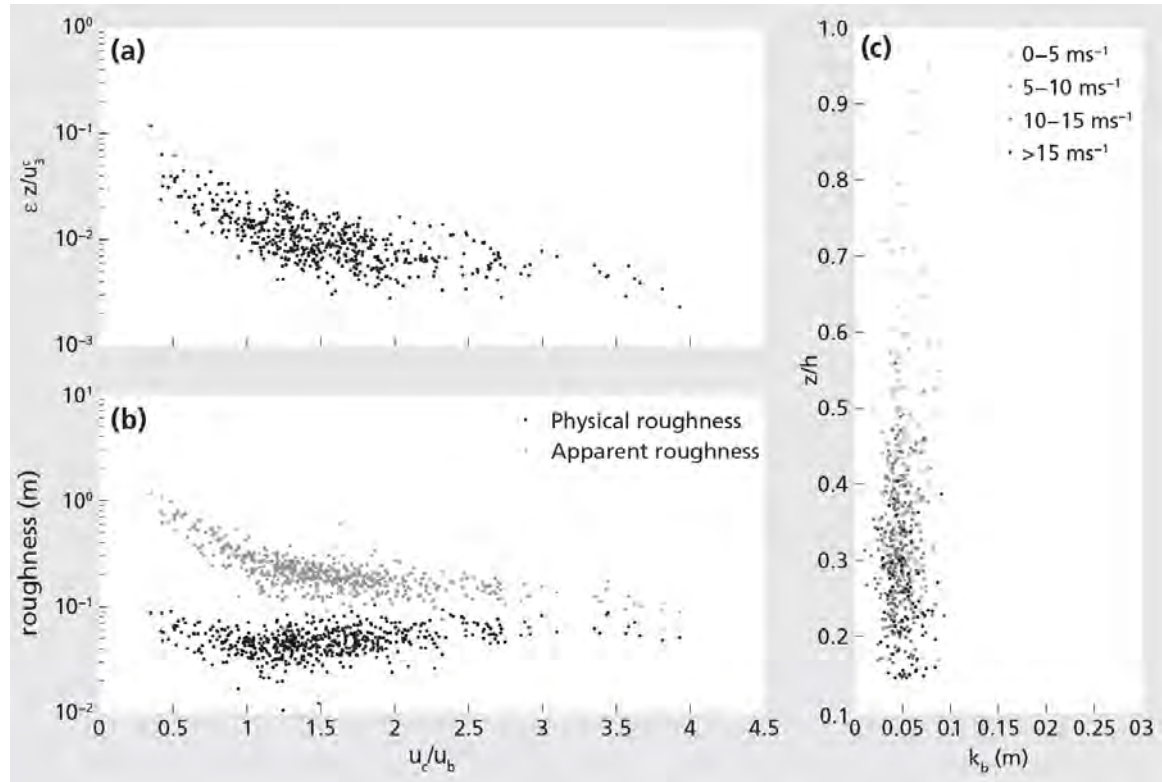


Figure 2.3 In panel a. the dimensionless dissipation of TKE as a function of the scaled current velocity. y-axis is logarithmic. In panel b. the apparent physical roughness and the physical roughness as a function of the scaled current velocity. All plots are shown for measurements performed during flood at station 5. In panel c. the physical physical roughness is shown as a function of the relative water depth for 4 wind velocity regimes.

We start by the local estimation of the physical roughness. The physical roughness is estimated from the ADV velocity measurements using the method described in section

2.2.1. First, the dissipation of TKE is scaled with the current velocity and the height above the bed (see Equations 2.2 and 2.1). In Figure 2.3a the scaled dissipation of TKE is plotted as a function of the scaled current velocity (the current velocity divided by wave orbital velocity). When no additional turbulent kinetic energy would be created by waves the law of the wall (Equation 2.2) predicts that dimensionless turbulent dissipation rate ($\epsilon z u_c^{-3}$) should be constant. Results show that for increasing relative current velocities the scaled dissipation decreases. This shows that wave orbital motion creates additional turbulence and that the effects of wave-current interaction should be considered to estimate the physical roughness. In Figure 2.3b both the apparent roughness and the physical roughness are plotted as a function of the scaled current velocity. The apparent roughness decreases as a function of u_c/u_b and this shows that the apparent roughness is influenced by turbulence generated by wave motion in the wave boundary layer. In contrast to the apparent roughness the physical roughness shows no relation with the scaled current velocity, this suggest that the wave bias is successfully removed. For all analyzed records an average physical roughness of $0.050 \pm 0.015 \text{ m}$ was found. Since, during the measurement period wind speeds were often larger than 10 ms^{-1} , the effects of wind shear might increase the turbulence intensity (Jones and Monismith, 2008) which consequently would lead to an overestimation of the TKE dissipation rate and thereby the physical roughness. To test the influence of wind shear on the physical roughness estimates, the obtained values are shown as a function of relative water depth for four different wind conditions in Figure 2.3c. Results show that for all wind forcing regimes estimates for the physical roughness have approximately the same range and do not vary substantially, this is quantified by averages shown in table 2.2. This indicates that the obtained values of the physical roughness are not influenced by wind shear. Also, there is no trend between the relative water depth and the estimate for the physical roughness.

wind speed	roughness (m)
$< 5 \text{ ms}^{-1}$	$0.056 \pm 0.017 \text{ m}$
$5 - 10 \text{ ms}^{-1}$	$0.047 \pm 0.013 \text{ m}$
$10 - 15 \text{ ms}^{-1}$	$0.046 \pm 0.013 \text{ m}$
$> 15 \text{ ms}^{-1}$	$0.053 \pm 0.015 \text{ m}$

Table 2.2 Average estimated values of the roughness length in four wind regimes.

Next, the physical roughness is estimated from wave attenuation following the method described in section 2.2.2. First, the occurrence of wave breaking is investigated. Figure 2.4a shows the wave height (H_{rms}) versus water depth together with the minimal breaking criterion (red line). This minimal breaking criterion is hardly ever met and if so the deviation is so small that no significant effects on the energy budget will occur. This means further analysis can proceed without the consideration of wave breaking. Second, the loss of wave energy over the mussel bed is inspected. In Figure 2.4b the loss in wave energy between stations three and five is shown as a function of the Keulegan Carpenter Number (KCN) $U_{\text{rms}} T_p l^{-1}$, a dimensionless quantity which describes the relative importance of drag with respect to inertia (Keulegan and Carpenter, 1958). With T_p being the

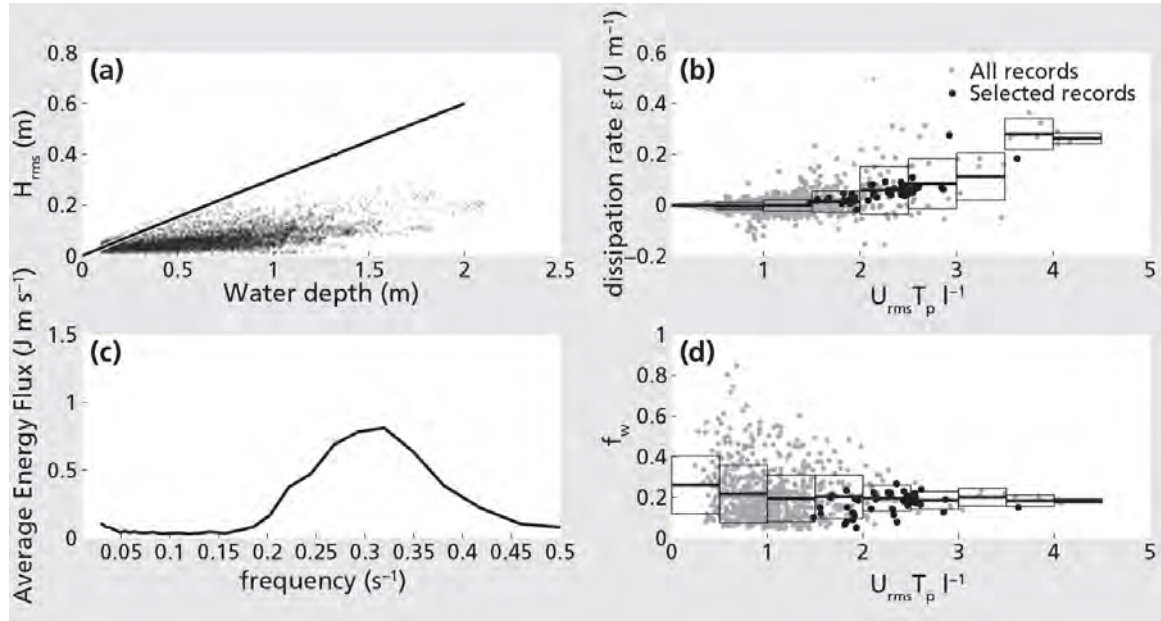


Figure 2.4 Panel a. shows the root mean squared wave height as a function of water depth; the red line here illustrates the line $H_{rms}/h = 0.3$ which is the minimal condition for breaking. Panel b shows the energy dissipation as a function of the Keulegan Carpenter number $U_{rms} T_p l^{-1}$ over the transect between stations 3 and 5. All estimates are shown in gray while those who passed the quality control are shown in black. The red line represents the mean dissipation rate for each part of the values on the x-axis and the boxes show the uncertainty by means of the standard deviation. Panel c. shows the average wave energy flux for each frequency component for records that past the selection criteria. Panel d. shows the wave friction factor as a function of the Keulegan Carpenter number $U_{rms} T_p l^{-1}$ over the transect between stations 3 and 5. Again the black dots represent records that past the quality control, center lines show the mean for each group and boxes show the standard deviation.

peak period and l being the mussel length ($l = 0.04m$). This quantity is determined from wave characteristics measured at station three. For further analysis only records are used which pass the criteria described in section 2.3.5. The average orbital velocity of data that passed the data selection was $0.26 \pm 0.03 \text{ ms}^{-1}$.

transect	f_w	roughness (m)
3 - 5	0.16 ± 0.06	0.056 ± 0.023
3 - 6	0.12 ± 0.04	0.036 ± 0.018
3 - 8	0.13 ± 0.03	0.041 ± 0.016
4 - 6	0.11 ± 0.04	0.032 ± 0.016

Table 2.3 Wave friction factors and Nikuradse roughness determined from wave dissipation over different transects.

Using the method described in section 2.2.2 the representative wave friction parameter f_w is determined for each measurement period. In Figure 2.4d the representative

wave friction parameter is shown as a function of the KCN. For small near bed orbital velocities the observations of the representative wave friction parameter appear as scatter (gray in Figure 2.4d), measurements converge for higher KCNs. Some values for low KCNs are even negative; this occurs when the reduction in wave energy flux due to wave attenuation is in the same range as the measurement error. The wave friction factor is estimated from observations that pass the selection criteria (black in Figure 2.4d) at 0.168 ± 0.055 . This result and the results of three other transects are shown in Table (2.3). Subsequently, calculated values for the physical roughness for transect 3-5 are significantly higher than those derived for the other transects. For transect 3-6 and 3-8 similar results are derived while the observed friction factor at transect 4-6 is smaller. These variations are attributed to variations in mussel density in particular the decrease between stations 5 and 6. Nikuradse roughness estimates for transects 3-6 and 3-8 compare quite well with the values derived using the turbulent dissipation method. Next, for the observations in transect 3-6 with a relative wave height higher than 0.18 m the average wave energy flux (Equation 2.5) is calculated for each frequency component. The results are displayed as a function of wave frequency in Figure 2.4 c. Results show that for frequencies higher than ($> 0.2 \text{ s}^{-1}$) a large wave energy flux is observed.

2.4.3 Forcing

The estimated roughness from dissipation of TKE (0.050 *m*) is used to calculate the total bed shear stress (Equation 2.15). This value is chosen because it represents the physical roughness at the measurement location the best and has the smallest error. Using Equations 2.14 and 2.13 the bed shear stress by the currents and waves are calculated and compared to estimates of the total bed shear stress. The time series displayed in Figure 2.5a show that the contribution of the current to the total bed shear stress is always much lower than the wave contribution. This is further illustrated by a short period of the complete time series in Figure 2.5b. Time series, of a stormy period, shows that both during more energetic periods and high water slack shear stresses exerted by waves are dominant. Only during ebb in the morning of the 24th of October the current substantially contributes to the total bed shear stress. However, for most periods wave forcing is clearly dominant. Hence, the model study is focused on wave forcing.

2.4.4 Wave model

A wave model was used to model the spatial distribution of wave forcing over the tidal flat. The effect of increased roughness is compared with a model run in which the roughness is constant over the tidal flat. The height measurements performed during the fieldwork cover only a small portion of the total grid therefore the model grid generated from the DGPS measurements (DGPS grid) is nested in a larger grid (RWS grid) which is based on the most recent soundings (January 2009) performed by Rijkswaterstaat (RWS). During these soundings, which are performed at a resolution of $20 \times 20 \text{ m}$, the mussel bed was not yet present. Model runs were performed for the two dominant wave directions being 15° and 80° degrees for the largest wave conditions for these directions. Using the wave model SWAN (Booij et al., 1999) in total six model runs were performed, three

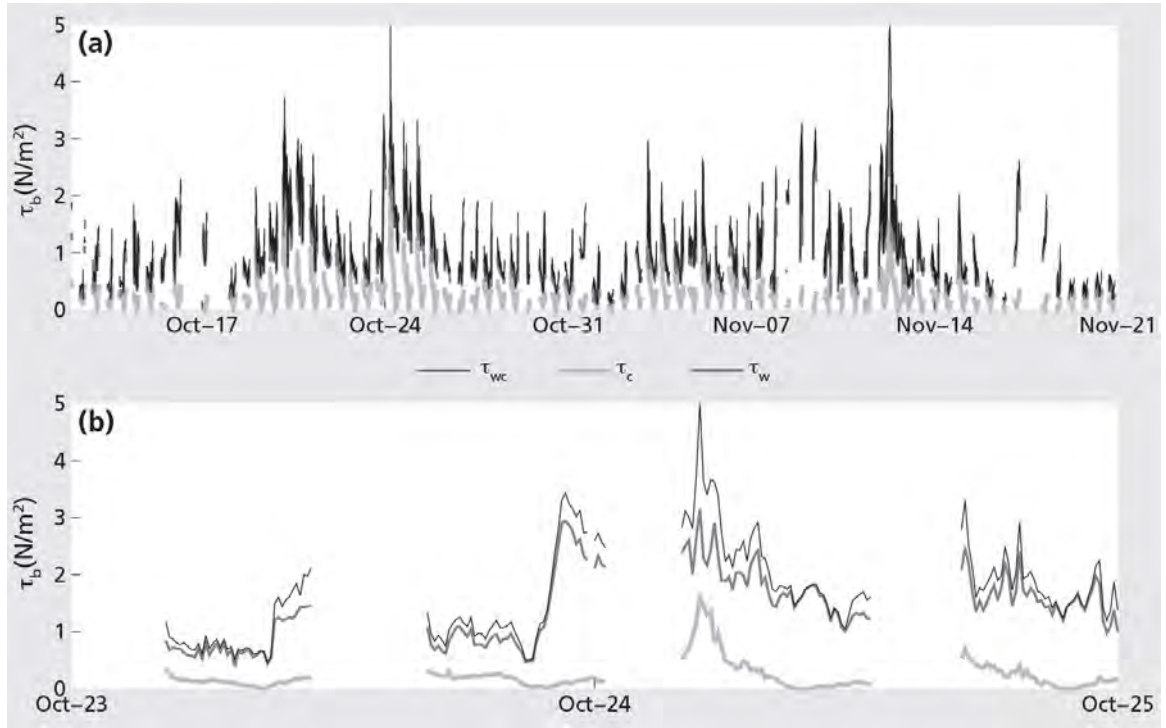


Figure 2.5 Time series of the total bed shear stress and the theoretical values in the case of waves only and currents only. Panel a. shows the shear stresses for the entire measurement period. Panel b. shows the shear stress during one of the most energetic periods (23th of October to the 25th of October).

for each condition, of which the model settings are shown in Table 2.4. The first two runs are performed using the RWS grid, from which wave forcing over a large portion of the tidal flat as well as boundary conditions for the nested DGPS grid are determined. Next, using the obtained boundary conditions for each wave condition two model runs are performed using the DGPS grid: one with the increased roughness and one without. In model runs bed friction is incorporated using the Madsen friction method, which uses the same equations as derived in section 2.2.2. The Nikuradse roughness for the uncovered part of the flat is estimated from observations at 0.02 m, while for the covered area's a representative value of 0.05 m is used. Triad wave interactions, wave breaking and white capping are taken into account. Wave generation by wind and quadruplets are switched off. In order to test if diffraction effects are important, two SWAN runs were performed in stationary mode, one with and one without taking diffraction into account. This was done at a low water level when the highest parts of the bed are just covered with water. The most diffraction is expected at these water levels. During this run the conditions for run 1 were used (see Table 2.4).

Wave forcing over uncovered flat

The focus is on the area around the measurement site. For this area the bathymetry of the RWS grid is shown in Figure 2.6a, the axis is rotated so that isobaths are nearly parallel

Parameter	run1	run2	run3	run4	run5	run6
Grid	RWS09	RWS09	DGPS10	DGPS10	DGPS10	DGPS10
Wave height (m)	0.20	0.28	0.20	0.28	0.20	0.28
Wave direction (°)	15	80	15	80	15	80
Peak period (s)	3	3	3	3	3	3
Directional spreading (°)	20	20	20	20	20	20
Mussel roughness	no	no	no	yes	no	yes

Table 2.4 Settings for the Swan wave model runs. RWS09 is the Rijkwaterstaat bathymetry of 2009 and DGPS10 is the bathymetry gathered during the fieldwork.

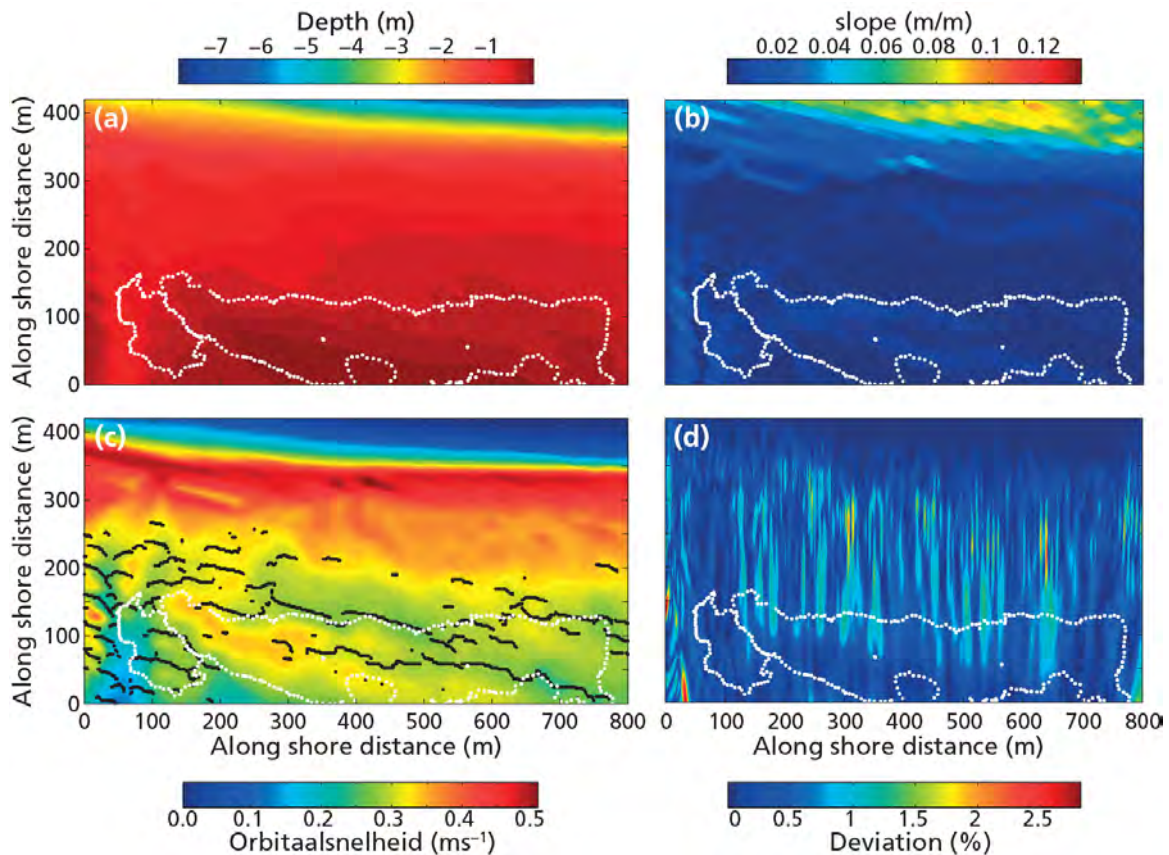
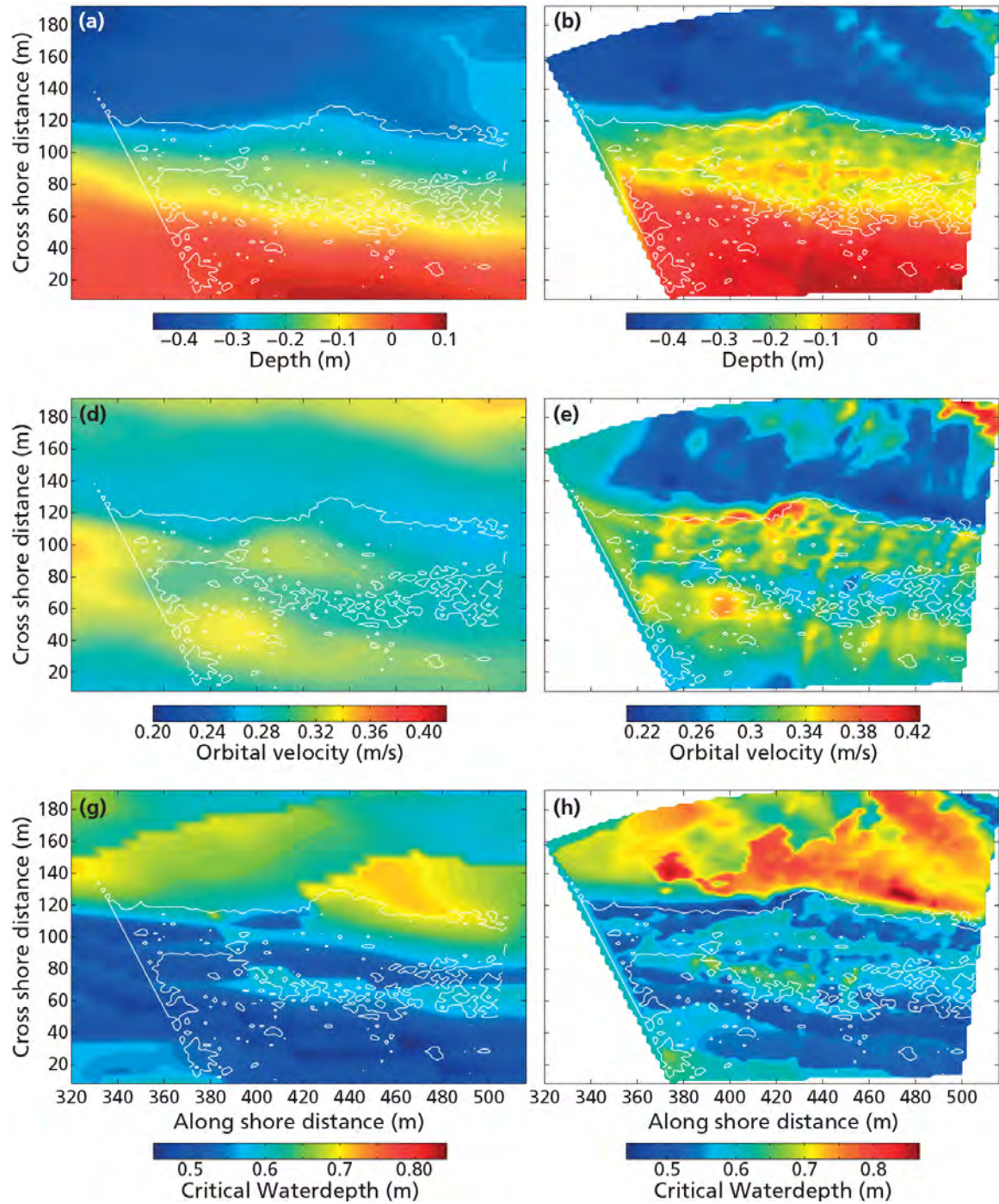


Figure 2.6 Panel a. shows the RWS bathymetry of the modeled area. In all figures the edge of the current mussel bed (as measured in January 2011) is illustrated by white dots. In Panel b the bed slope of the bed is shown. Panel c. presents the modeled near bed orbital velocities. Black dots represent local minima in orbital velocity. Again white dots are used to illustrate the edge of the bed as it was measured in January 2011. Panel d. shows the deviation in orbital velocity for a model run with and without diffraction effects taken into account.

to the x-axis (the map is rotated 31 degrees in anti-clockwise direction). The bed slope is shown in Figure 2.6b. Only at the sea side edge of the bed large slopes are found and over the tidal flat the bed slope is on average 0.01. For two incoming wave conditions



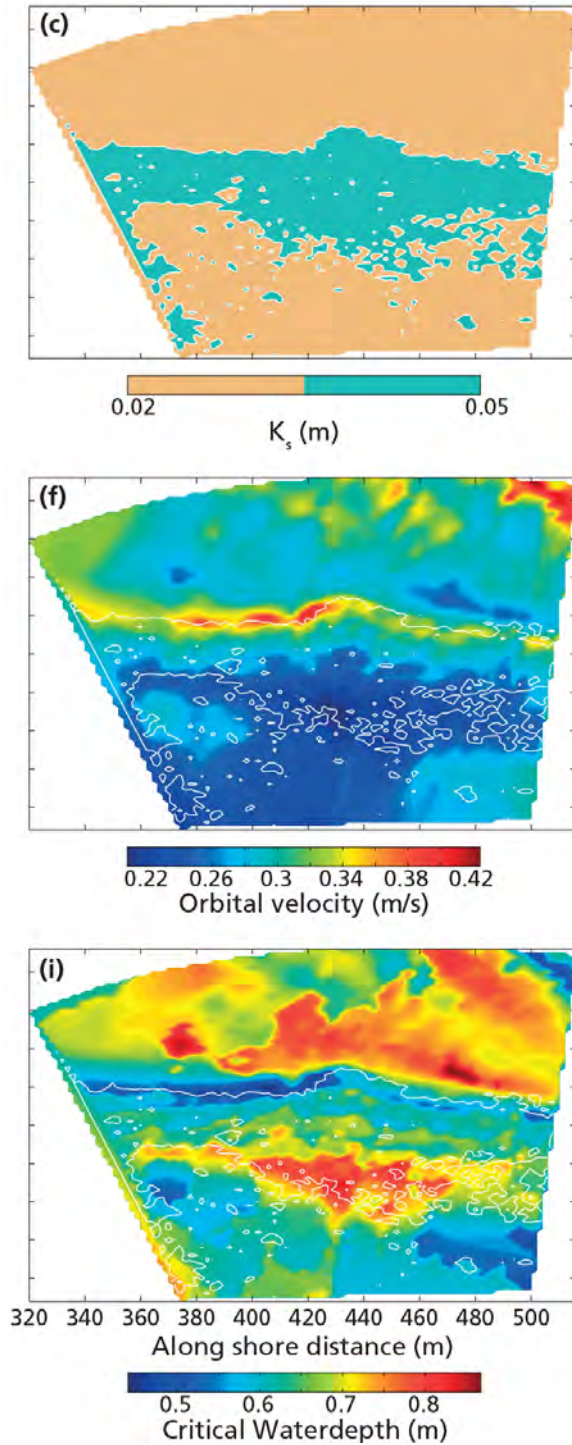


Figure 2.7 Model results of wave forcing in the study area. The left panels (a,d and g). show model bathymetry (a.) and results for a model run using the RWS bathymetry of 2009 and a constant homogeneous frictional coefficient. Center panels (b,e and h) show model bathymetry (b.) and results for a model run using the DEM created from DGPS measurements in the field and also uses a constant friction parameter. The model run represented by panels on the right hand side (c, f and i) show model results for a model run based on bathymetry shown in panel (b) In addition the bed friction is varied for this case based on mussel coverage. This is illustrated by the friction grid shown in panel (c). Mussel cover was determined from the aerial photographs shown in section 2.8. In panel (d.,e, and f), the modeled orbital velocity is shown for the study area. The bottom panels (g. h. and i) show the modeled critical water depth. The critical water depth is the water depth at which locally the highest bed shear stress is modeled. The used coordinate system for all figures is the same as used in Figure 2.6.

the spatial distribution of wave forcing over a tidal cycle was determined. The maximum wave forcing is illustrated by the maximum near bed orbital velocity over a tidal cycle, results are shown in Figure 2.6c. In this figure also the outline of the mussel bed, measured in January 2011, is indicated. The figure shows the near bed orbital velocity instead of the bed shear stress which are related through Equation 2.13. This allows for a better comparison of the results when later on in the analysis for the mussel covered area the friction factor is increased and forces will be much larger than in the uncovered area. Local minimums in the maximal wave forcing are highlighted in the figure. The current Wadden Sea side edge of the bed is, for a large part, overlapping with areas where there is a minimum in the maximal wave forcing. This suggests a relation between the location of the edge of the bed and a minimum in wave forcing. Finally, Figure 2.6d shows the deviations in wave orbital velocity caused by diffraction they are never larger than 3 % and are therefore unimportant.

Wave forcing over the mussel bed

Next, wave behavior above and around the mussel bed is studied. The effect of the differences in bathymetry between the RWS grid (January 2009) and the model grid obtained for the DGPS grid (autumn 2010) are studied. Furthermore, the effect of the increased roughness due to the presence of mussels inside the bed is investigated. For all three cases the maximum orbital velocity over a tidal cycle under the maximum wave conditions observed during the measurement campaign and the local water depth at which these values were obtained. The water depth at which orbital velocities peaked will be referred to as the critical water depth. The larger critical water depth the more sheltered the location is. First, the orbital velocity for the RWS and DGPS grids (shown in Figure 2.7d and Figure 2.7e) are compared. In these model runs the bed roughness is not increased for mussel coverage. For both model runs the spatial distribution of the orbital velocity appears to peak in similar areas. Also the spatial distribution of the critical water depth, shown in Figure 2.7g and Figure 2.7h, shows a similar pattern. Exact comparison between both model results is however complicated because the RWS grid is much coarser than the DGPS grid. Second, the wave forcing derived from both fine grid model results for both the model run with and without the increased roughness in the mussel covered area are compared. The modeled maximal orbital velocity, illustrated in Figure 2.7e and Figure 2.7f, shows large differences for both model runs. While in the model run without the increased roughness there are several maxima in orbital velocity, the model run with the increased roughness shows a clear decrease in orbital velocities over the bed in shoreward direction. For both models however the maximal orbital velocity appears to increase again shoreward of the mussel bed. Subsequently the model results for the critical water depth are investigated. Results show that the spatial distribution looks fairly similar with an increase in the critical water depth towards the shore. For the model run without the effect of the increased roughness the critical water depth peaks at 0.65 m while for the model run with this effect the critical water depth at the mussel bed reaches values up to 0.80 m.

2.4.5 Observations of coverage

In order relate predicted wave forcing from the model study to changes in mussel coverage, aerial photographs were taken just after the measurement period ended, half a year later and 10 months later. Photographs of the area surrounding the measurement array are presented in Figure 2.8a. The spatial distribution of mussel cover is similar in all three photographs. There are however some small changes. The amount of mussels in the area shoreward of the mussel bed has decreased. This is most pronounced left of station 5 (white cross in Figure 2.8), near the measurement frame. When this is compared with model results, it appears that these areas coincide with the regions with the strongest predicted bed shear stresses (apart from the sea side edge of the bed). These differences are however small and not conclusive. Finally, "cross-shore" profiles measured across the mussel bed are compared; DGPS surveys along the main array were carried out in November 2010 and May 2011, respectively. Figure 2.8b shows profiles for both periods. There is little variation in bed height in the mussel covered area between both measurement periods. The largest differences in bathymetry are caused by the migrating bed forms in front of the bed.

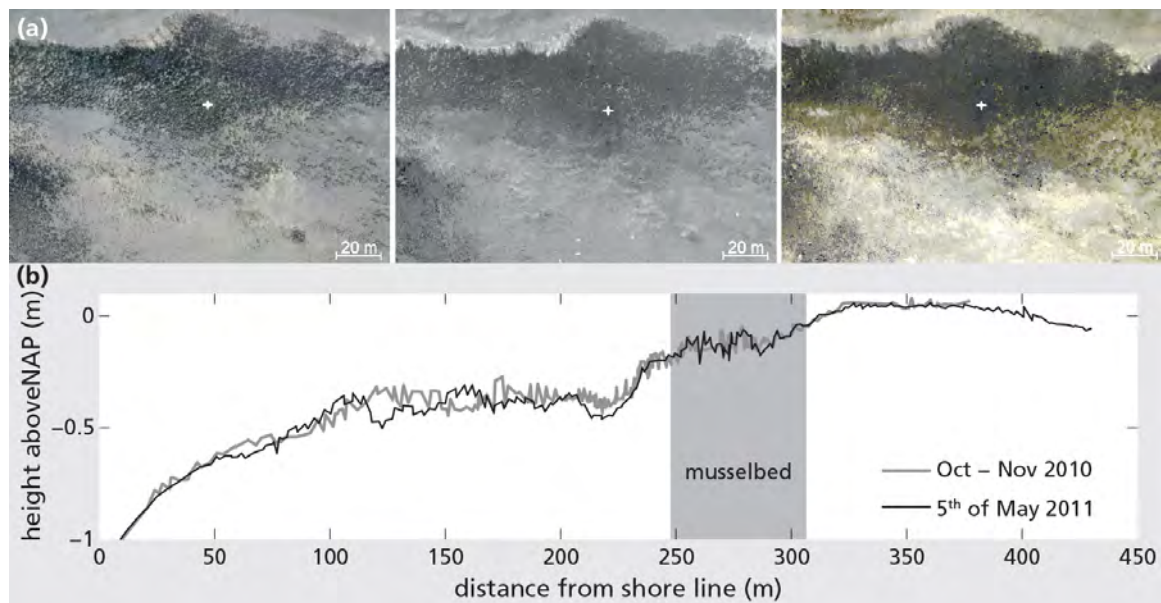


Figure 2.8 Panel a shows aerial photographs of the measurement area. The left aerial photograph was taken on 23rd of November 2010. The photograph in the center was taken on the 5th of May 2011. The photograph on the right hand side was taken on the 30th of August 2011. In all three images the location of observation station 5 is shown by a white cross. Panel b shows DGPS measurements of surface height along the measurement transect with a radius of 3 m around the transect. The black line represents the measurements done during the measurement period (6th of October 2010 up to 23th of November 2010). Grey line represents measurements from a single transect performed on May 5, 2011.

2.5 Discussion

2.5.1 Roughness

The physical roughness of the mussel bed was estimated using two methods. First, high frequency velocity measurements combined with the Madsen (1994) wave current interaction model were used to estimate the physical roughness of the mussel bed. The physical roughness at the measurement location is estimated at 0.050 ± 0.0150 m. It was shown that this estimate remains constant for different current velocities and also under different wave conditions. Also, possible effects of wind shear on values of the physical roughness were investigated and no relation was found. Furthermore, at small water depths during strong winds no records passed the quality control. A likely cause for this is given by Jones and Monismith (2008), who demonstrates that turbulence by wind shear is generated in the part of the spectrum that was used to determine the dissipation rate. Variations in physical roughness estimates can be attributed to mussel feeding activity (Van Duren et al., 2006). The obtained value is much smaller than the roughness value that is obtained by Van Duren et al. (2006) using flume experiments, their estimates for $k_b (= 30z_0)$ vary up to 0.202 ± 0.030 m. Their estimates close to the bed for inactive feeding are in better agreement with the results (0.0396 ± 0.0009 m for 0.13 m s^{-1}). In contrast to their experiment the obtained value for the physical roughness compares well with the physical size of the larger mussels (0.04 m).

Second, to estimate the roughness on a larger spatial scale, changes in the wave energy flux have been used to determine the physical roughness. Values of the representative wave friction factor f_w (see table 2.3) are more than 10 times larger than typical literature values ~ 0.01 for tidal flats (Thornton and Guza, 1983). The derived estimates for the physical roughness are also similar to the estimate from high frequency velocity measurements. The obtained value provides thus a robust estimate for the physical roughness which can be used in modeling. Furthermore, the results indicate a relation between the effective wave friction factor and mussel density. Obtained values for the wave friction factor and physical roughness are smaller for the transect between stations 4 and 6; this is attributed to a decrease in mussel density as can be observed from the aerial photographs shown in Figure 2.8. Only estimates for high waves ($H_{\text{rms}} > 0.18 \text{ m}$) were included in the analysis, since the effects of bottom friction become more pronounced at higher relative wave heights (De Swart and Zimmerman (2009)), reducing the relative amount of noise in the wave field. This will lead to more accurate estimates of the physical roughness. There are however still sources for errors in estimates in the wave friction factor and physical roughness. Firstly, errors can occur due to variation in wave fields passing both stations since stations are imperfectly aligned with respect to the incoming wave direction. Secondly, values can deviate due to the fact that most waves observed during the measurement period were relatively small so only a small band of wave frequencies contained enough energy to substantially contribute to the estimates of the frictional parameters.

2.5.2 Forcing

The time series of shear stresses have shown that wave forcing is the dominant source of hydrodynamical forcing over the mussel bed. The subsequent wave model study on the relation between current mussel cover and the wave forcing prior to settlement of the bed suggests a relation between the two. A clear indication of this is that a minimum in wave forcing on the uncovered tidal flat is coinciding with the current sea side edge of the mussel bed. This relation is mainly attributed to the bed slope which is the smallest near the sea side edge of the mussel bed. Results also showed that diffraction has no significant effect (<3%) on the spatial distribution of wave forcing. In addition, the model study of the present situation, in which the mussel bed and its wave attenuating effects are taken into account, demonstrates that at this sea side edge the largest wave forces are exerted. This run also shows that by attenuation of waves over the bed, more shoreward located mussels are sheltered from large wave forcing. Notice that the forcing behind the mussel bed again slightly increases. These model results suggest that the current location of the sea side edge of the bed is optimal with respect to wave forcing. Since observations of mussel bed cover right after settling and during the early stages of development are lacking, it remains unclear during which phase of development and under which meteorological conditions the shape of the mussel bed was influenced the most.

2.5.3 Implications for mussel bed survival

The settling phase, during which the mussels still have to attach to the substrate, is a critical phase in mussel bed development. Denny (1995) showed that in the period after the initial attachment, the attachment is relatively the strongest since forcing depends on the surface area which increases quadratically while the attachment strength does not. Also during this phase mussels are closer to the bed where shear stresses are smaller, and seek shelter behind larger shell fish or their remainders (McGrorty et al., 1990). However, during this period the sheltering effect, which depends on the roughness of the mussel layer, is much smaller. When mussels grow effects of sheltering increase, while also the relative wave forcing on the exposed sea side edge will grow. Also seasonal variations in attachment strength results in increased risk of erosion during winter and early spring storms (Hunt and Scheibling, 2001; Moeser and Carrington, 2006). In order to survive exposed mussels on the sea side edge need more food. For this particular site the exposed seaward side of the bed is submerged the longest, it's subjected to stronger currents, and it is closer to the gully. These factors suggest increased food availability for the sea side edge. Since the seaward side of the bed is also exposed to flood currents, which transports the most food, it is likely that food availability reduces in shoreward direction (van de Koppel et al., 2005). The role of food depletion is supported by the aerial photographs which show a reduction in mussel density in shore ward direction. This increased scarcity of food in shore ward direction could explain why the shoreward edge appears where the wave forcing is just slightly increased.

2.6 Summary and Conclusions

Wave forcing on mussel beds has long been studied by means of simple physical models or statistical evidence and focused on predicting survival chances. This chapter investigated the spatial distribution of mussel cover and local wave forcing. Results from a six week field experiment show that wave -generated bed shear stress is responsible for the majority of the hydrodynamical forcing on a mussel bed located on an inter tidal flat. Dissipation by bed friction is found to be the main mechanism for wave dissipation over the mussel bed, wave breaking is found to be of minor importance due to the small slope and relatively small waves. This is similar to observations performed over coral reefs (e.g. Lowe et al. (2005)) . Using the method from Lowe et al. (2005) estimates are made for the physical roughness of the bed which are smaller than physical roughness determined by flume studies (i.e. Van Duren et al. (2006)). The estimates compare well with the physical size of mussels. The increased roughness of the bed results in a strong increase of wave attenuation over the bed resulting in the seaward parts of the bed absorbing more wave energy and thereby protecting the more shore ward lying areas of the bed.

A subsequent model study based on results of the field measurements demonstrates similar developments. Near bed orbital velocities peak on the seaward edge of the bed and reduce over the bed in shoreward direction. In the model the bed coverage is determined from aerial photographs and a single roughness value is used to represent the mussel bed. Behind the mussel bed an increase in wave orbital velocity is observed, mussels in this area seem highly vulnerable to erosion. Finally, the model study was expanded to determine the wave forcing over the bed before the mussel bed was present. A minimum in wave forcing is found to largely coincide with the present seaward edge of the bed. This suggests that the bed has established in such a way such that the wave forcing on the bed was minimized. In order to confirm this relation between mussel cover and wave forcing this research will be extended to other mussel beds.

3 How mussel hummocks influence flow patterns and food uptake in intertidal mussel beds

This chapter is based on:

DONKER, J. J. A., VAN DER VEGT, M., HOEKSTRA, P. (2015), How mussel hummocks influence flow patterns and food uptake in intertidal mussel beds. Submitted to: Journal of Geophysical Research: Oceans.

Abstract

Intertidal mussel beds are a key species in the ecosystem of the Dutch Wadden Sea. They accumulate and stabilize sediments and therefore create possibilities for coastal protection. While some mussel beds remain uniform and flat others form elevated hummocks. Here, the influence of hummocks on hydrodynamics and food availability is investigated and the benefits for hummock creation in current-dominated intertidal mussel beds are evaluated. A field campaign revealed that hummocks (height 0.4 m) substantially influences flow patterns. At low tide, the flow velocity between hummocks is strong but is relatively weak over the hummock. At intermediate water levels, flow over the hummocks becomes larger than between hummocks. At high water levels the velocity differences between flow over and along hummocks appears to be small. To upscale the observations, the SWASH model was used to simulate flow over an idealized hummock geometry. Results confirm the flow regimes observed in the field and show that they are sensitive to length, width and height of the hummock and to the roughness of the mussels. The modeled flows were used to solve an advection-diffusion model to simulate the presence and supply of food near the bottom. Uptake of algae by mussels is explicitly taken into account. The results demonstrate that when flow is accelerated over the hummock the mussels have better access to food. When flow is larger around the hummock less food is available. Both field data and model results suggest that wide hummocks improve survival chances of mussels.

3.1 Introduction

Mussels are ecosystem engineers who adapt and maintain their habitat by accumulating and stabilizing sediments (Wright and Jones, 2006). This makes them a key species in the Dutch Wadden Sea as they influence the (fine) sediment budget (Van Leeuwen et al., 2010)). Ecosystem engineering activities result in various morphological features and

patterns at different mussel beds as shown in Figure 3.1 (uniform coverage (Chapter 2), regular banded mussel beds (van de Koppel et al., 2005) and small elevated patches). As suggested by van de Koppel et al. (2012) these features are the result of a combination of self-organization on the small-scale and large-scale physical forcing. These self-organized patterns in mussel cover and bed elevation will also influence flow patterns on the mussel beds, and thereby the sediment transport and the transfer of food to the mussels. However, in studies on pattern formation in mussel beds (van de Koppel et al., 2005; Liu et al., 2014a,b), for which food availability plays a key role, these effects have been neglected as constant flow velocities and vertical mixing have been assumed. The formation of elevated patches or 'hummocks' is of particular interest, as their use for coastal protection is investigated (Piazza et al., 2005; Borsje et al., 2011; Scyphers et al., 2011).

In this study the effects of hummocks formed by the blue mussel, *Mytilus edulis* L., on local hydrodynamics and the consequences for food uptake are investigated. Differentiation is made between non-elevated mussel 'patches', and elevated mussel 'hummocks'. The formation of hummocks is the result of sedimentation processes inside mussel patches. Due to the enhanced surface roughness and the effects of filtration by mussels often sedimentation occurs inside mussel patches. Patches offer an advantage for mussels in terms of resistance to wave disturbance as well as it reduces predation (Bertness and Grosholz, 1985; Okamura, 1986; Côté and Jelnikar, 1999; Hunt and Scheibling, 2001). However, when mussels are located in close proximity to each other food demand is high, leading to depletion of food from the bottom boundary layer (bbl). Therefore, in order to replenish the bbl, often bare patches of sediment are found between subsequent mussel covered areas (Butman et al., 1994; Gascoigne et al., 2005; Saurel et al., 2013). Results from flume studies suggest that these bare patches cause a renewal of the bbl and optimizes food uptake by mussels in the observed patchy structure (Widdows and Brinsley, 2002; Van Duren et al., 2006; Folkard and Gascoigne, 2009). When mussels become buried they are capable of repositioning themselves on top of the sediment, thereby reassuring their access to food again. As the height of the hummock increases it increasingly influences the 3D structure of both flow and mixing.

A major drawback of flume studies is that the size of the flume is often small with respect to the size of hummocks found in the field. Therefore only the 2D (vertical and along-flume) effects of mussel patches and hummocks on the flow could be quantified. Hence, 3D effects such as possible routing of flow alongside the patches have not been taken into account, although results from the field for other benthic structures such as sea grass patches show clear evidence that this phenomenon is an important aspect (Zong and Nepf, 2010). Likewise, model studies (van de Koppel et al., 2005; Simpson et al., 2007; Liu et al., 2014b) often ignore bathymetric variation, and simulate the mussel bed by applying an increased roughness to a flat area. This can be an appropriate approximation for flat beds, or for hummock type beds in deep water. However, in intertidal areas where hummocks at some point during a tidal cycle occupy the full water column the flow and mixing processes will be affected. Due to the limited through flow area, flow will have to accelerate. Depending on the surface roughness and water level this will be either over the hummock or around it, increasing the forcing on top of the hummock or in adjacent

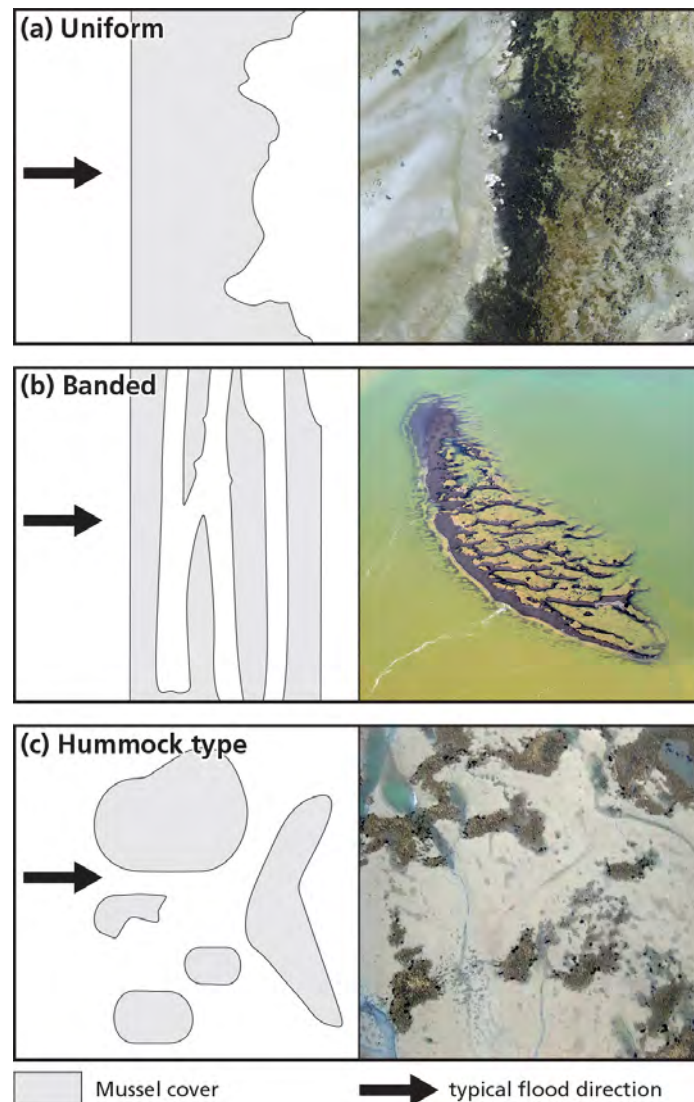


Figure 3.1 Overview of typical mussel bed types with sketches and aerial photographs. In panel a uniform covered mussel bed. In panel b and c a banded mussel bed and a hummock type mussel bed, respectively.

areas respectively, similar to flow patterns observed in vegetation patches (Zong and Nepf, 2010).

Hummocks will affect food dynamics because they influence flow and mixing. It has been shown by Liu et al. (2012) that height variation can promote uptake. Their simplified approach, however, ignored the strong temporal and spatial variation in hydrodynamics over the hummock. Apart from the obvious effects of changes in advection on food availability also changes in vertical mixing, resulting from hummock presence, influence food uptake. The role of vertical mixing has been shown to be of great importance to compensate the rapid depletion of the bbl (Fréchette and Bourget, 1985; Dolmer, 2000; Butman et al., 1994; Ackerman et al., 2001; Simpson et al., 2007). Therefore, knowledge

on the effects of hummock formation in relation to the three dimensional structure of flow and mixing processes are of importance when studying the evolution and survival of mussel beds.

The objective of this study is to investigate how elevated hummocks which are limited in length and width influence flow behavior, and as a consequence food availability in mussel beds. Furthermore, the study aims to determine under which conditions and for which geometry hummock formation is beneficial for mussel bed survival. This is done by analyzing observations of currents around a mussel hummock over multiple tidal cycles. Subsequently, a model is used to mimic the observed flow variations and to study the scale dependent effects of mussel hummocks on flow routing and acceleration. Finally, the model is used to investigate the effect of hummock presence on food uptake.

3.2 Materials and Methods

3.2.1 Field experiment

Physical setting

The field observations were performed from the 5th to the 27th of April in 2012, on one of the smaller hummocks in a mussel bed in the Dutch Wadden Sea. The bed is located on Brakzand, an intertidal shoal located between the Dutch mainland coast and the barrier island of Schiermonnikoog (54°26,5'N, 6°12'O). A height map of the area surrounding the measurement location is shown in Figure 3.2. The mean elevation is 0.6 m below mean sea level (MSL) in uncovered areas while the top sections of mussel hummocks reach up to 0.1 m below MSL. The area is mainly populated with blue mussels *Mytilus edulis* (40%) and Japanese oysters *Crassostrea gigas* (60%) with a concentration of 3350 individuals per square meter. There is a lot of variation in hummock shape, small hummocks tend to be rectangular or circular, while larger hummocks tend to form banded structures.

The shoal is dominated by tidal currents. The astronomical tidal amplitude varies between ~1.6 m and ~0.7 m over a Spring-Neap cycle. The tidal wave enters the basin through the tidal inlet between Schiermonnikoog and Ameland (barrier island West of Schiermonnikoog). During flood the flow is directed towards the SSE, ebb flow is to the NNW. Spring tide occurred at the 8th and 22th of April and Neap tide on the 15th April. During the period little set-up or set-down was observed. During the first two days and on the 18th of April there is a clear set-down (< -0.4 m). Clear set-up (> 0.4 m) was observed on the 7th and around the 11th of April. Waves are locally generated in the Dutch Wadden Sea (Chapter 2) as most waves from the North Sea dissipate on the ebb-tidal delta in front of the inlet. Wave characteristics are strongly modulated by the tide as both wave generation and propagation are limited by the water depth and fetch length. At the measurement site the root mean squared wave height during the measurement period peaked at 0.12 m.

Data acquisition and processing

In April 2012 two measurement rigs were deployed to determine wave and current characteristics on and next to a mussel hummock. The rig on top of the mussel hummock

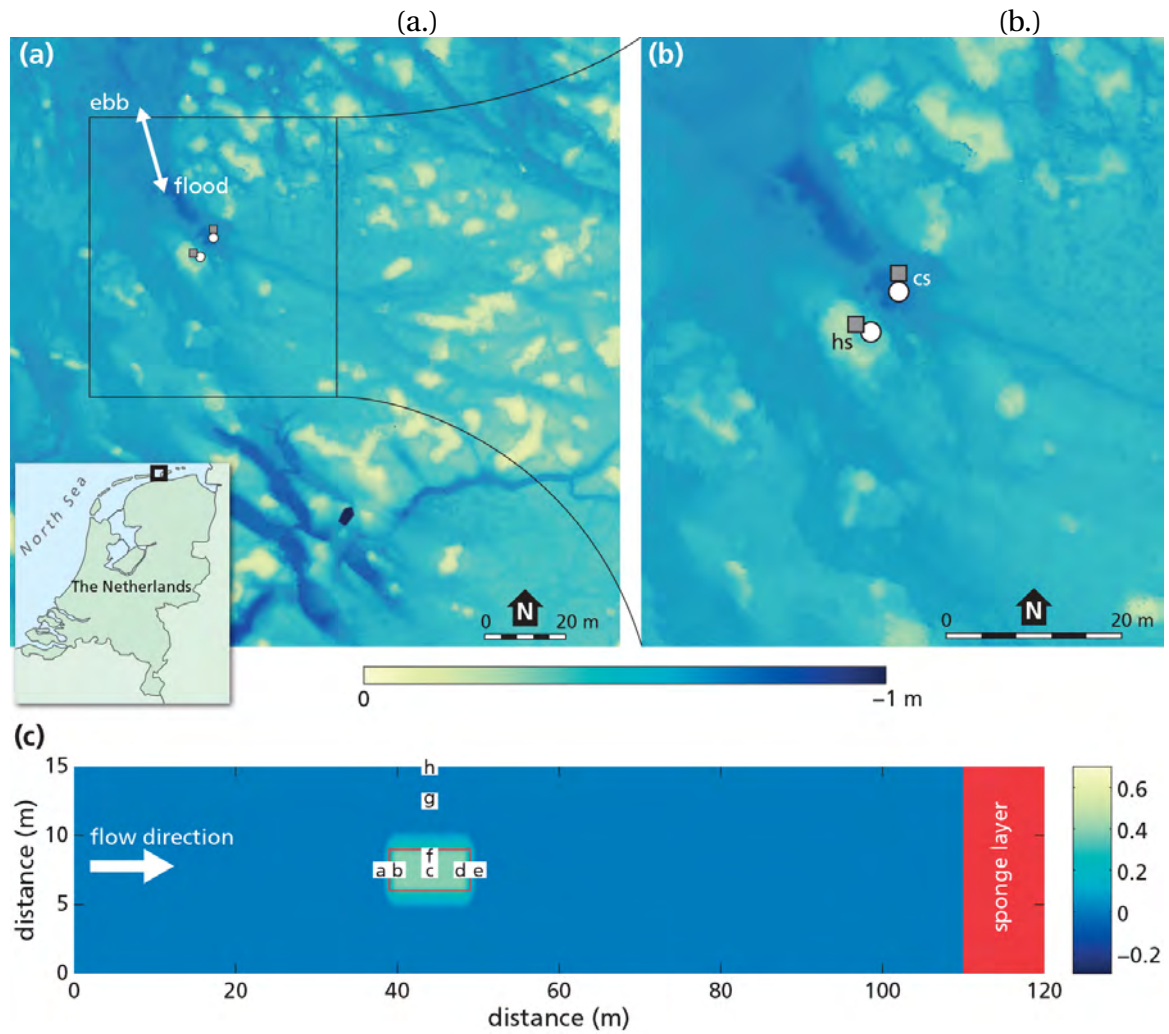


Figure 3.2 Panel a. gives an overview of bed level around the measurement location. Locations of velocity (gray squares) and pressure (white circles) measurements are marked. In the bottom left an inset of the Netherlands with the location of the measurement area is displayed. Panel (b.) an enlarged region of the area surrounding the studied mussel hummock is shown together with the location of the hummock sensors (hs) and the channel sensor (cs). In Panel c the applied model bathymetry and set-up is illustrated, the red rectangle shows the area covered with mussels on top of the hummock. The flow direction is from left to right and in purple the location of the sponge layer is indicated. White squares highlight locations from which flow velocities were analyzed.

contained two Acoustic Doppler Velocimeters (ADV; type Nortek Vector cabled version) and one pressure sensor (type Ocean sensor systems OSSI-010-003B Wave Gauge). The rig next to the mussel hummock contained one ADV and one pressure sensor. In order to minimize influence of the measurement rig ADV's were orientated horizontally looking towards the west (opposing the dominant direction of flood currents). The ADV's measured continuously throughout the measurement period at a frequency of 16 Hz. The pressure sensors measured at 10 Hz. In table 3.1 the orientation, height and key settings of the deployed sensors are listed.

Sensor name	Sensor height Type	above bed	Measurement frequency	Orientation
<i>upper hummock sensor (uhs)</i>	ADV	0.56 m	16 Hz	326°
<i>lower hummock sensor (lhs)</i>	ADV	0.15 m	16 Hz	326°
<i>channel sensor (cs)</i>	ADV	0.28 m	16 Hz	327°
<i>hummock pressure sensor</i>	OSSI	0.155 m	10 Hz	-
<i>channel pressure sensor</i>	OSSI	0.125 m	10 Hz	-

Table 3.1 Overview of the level, orientation and measurement frequency of the used measurement devices

The time series retrieved by the ADV were binned into 10 minute records. The data was quality controlled using the guidelines proposed by Elgar et al. (2005) and subsequently de-spiked using the method described by Mori et al. (2007). When both methods resulted in less than 1% of the points being rejected, the rejected points were interpolated. More rejected points resulted in rejection of the complete 10 minute record. Next, the quality controlled time series were time averaged to determine mean velocity components. The orbital velocity was determined and the wave directional spectrum was created following a PUV method (Gordon and Lohrmann, 2001). Subsequently, the wave bias was removed from the sensor by means of the adaptive filtering method proposed by Feddersen and Williams III (2007). At the channel sensor pressure data was used to remove the wave bias as no second ADV was available there. After removing the wave bias the total amount of Turbulent Kinetic Energy (TKE) and Reynolds stresses were determined. Estimates of TKE are only used when orbital velocities are small ($<0.05 \text{ ms}^{-1}$) to avoid a large contribution from waves on the roughness the flow experiences (Grant and Madsen, 1979). Only flood measurements are considered for turbulence analysis as flow passes through the rig during ebb. Flood velocity estimates are not expected to be affected by this process. Pressure time series gathered by the OSSI pressure sensors and the ADV's internal pressure sensor were processed in a similar fashion. All records during which the pressure sensors were covered with less than 10 cm of water were rejected, this to guarantee that the sensors were submerged during the whole 10 minute period.

Elevation

The local morphology was measured using a terrestrial 3D laser scanner Riegl V400. The scans were georeferenced using reflectors of which the location (x,y,z) was measured using a dGPS device. These reflector sites were also used as tie points, and could be used to link individual scans from different locations to each other. One scanner location was on top of a 9 meter high camera pole. The scans were pre-processed using the program Riscan pro. The measurement rigs and poles were removed from the scans. The scans were mapped on a $0.1 \times 0.1 \text{ m}$ grid, and data of individual scans were combined. When multiple scans have a value for the same position the data from the scan which had the smallest angle with respect to the vertical was used. Since, the laser scanner is unable to

perform measurements in water covered areas, additional measurements with the dGPS device were performed in water covered areas to map the entire research area.

3.2.2 Model Simulations

Model description

Flow behavior around an intertidal mussel hummock was simulated using SWASH; a full description of the model is given in Zijlema et al. (2011). SWASH is a three-dimensional hydrodynamic model which solves the non-linear shallow water equations with the addition of non-hydrostatic pressure in the horizontal momentum equation and a vertical momentum equation. Furthermore, a vertical momentum equation is added. Therefore in SWASH, rapidly varying flows and their effects on the free surface elevation can be modeled. This is essential when modeling the effects of large and rapid variations in bed topography, as those caused by the mussel hummock, on flow. The equations are solved over a three-dimensional spatial grid. In the vertical the model grid is divided into terrain following sigma coordinates.

Model setup

The model bathymetry, domain and set-up are shown in Figure 3.2c, model grid length is 120 m and width is 15 m. Horizontal grid size is 0.1×0.1 m, time stepping is determined using the Courant criterion. In 3D mode the water depth is divided into six layers and the thickness of the layers increases from the bed towards the surface. The layers cover 5%, 10%, 10%, 20%, 25% and 30% of the water column respectively. Flow is generated at the westward boundary and any reflection is damped near the eastward boundary by a 10 m thick sponge layer. Boundary conditions in the y -direction are cyclic which means that the effects of multiple parallel located hummocks on flow are simulated; the spacing between adjacent hummock edges is 7 m. To facilitate interpretation the model bathymetry is kept as simple as possible. The hummock top is assumed to be rectangular and flat and its size in the *default* run is 8×2 m. To ensure a good transition from flat to hummock the 2 meter thick edge has a convex to concave profile. The hummock is covered with mussels in a rectangular area which extends 0.5 m from the edges of the top of the hummock, thus in the *default* run 9×3 m is covered with mussels (red rectangle in Figure 3.2c). The front edge of the hummock top is located 40 meters from the upstream boundary in the middle of the grid. For the 3D model runs, which all have an input velocity of 0.2 ms^{-1} , 12 minute simulations were performed of which the final 8 minutes were used to derive averages. For the 2DH model simulations, which were performed with varying velocities here, the final 8 minutes of 16 minute simulations were used to obtain averages. Flow velocities, throughout the domain were initialized at the input velocities to decrease adaptation time.

3.2.3 Advection-diffusion model with explicit food uptake

To determine how hummocks affect the algae concentration in the water, an advection-diffusion model with explicit uptake is designed to interpret the transport and uptake

of algae over the mussel hummock. The model is based on the 1D models for plankton transport and filtration developed by Fr  chette et al. (1989) and Simpson et al. (2007) of which the latter formulation was implemented. The advection-diffusion model is extended to 3 dimensions and a horizontal eddy viscosity is added. Mussels have direct access to algae in the bbl (Wildish and Kristmanson, 1984), which they acquire by filtering the water in this layer. Over a given period of time the uptake of water is constant and the amount of algae extracted depends on the concentration in the near bed boundary layer. Algae concentration in the bottom boundary layer can be renewed by lateral advective transport and vertical diffusion. It is assumed that algae have no sinking velocity and that there is no algae growth. This leads to the following formulation for algae concentration in time:

$$\frac{\partial C}{\partial t} = -\vec{u} \cdot \vec{\nabla} C + \frac{\partial}{\partial x} \left(K_h \frac{\partial C}{\partial x} \right) + \frac{\partial}{\partial y} \left(K_h \frac{\partial C}{\partial y} \right) + \frac{\partial}{\partial z} \left(K_v \frac{\partial C}{\partial z} \right), \quad (3.1)$$

in which C is the algal concentration, \vec{u} is the average velocity vector. Horizontal mixing parameter $K_h = 0.002 \text{ m}^2 \text{ s}^{-1}$, based on smagorinsky, is constant in space while the vertical Eddy diffusivity K_v is obtained from the output of SWASH. As both average velocity and Eddy diffusivity are constant in time a steady state solution $\frac{\partial C}{\partial t} = 0$ is sought in which the outcome is controlled by the boundary conditions. Boundary conditions are given by a vertically well mixed algae concentration $C(x = 0, y, z) = C_0$ at the upstream boundary. On the downstream boundary at $x = L$ no spatial gradient in concentration is assumed i.e., $\frac{\partial C}{\partial x} = 0$. Boundary conditions near the surface and bottom are given by no flux at the surface and a flux near the bed caused by mussel filtration:

$$K_v \frac{\partial C}{\partial z} = 0, \quad (3.2)$$

$$K_v \frac{\partial C}{\partial z} = FC_b, \quad (3.3)$$

Here, F is the filtration rate (ms^{-1}) of mussels and $C_b(C(z = z_0))$ is the algal concentration in the near bed boundary layer.

Input for the advection-diffusion model with explicit food uptake was obtained from output data of the SWASH simulations. In total five input grids were retrieved from the SWASH model output; averaged values for the horizontal velocities and vertical mixing were directly outputted by SWASH. Average layer depth and vertical velocities, are not standard output parameters of SWASH. These were outputted at 5 s intervals and averaged over the final 8 minutes. In the horizontal, equations were solved using a second order central differencing scheme for spatial gradients. The application of a sigma layer grid caused variation in the grid size over the vertical. The vertical concentration gradient ($\frac{\partial C}{\partial z}$), is discretized as follows: the concentration was linearly projected on the edge between the grid cells, using a first order Taylor expansion. This leads to the following description of the concentration gradient:

$$\frac{\partial C}{\partial z}_{1,2} = \frac{(C_2 - C_1) \frac{h_2^2}{2} + (C_1 - C_2) \frac{h_1^2}{2}}{\frac{h_1^2}{2} \frac{h_2}{2} + \frac{h_2^2}{2} \frac{h_1}{2}}. \quad (3.4)$$

Here, C_2 and C_1 are the concentrations in two vertically adjoining grid cells with respective heights h_1 and h_2 , C_{12} is the projected concentration at the edge between these grid cells. In the vertical food concentrations from the center of the grid boxes are projected, on the box edges. These are subsequently used to determine vertical gradients in concentration in the box centers. The differential equations are solved numerically until a steady state solution is reached.

3.2.4 Simulations Overview

An overview, of the simulations performed with SWASH is given in Table 3.2. First, a *default* run is defined, in this run the water level is set at 0.6 m above the bed, with a hummock height of 0.4 m. The input velocity at the western boundary is set at 0.2 ms^{-1} , this input velocity is used for all runs except *wlrns*. Background viscosity is set at $10^{-4} \text{ m}^2\text{s}^{-1}$ to obtain stable results.

Second, the importance of flow routing and flow acceleration at different water levels and for different hummock geometries are tested in 2DH mode. The effects of water level (*wlrns*) were tested with input velocities based on those observed at the channel station for these water levels. These velocities are based on the flood part of a typical tidal cycle. SWASH was run at different water levels from low water (0.05 m) to high water (1.6 m) with a step size of 0.05 m. Velocities for water levels below 0.6 m are set at 0.21 ms^{-1} . Similarly, during high water when observed velocities become really small the input velocity is increased to 0.05 ms^{-1} , as low flow velocities require a larger adaptation period. To test the effects of geometry, model runs for varying hummock length (*lrns*), hummock width (*wruns*), and surface roughness (*rrns*) were performed. These runs were carried out at constant water level (0.55 m). For model runs with varying hummock width, the width of the model domain was also increased to maintain channel width.

Third, to model food uptake by the mussel hummock the full 3D capability of the SWASH model is used. This is done for the *fdefault* run (*default* run with food uptake), a run without enhanced surface roughness on top of the hummock (*fsmooth*) and a run without surface elevation (*fflat*). Also, a simulation with an enhanced surface roughness of 0.09 m (*frough*) is performed. Other model parameters are the upstream algae concentration which is set at 0.002 g l^{-1} based on the value in Simpson et al. (2007). However, since uptake depends linearly on near bed concentration, all results are scalable with respect to the input concentration. Also, the filtration rate for the default run is set to $2 \times 10^{-3} \text{ m s}^{-1}$ which represents a mussel concentration of 3750 individuals per square meter (Simpson et al., 2007). To test the effects of the filtration rate on the difference between an elevated hummock and the flat patch a sensitivity analysis is performed. For this sensitivity analysis model runs *fdefault* and *fflat* were run for different filtration rates, these runs are named *fuptake* and *fuptakeflat* respectively.

Finally, the effect of three different geometries on food availability is tested: (1) a large flat mussel covered area (*fflatbig*) which is 2 times as big as the mussel covered area in *fflat*. The filtration rate is adapted such that the total amount of water filtered per second, and thus the amount of mussels, is similar to that of the *default* run. (2) An elevated band (*fband*) where the hummock of the default run is extended in width to cover the

whole width of modeled area. (3) A checkerboard pattern (*fchecker*), where an additional hummock is added (same size as used in the *default* run), 4 meters behind the hummock in and in the center of the channel.

3.3 Results: field observations

In this section field measurements around a mussel hummock are used to study the effects of an hummock on flow and turbulence. First, a short overview of the tidal flow velocities and wave conditions during the measurement period are given. Secondly, velocity observations are used to study the effect of an hummock on flow patterns. Thirdly, turbulence characteristics are analyzed to determine the effect of a hummock on vertical mixing.

Tides and Waves

Conditions during the measurement period are studied using data from the channel station. Observed current velocities and water levels at this station are shown in Figure 3.3a. Current velocities reached up to 0.47 ms^{-1} during flood and 0.30 ms^{-1} during ebb tide. Velocities peak when the hummock is covered with a small layer of water. High water levels varied between 0.8 m and 1.5 m above mean sea level. Waves (data not shown here) at the site were small with wave heights peaking at 0.12 m. Highest waves occurred at days with high wind speeds. Measured wave height time series show sharp peaks around maximum water level, indicating limitation of wave height by water depth and/or fetch. Waves at the field site are relatively short with maximum wave periods of 3 s. This confirms that waves are only small and of secondary importance in this area.

Flow behavior

The analysis of flow patterns focuses on two processes which occur when the flow area becomes limited: (1) flow acceleration, flow being forced over the hummock and (2) flow routing, flow being forced to flow around the hummock. Average ebb and flood directions are indicated in Figure 3.2. During flood, flow has passed over the hummock for 1.5 m before it reaches the sensor. During ebb, flow has passed the covered area 0.5 m before it reaches the sensor.

First, flow behavior during a representative tidal cycle (on April 14) is analyzed. In Figure 3.3b the measured absolute velocities at the lower hummock sensor (lhs), the upper hummock sensor (uhs) and the channel sensor (cs) are shown together with the water level measured at the channel station. As the lower hummock sensor is approximately at the same absolute vertical position as the channel sensor my analysis focuses on a comparison between these two sensors. Note, that the lower hummock sensor is closer (0.15 m) to the bed than the channel sensor (0.28 m). During most periods when both sensors are submerged, except during high water flood, velocities at the lower hummock sensor are larger than those observed at the channel sensor. Velocity differences increase with decreasing water level. During the largest part of the tidal cycle flow is thus accelerated at the lower hummock sensor. Notice, that when the lower hummock sensor emerges there

Run	Water level	Nikuradse roughness	2DH/3D	Specifics
<i>default</i>	0.6 m	0.05 m	3D	none
Geometry runs				
<i>wlrns</i>	[0.05-1.6 m]	0.05 m	2DH	Various water levels from 0.05 to 1.6 m with step size of 0.05 m
<i>lrns</i>	0.55 m	0.05 m	2DH	Hummock lengths: 1, 2, 4, 8, 12, 16, 30, 40 m
<i>wruns</i>	0.55 m	0.05 m	2DH	Hummock widths: 1, 2, 4, 6, 8 m Domain width is increased to keep channel width constant
<i>rrns</i>	0.55 m	varies	2DH	Hummock Nikuradse roughness 0.02, 0.04, 0.05, 0.06, 0.08, 0.10, 0.12 m
Food runs				
<i>fdefault</i>	0.6 m	0.05 m	3D	uptake results of food model for <i>default</i>
<i>fsmooth</i>	0.6 m	0.02 m	3D	No increased surface roughness
<i>fflat</i>	0.6 m	0.05 m	3D	No elevation
<i>frough</i>	0.6 m	0.10 m	3D	Increased surface roughness
<i>fuptake</i>	0.6 m	0.05 m	3D	<i>fdefault</i> run with different filtration rates: 0.1, 0.2, 0.5, 1.0, 2.0, 4.0 and $8.0 \times 10^{-3} \text{ m s}^{-1}$
<i>fflatuptake</i>	0.6 m	0.05 m	3D	<i>fflat</i> run with different filtration rates: 0.1, 0.2, 0.5, 1.0, 2.0, 4.0 and $8.0 \times 10^{-3} \text{ m s}^{-1}$
Food and geometry runs				
<i>fflatbig</i>	0.6 m	0.05 m	3D	Larger flat area with lower mussel concentration
<i>fband</i>	0.6 m	0.05 m	3D	Hummock extends over entire domain width
<i>fchecker</i>	0.6 m	0.05 m	3D	Additional hummock 5m behind hummock in center of channel

Table 3.2 Overview of model simulations, with their specifics. Water levels, surface roughness, and the use of vertical layers are indicated.

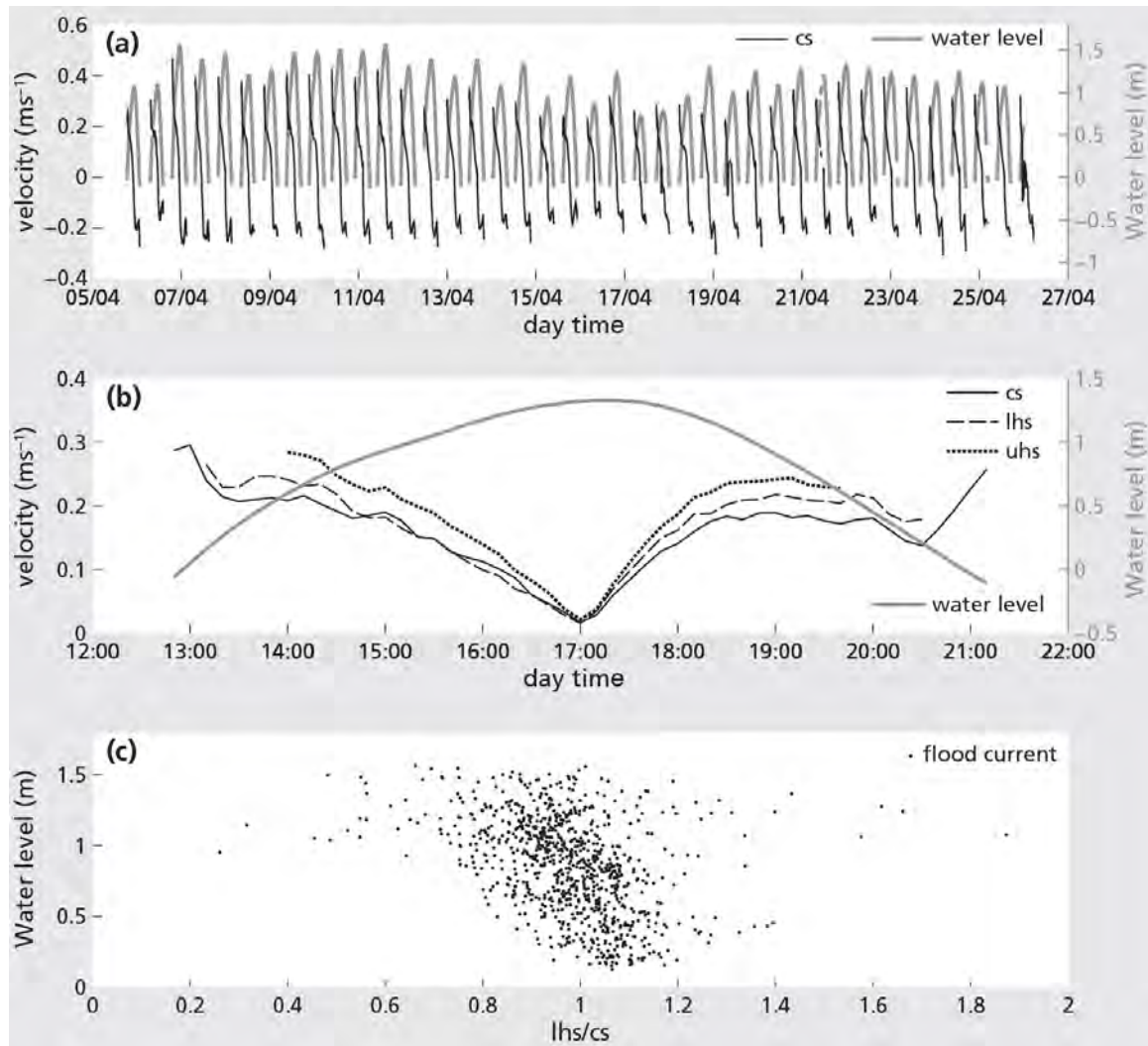


Figure 3.3 Observations of the effects of hummock presence on flow. Panel a. shows a time series of the measured total velocity measured at cs. Flood flows are positive and ebb flows are negative. Panel b. shows measured flow velocities for all sensors together with the water depth measured at cs 3 on April 14 2012. When submerged lhs and uhs are nearly always larger than cs except during high water flood. Panel c. shows how the ratio of flow at lhs and cs is influenced by the water depth during flood.

is a strong increase in flow velocities recorded by the channel sensor. This could indicate that flow routing becomes important at very low water levels.

Second, the dependence of the observed flow acceleration on water levels during ebb and flood are studied in more detail. This is done by analyzing the ratio between flow velocities measured at the lower hummock sensor(lhs) and the channel sensor(cs) over the whole measurement period. In Figure 3.3c these ratios are shown as a function of water level for flood conditions. Results indicate that during flood, flow acceleration depends on water level and the ratio increases from 0.92 ± 0.19 at high water levels ($h > 1$ m) to 1.06 ± 0.08 at low water levels ($h < 0.4$ m). Thus a small deceleration during high water

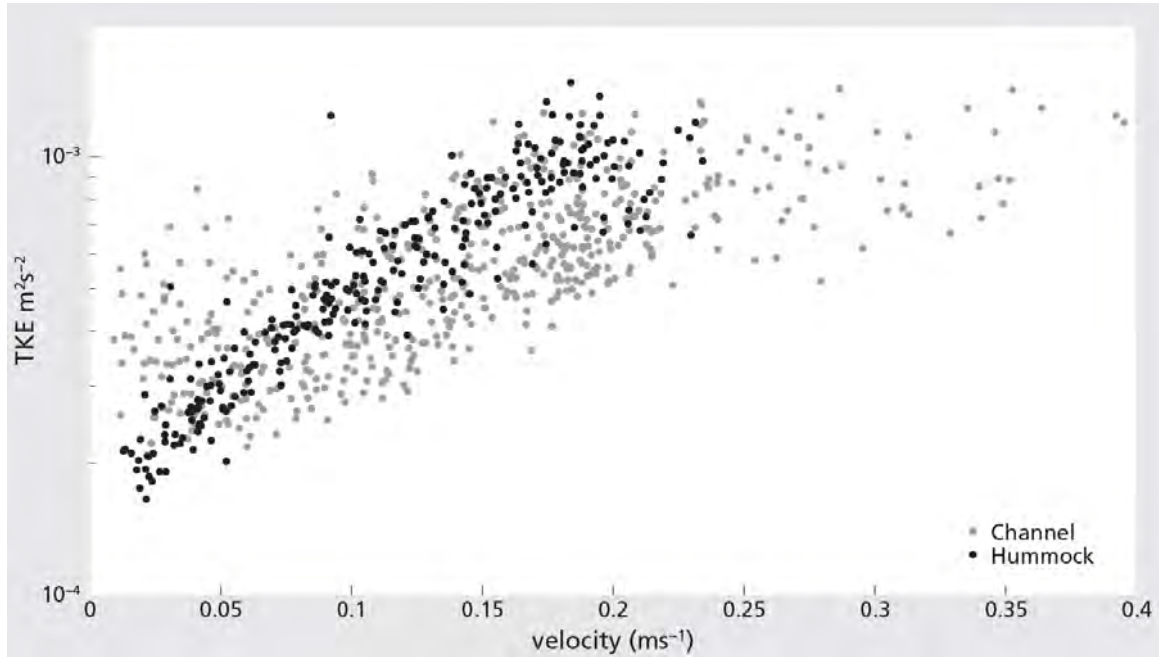


Figure 3.4 Observed TKE in the channel and over the hummock during flood as a function of flow velocity.

and acceleration during low water. It is expected that the ratios are also underestimated as the lower hummock sensor is located closer to the bed. In addition there is increased roughness over the hummock resulting in a thicker bottom boundary layer. This might lead to a reduction of the velocity measurements at the sensor heights. This is confirmed by the large velocity difference between the upper and lower hummock sensor.

Flow acceleration occurs at most water levels, except high water flood and it becomes less apparent with increasing water levels. The only indication of flow routing is based on measured large current velocities in the channel at very low water levels ($<0.15\text{m}$) above the hummock.

Turbulence

Next, the effects of hummocks on turbulent kinetic energy are studied. In Figure 3.4, the TKE is plotted as a function of flow velocity, as mentioned only periods with small orbital velocities are shown. At high flow velocities TKE is larger at the lower hummock sensor than in the channel. Averages of TKE over the hummock range between $5.2 \times 10^{-4} \text{m}^2 \text{s}^{-2}$ at 0.1ms^{-1} and $9.6 \times 10^{-4} \text{m}^2 \text{s}^{-2}$ at 0.25ms^{-1} . While in the channel TKE values for these velocities are $4.5 \times 10^{-4} \text{m}^2 \text{s}^{-2}$ at 0.05ms^{-1} and $7.4 \times 10^{-4} \text{m}^2 \text{s}^{-2}$ at 0.25ms^{-1} . Thus, TKE is increased over the hummock.

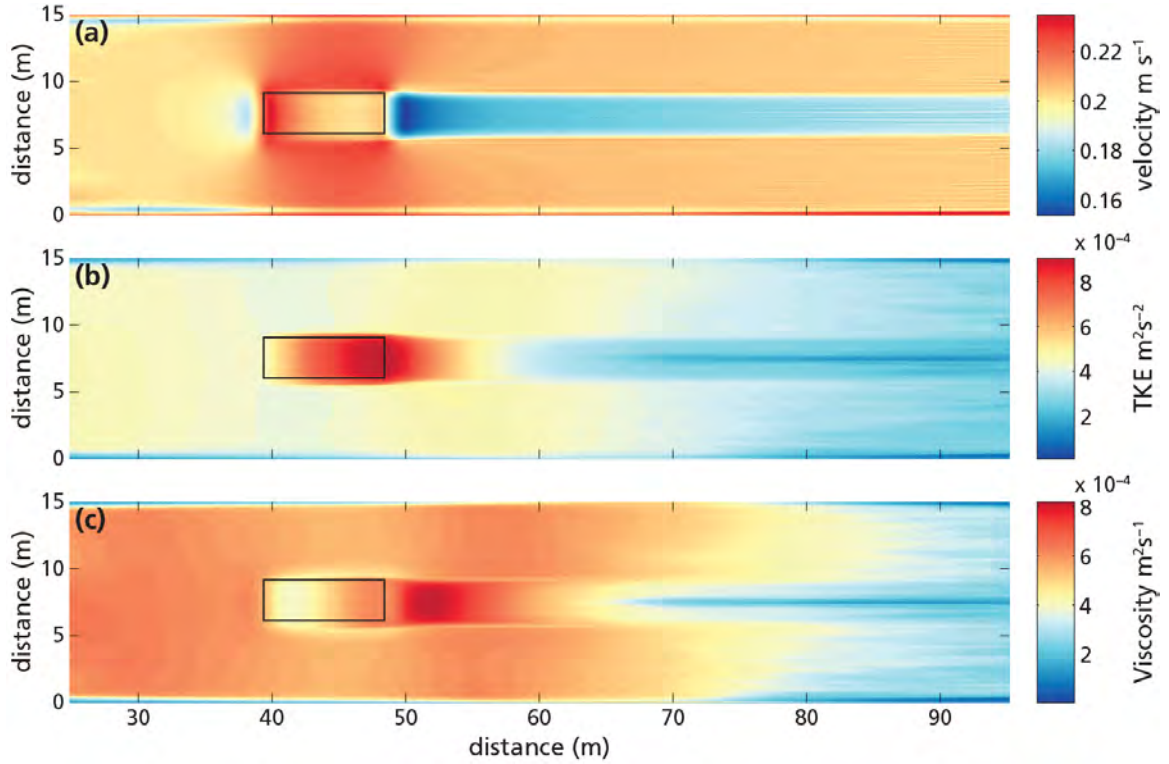


Figure 3.5 Modeled effects of an hummock on the spatial depth averaged distribution of flow and turbulence for the *default* run. Panel a. shows the modeled absolute velocity. Panel b. shows the depth averaged modeled TKE for this run. Panel c. shows the depth averaged viscosity. Rectangles indicate the mussel covered area of the hummock.

3.4 Results: model simulations

Flow behavior, especially the role of flow routing and acceleration, around mussel hummocks is now further investigated using the SWASH model. An overview of the model runs is given in Table 3.2. Firstly, the flow patterns as well as turbulence characteristics of the default model run are discussed and model results are compared with observations. Secondly, a sensitivity analysis of flow routing and acceleration is performed, for different water levels and hummock geometries. Thirdly, the advection-diffusion model with explicit food uptake by the mussel bed is applied to study the effects of the modeled flow patterns and vertical mixing on food uptake by the mussel hummock. In the final section, food uptake for different geometries and mussel coverages are compared.

3.4.1 Influence of hummock on flow behavior

The depth averaged flow velocities for the *default* run are shown in Figure 3.5a. Model results show that at the leading edge of the hummock and in the adjacent channel flow velocities accelerate with respect to the input velocities. Depth averaged velocities in the meter behind the leading edge are 0.23 m s^{-1} on the hummock and 0.22 m s^{-1} in the channel which gives a velocity ratio between hummock and channel of 1.04, similar

to my observations. Increased velocities over the hummock as well as in the channel show that part of the flow is routed around the hummock and part is accelerated over the hummock. In downstream direction, a large part of the flow is routed around the hummock as flow velocities over the hummock reduce, and increase in the channel. At the downstream edge there is an increase again in velocities over the hummock. Both in front as behind the hummock there is a decrease in flow velocity. In front of the hummock this is caused by a stagnation point. Behind the hummock there is a strong wake as a large portion of the flow is routed through the channel. The effects of these flow patterns on turbulent kinetic energy are shown in Figure 3.5b. The figure shows the depth averaged TKE levels. Simulated TKE values over the hummock are close to those observed in the field, average value over the mussel hummock is $(7.6 \pm 1.3) \times 10^{-4} \text{ m}^2 \text{ s}^{-2}$. While values in the channel are slightly lower than observed values with an average value of $(4.6 \pm 1.37) \times 10^{-4} \text{ m}^2 \text{ s}^{-2}$. A strong increase in TKE is simulated on top of the hummock, it starts increasing in front of the hummock and reaches a maximum at the downstream edge. In the channel adjacent to the hummock there is a small increase in turbulence levels as flow velocities increase. In the wake of the hummock simulated depth averaged TKE reduces rapidly again. The increased TKE levels are reflected in the depth-averaged vertical viscosity shown in Figure 3.5c. Results reveal that depth averaged viscosity peaks at the downstream side of the hummock, but also high levels in vertical viscosity are found in the wake of the hummock. Routing of flow along the hummock reduces horizontal transport over the hummock, while the turbulent kinetic energy and thus vertical turbulent mixing is enhanced.

3.4.2 Effects of water levels and geometry on flow patterns

Observations showed that the ratio between flow acceleration and routing is influenced by water levels as well as hummock geometry. The effects of water level are investigated using simulations at different water levels, based on observed velocities. Furthermore, effects of geometry are studied using simulations for different hummock length (*lruns*), width (*wruns*) and surface roughness (*rruns*).

The model runs for different water levels (*wlrns*) are compared with observations. Results are compared for the flood period only at a location 1 meter from the leading edge. The comparison, shown in Figure 3.6a, reveals that the modeled velocity ratio estimates on top of the hummock are higher than the average observed ratio but within the range of the observations. Note, that observed values are a comparison of point measurements while modeled depth averaged values are compared. Based on the lower sensor height and thicker bottom boundary layer over the hummock, observed values likely underestimate the velocity difference.

The flow velocities at different water levels and for different locations (see Figure 3.2c) on and around the hummock are shown in Figure 3.6b and c. Results for locations along the flow direction over the hummock (Figure 3.6b) reveal that there is a stagnation point upstream (location: Front) and a wake downstream (location: Wake), with lower velocities. Downstream the velocity decrease is stronger and reveals negative velocities when the hummock is emerged. On top of the hummock velocities are always the largest on the

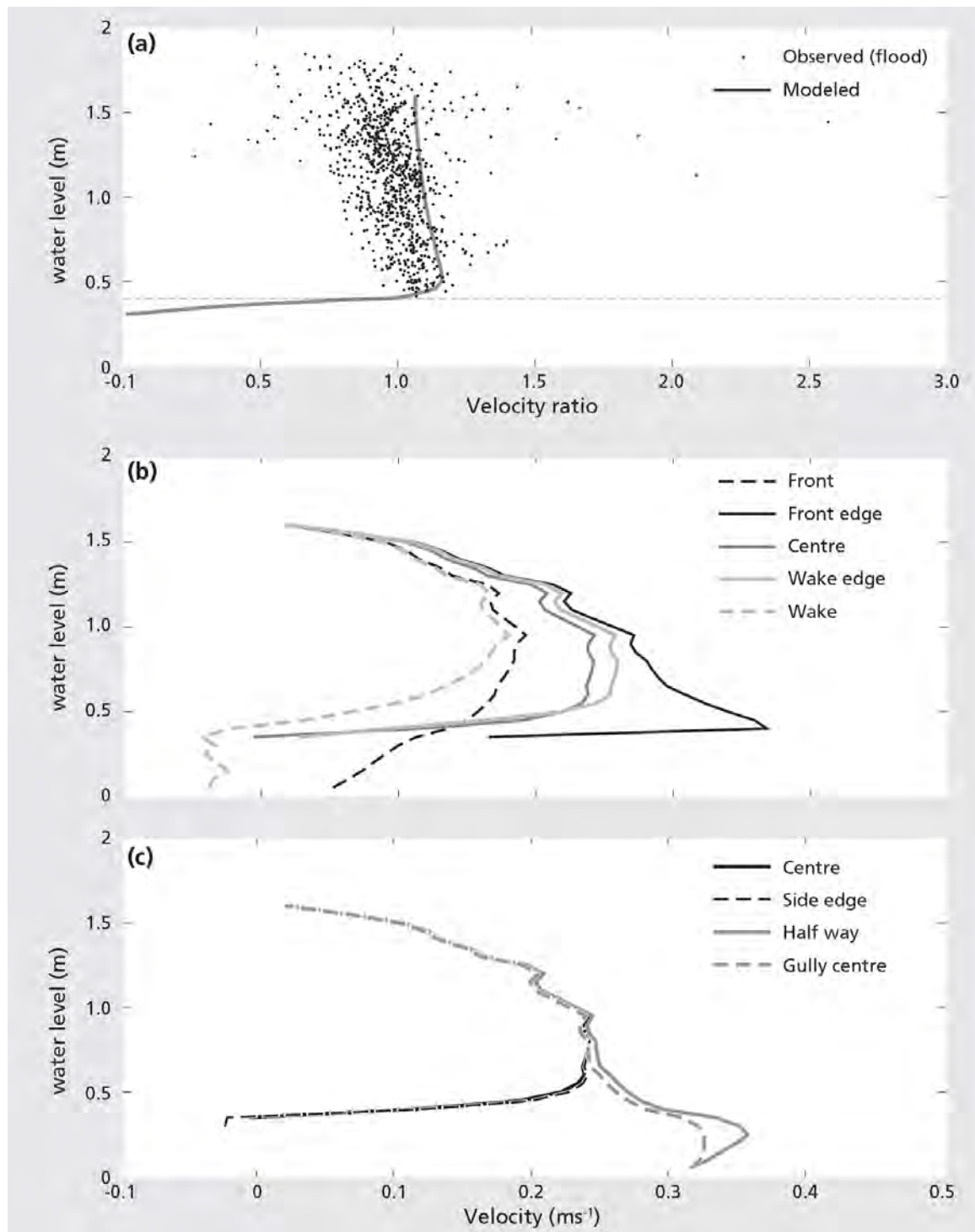


Figure 3.6 Modeled effects of hummock on flow velocities at different water levels. Panel a. shows a comparison between the modeled and observed velocity ratios for flood, at a location similar to the observation location for different water levels. The dashed line indicates the height of the hummock. Panel b. shows the effects of modeled velocities for locations a,b,c,d, and e in Figure 3.2. Panel c. same as b. but than for locations c, f,g and h.

upstream side (location: Front edge) of the hummock, they peak at 0.36 ms^{-1} when the hummock becomes covered by water which is 180% of the input velocity. The lowest velocities are observed in the center. In a line perpendicular to the hummock (Figure 3.6c) the largest velocities are modeled in the channel while the hummock top is still dry. At intermediate water levels the velocity at the edge of the bed peaks, at higher water levels the velocity at the center of the hummock becomes the largest.

As hummock geometry changes, the relation between the amount of flow that is accelerated over the hummock versus the amount routed around the hummock is expected to vary. The effects are analyzed by comparing depth averaged velocities on top of the hummock with average values in the channel. As depicted by Figure 3.7a, increasing the hummock length leads to an increase in velocities in the channel while velocities on top of the hummock are reduced. Thus more flow is routed around the hummock as hummock length is increased. However, as length increases the relative increase in the amount of flow that is routed decreases. For larger hummock lengths the velocity over the hummock becomes smaller than the input velocity at the upstream boundary.

For increasing hummock width (results shown in Figure 3.7b) both hummock as well as channel velocities increase. A logic response since a wider hummock blocks a larger part of the flow area. Apart from the velocity increase also the ratio between flow accelerated over the hummock and flow routed around the hummock increases with increasing hummock width. Consequently, a larger part of the flow is accelerated over the hummock. A wider hummock thus leads to an increase in advective transport towards the hummock per unit area.

Nikuradse roughness is not only a key parameter which influences advection of flow but also strongly influences vertical mixing. Results presented in Figure 3.7c show that by increasing the surface roughness more flow becomes routed around the mussel hummock. For a large Nikuradse roughness ($>0.07 \text{ m}$) the average velocity over the hummock is reduced with respect to the input velocity. Meanwhile, the vertical exchange is strongly enhanced for higher values of the Nikuradse roughness as is revealed by the depth averaged vertical viscosity (K_v) illustrated in Figure 3.7d. However, a larger increase in Nikuradse roughness length from 0.05 m to 0.09 m results in a decrease in average viscosity on top of the hummock. This is investigated further when food uptake is studied.

3.4.3 Influence of hummock on food uptake

The effects of hummock presence on food uptake are investigated using the advection-diffusion model with explicit food uptake presented in Section 3.2.3. In Figure 3.8a the spatial distribution of food uptake is shown. Average uptake is $2.66 \times 10^{-6} \text{ gm}^{-2}\text{s}^{-1}$, and varies strongly over the hummock. Largest uptake ($3.81 \times 10^{-6} \text{ gm}^{-2}\text{s}^{-1}$) is simulated near the leading edge and reduces in downstream direction to $2.23 \times 10^{-6} \text{ gm}^{-2}\text{s}^{-1}$. To test the effects of the elevation of the hummock on uptake, results of *fdefault* are compared to those of *fflat*. On average uptake over the elevated hummock is increased by 3%. In Figure 3.8b the spatial distribution of uptake differences with respect to run *fflat* are shown. The uptake of the *fdefault* run is 2% lower compared *fflat* near the leading edge.

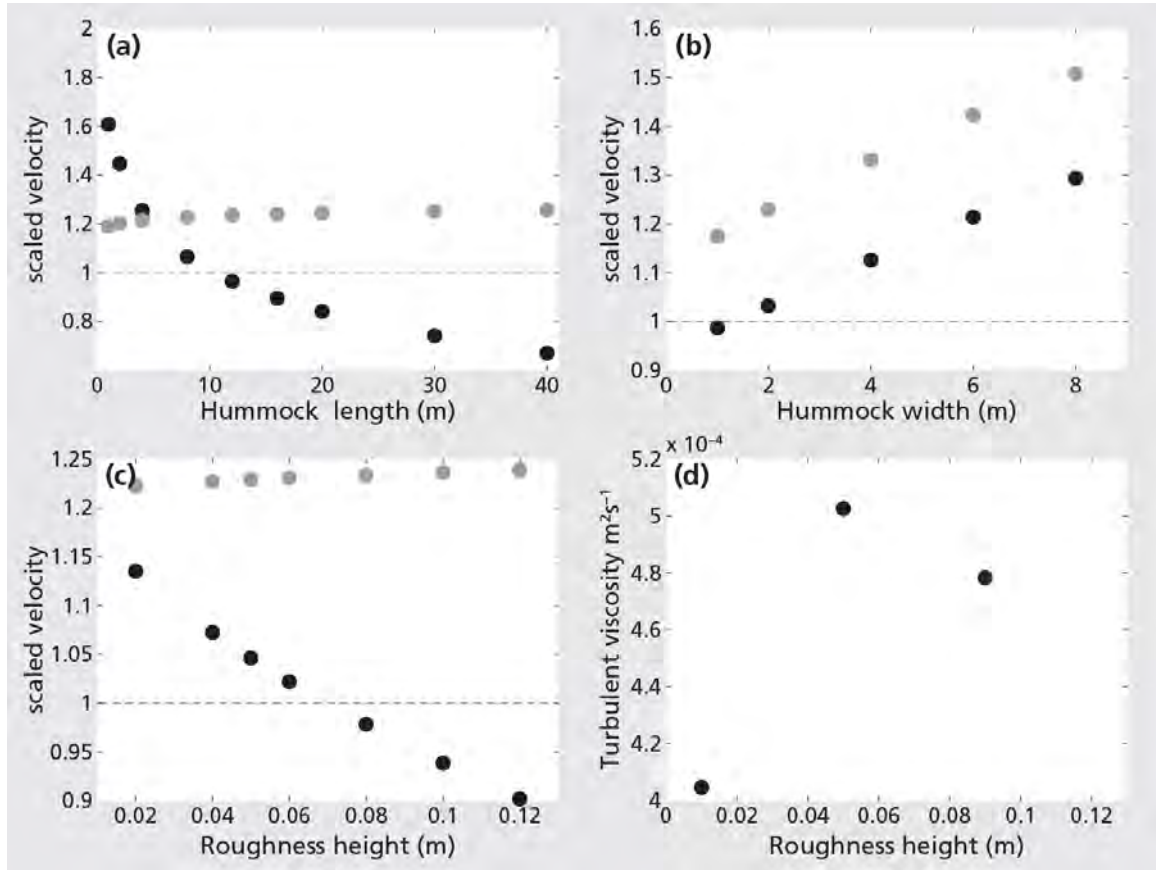


Figure 3.7 Sensitivity analysis of hummock geometry on flow routing and acceleration. In panels a, b, and c the velocity over the hummock (in black) and in the gully (in gray) are presented as a function of hummock length, width and Nikuradse roughness, respectively. The velocity is scaled with the velocity at the upstream boundary. In panel d, a sensitivity analysis for the Nikuradse roughness on turbulent viscosity is shown based on results of 3D model runs *fsmooth*, *fdefault* and *frough*.

However, further downstream the uptake difference becomes positive with an increase up to 5%.

The bottom two figures (Figure 3.8c and Figure 3.8d) highlight the large influence of roughness on food uptake. Figure 3.8c compares the uptake at intermediate Nikuradse roughness (0.05 m) from *fdefault* with that of a model run with no increased Nikuradse roughness (0.02 m) (*fsmooth*). Results show that for larger Nikuradse roughness increases the food uptake on average about 5%. Increases are the largest on the downstream side of the hummock. However, increased Nikuradse roughness can also enhance flow routing and thus reduce advective transport. This is the case for the high Nikuradse roughness (0.10 m) run *frough*. When uptake is compared to *fsmooth*, a strong decrease in uptake is found in the center of the downstream half of the mussel hummock. On average the uptake is 2% lower than for the smooth run. Thus in total 7% lower to the run with intermediate roughness.

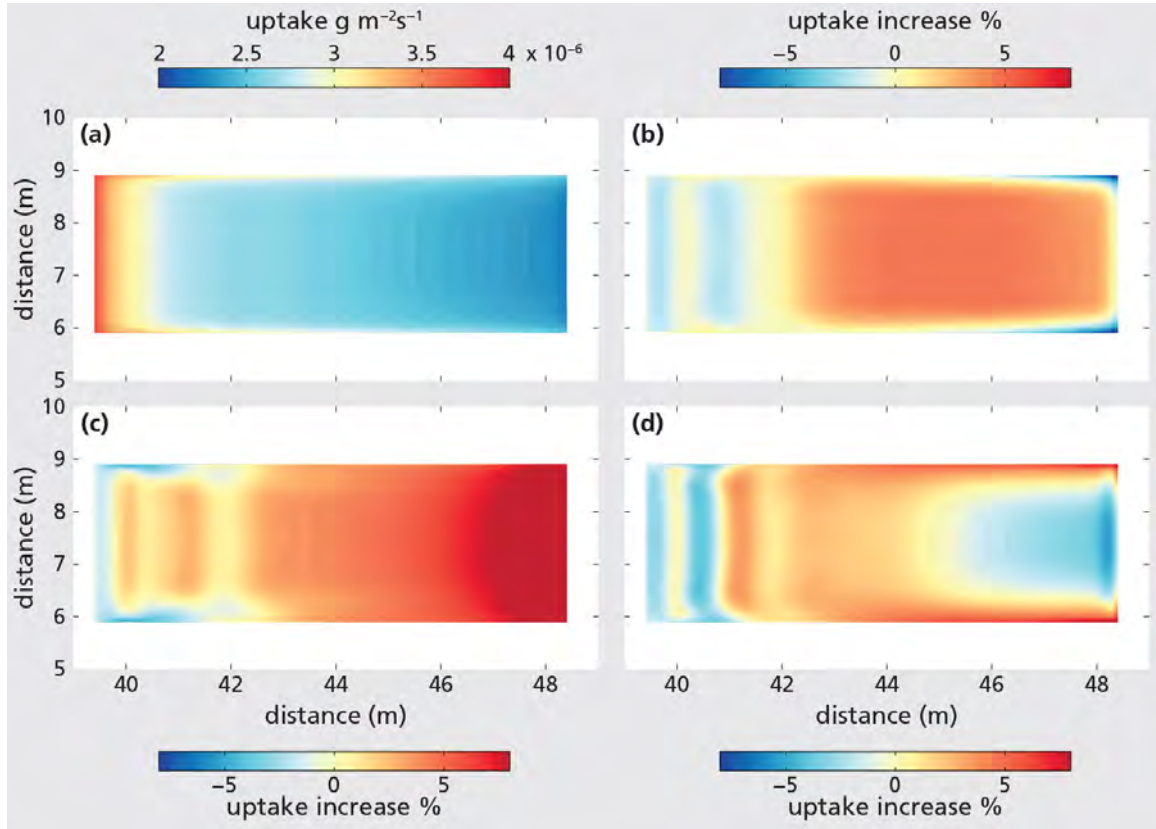


Figure 3.8 Model results using the food uptake model. Panel (a) shows the uptake modeled for the *fdefault* run. Panel (b) shows the relative increase of run *fdefault* with respect to *fflat*. Panel (c), shows the relative increase for *fdefault* to the model run without enhanced surface roughness *fsmooth*. Panel (d), shows the same but than for the *frough* run with increased hummock roughness compared to *fsmooth*.

Results also demonstrate that the filtration rate influences the uptake (Figure 3.9). Here model runs with elevation (*fuptake*) are compared with runs without elevation (*fflatuptake*). The simulations show that an increase in mussel filtration rate, leads to an increased difference in uptake for the elevated hummock from 1% at 0.0002 m s^{-1} to 4.5% at 0.008 m s^{-1} . As the uptake increases, the bottom boundary layer depletes faster and thus depends more on transport by vertical mixing. The benefits of increased vertical mixing are thus more important for higher uptake ratios.

3.4.4 Effect of hummock geometry on uptake

In the previous section results demonstrated that hummock formation influences food uptake and in this section results are compared for 3 different configurations of mussel distributions commonly found in field situations. These configurations or spatial patterns are: (1) mussels spread out uniformly over a larger area; (2) checkerboard pattern; (3) a banded pattern.

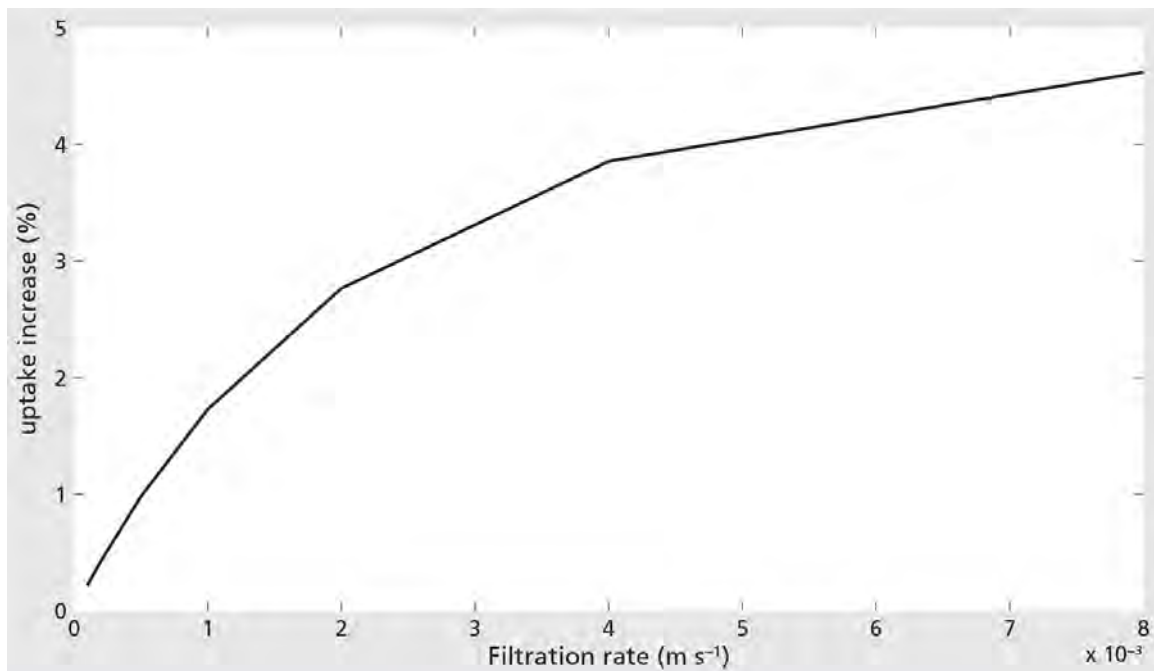


Figure 3.9 Percentage of uptake increase by the hummock (*fdefault*) with respect to a flat patch (*fflat*) at different filtration rates.

First, it is studied whether a high density hummock is more beneficial than mussels spread out over a larger area with no elevation. Therefore, uptake by the elevated hummock *fdefault* is compared to the uptake in simulation *fflatbig*. The prescribed filtration rate is halved, the area with mussels is doubled such that the amount of simulated mussels remains constant between this run and *fdefault*. Modeled uptake for model run *fflatbig* is shown in Figure 3.10a. Results show a small decrease in uptake from upstream to downstream over the flat patch, this decrease is much smaller than for *fdefault*. The lower filtration rate allows for more time for the flow to replenish the bottom boundary layer and this causes the total uptake to be 25% larger over the large flat area than over the hummock. Thus by reducing mussel density the same amount of mussels, spread out over a larger flat area, take up more food.

Next, using simulation *fchecker* the uptake of two hummocks in checkerboard configuration is investigated. This pattern is also observed around the observation site (Figure 3.2b). The uptake modeled for this hummock configuration is shown in Figure 3.10b. A comparison between uptake of both hummocks reveals that uptake over the second hummock is 3.6% larger than over the first hummock. While uptake over the first hummock does not differ significantly from *fdefault*. By routing of flow around the first hummock, advective transport towards the second hummock is increased leading to a small increase in uptake. The relative position of hummocks to each other may be beneficial for hummocks in the downstream direction due to modification of the advective transport.

Finally, uptake by the mussel band from model run *fband* is investigated. The modeled distribution of uptake is shown in Figure 3.10c. Simulated uptake is constant perpen-

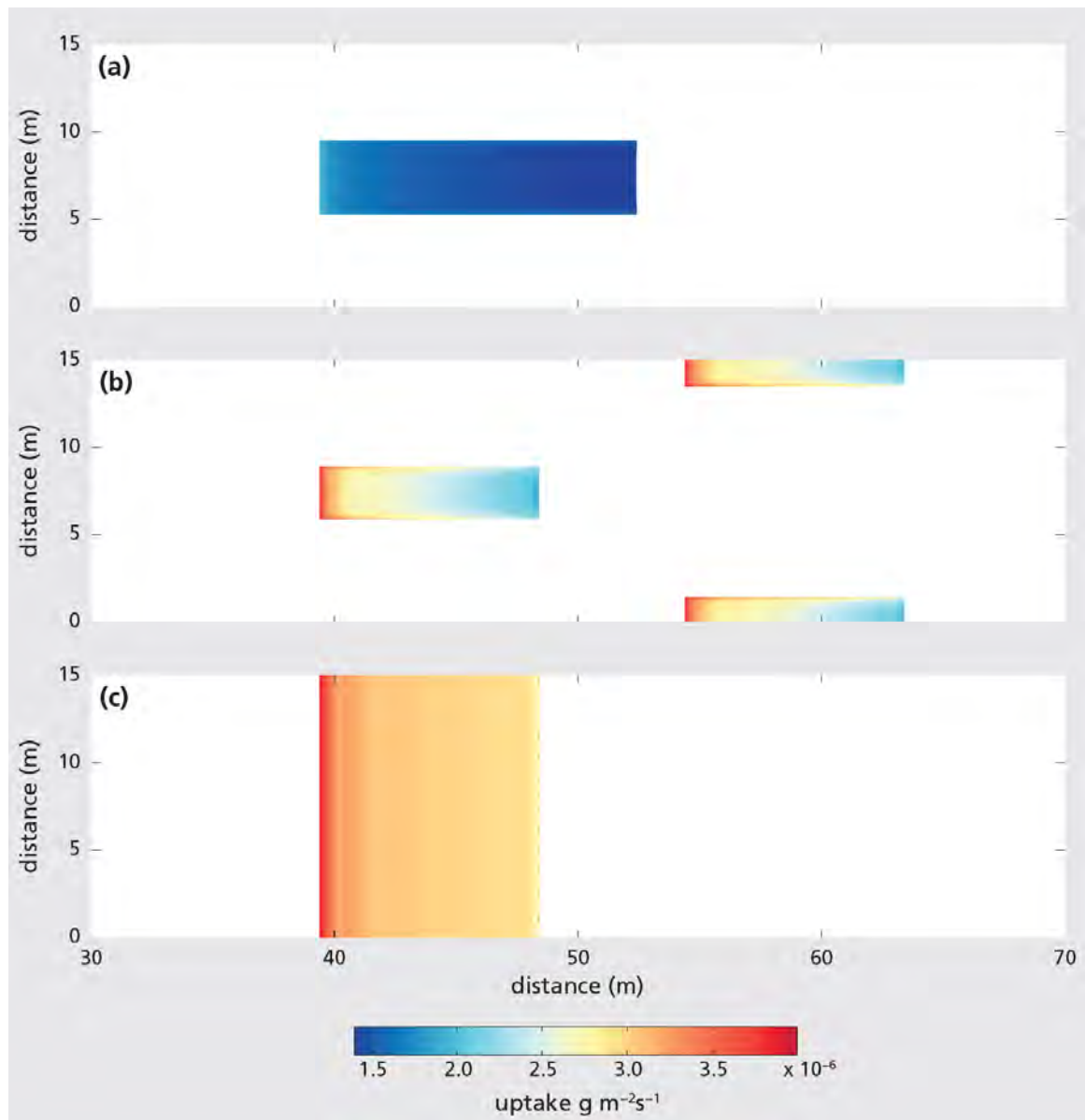


Figure 3.10 Food uptake by different mussel bed types. Panel a. shows uptake by a larger (100%) flat mussel bed with lower mussel density (50%). Panel b. shows uptake of two mussel hummocks in checker board configuration. Panel c. shows uptake by an elevated mussel band.

dicular to the flow direction over the band and reduces slowly in downstream direction. To study the effects of flow routing on uptake in the mussel covered area of the *fdefault* run is compared with uptake of *fband*. Only the part of the band that is also covered with mussel in run *fdefault* is used for this comparison. Over the band the uptake is 15% higher. This shows that routing of flow leads to a reduction in food uptake.

3.5 Discussion

In this study, the effects of hummock elevation and geometry on flow patterns and food uptake by mussels were investigated. Hummocks limit the flow area, resulting in acceleration of flow over the hummock as well as routing of flow around the hummock. Flow routing reduces the advection of food over the hummock, while flow acceleration enhances vertical mixing, increasing vertical transport of food towards the bed. My study revealed that the relative importance of these processes depends strongly on hummock geometry in relation to water level.

These results were obtained from field measurements and a model study. The field measurements indicated the presence of flow acceleration and flow routing, especially during flood. However, due to flow over a complex bathymetry during ebb and the problems to measure flow in limited water depths (several decimeters), no direct evidence of flow routing and acceleration during a tidal cycle could be deciphered from the data. Therefore also a model was set-up to simulate the effects of mussel hummocks on flow patterns. The model study confirmed the occurrence of flow routing and acceleration and showed good correspondence with the field data, despite the fact that effects of feeding activity by mussels (Van Duren et al., 2006) and waves (Grant and Madsen, 1979) were not considered in the model. Adding these processes would make the calculations more complex to interpret, and time consuming. Both waves and the effect of filter feeding are expected to increase the roughness the flow experiences on top of the hummock, and the effects are therefore captured by the sensitivity analysis of variations in Nikuradse roughness. A last aspect that can be discussed is that a constant uptake ratio is assumed. Some studies (Wildish and Miyares, 1990) suggest an adaptation of filter feeding activity to the flow velocity but more recent studies (Widdows et al., 2002; Nielsen and Vismann, 2014) show that in aggregations mussel feeding is independent of flow velocity.

Hummocks also occur in other intertidal structures, such as sea grasses (Nepf, 1999; Bouma et al., 2007), salt marshes (Temmerman et al., 2005) and algae mats (Escartin and Aubrey, 1995; Weerman et al., 2010) but also in subtidal corals (Hench and Rosman, 2013). These benthic structures all have in common that they influence the through flow area and have a different roughness than their surroundings. My simulations with SWASH show that length and height of the hummock will determine whether flow will go around the hummock or whether it will accelerate over it. The difference between mussel hummocks and other benthic structures is either caused by the flexibility (e.g., bending sea grasses) or the permeability (flow can go through vegetation, but not so easily through mussels) of the benthic structure.

Flow acceleration and routing influence food availability by advective and mixing processes. First, advection of food towards the hummock is dependent on flow routing (reduced transport of food to hummock) and flow acceleration (enhanced availability of food). Second, flow acceleration also increases vertical mixing, enhancing replenishment of food in the bbl as it becomes depleted. The importance of vertical mixing on food uptake in an intertidal mussel bed was mentioned by Simpson et al. (2007) and Saurel et al. (2013). The results demonstrate that also on a patch scale vertical mixing and its enhancement by geometry and roughness play a key role. Increased mixing can

compensate for the loss in advective transport. The benefits of hummock formation vary over the hummock, as the effects of reduced advection become more apparent towards the downstream edge of the hummock. Especially in the center of the downstream part of the hummock food availability is lowest, which is also reflected by mussel health conditions observed by Okamura (1986).

The model experiments show that both flow routing and acceleration are influenced by hummock geometry. Longer and rougher hummocks increase flow routing around the hummock. However, increased roughness also leads to an increase in vertical mixing which can compensate for the increased effect of flow routing. This also means that coverage of hummock by algae (Albrecht and Reise, 1994) or oysters (Reise, 1998), which make the hummock more rough, can substantially influence food uptake. A wider hummock increases food uptake, as it causes a smaller portion of the flow to be routed around the hummock. That flow routing has a large effect on food availability is highlighted by the increased uptake over the band and increased uptake by the second hummock in case of a checker board configuration.

This study suggests that aggregation is not beneficial for food uptake; mussels that are more spread out have an increased uptake. However, by making dense patterns, resistance against erosion is increased (van de Koppel et al., 2005). Results did show that higher uptake rates increase the benefits of hummock elevation. The formation of elevated banded structures thus appears to be the most beneficial for survival. This confirms previously performed model studies (van de Koppel et al., 2005; Liu et al., 2012, 2014a) which show that without perturbations self-organization leads to the formation of banded patterns in mussel beds. My results also show that such studies into pattern formation could be improved since these studies assume constant velocity and mixing. This study shows that the formed patterns influence flow patterns substantially, a feedback of flow velocity and the degree of mixing to mussel pattern formation can be expected. Bands formed in mussel beds often break up as the result of cumulative perturbations (Denny, 1987), for instance by storms, leading to patchy/hummock type mussel beds. The presented results show that such perturbations can drastically limit food availability as flow will be routed through the eroded area. These processes will progressively weaken the physical condition of mussels on the remaining hummocks, further exposing the bed to cumulative erosion.

Wave exposure, which is responsible for erosion in mussel beds, is also an important factor. As elevation increases wave forcing on the bed will increase making a mussel bed more prone to erosion. It is therefore that beds which are wave-exposed under calm conditions, such as the one studied in Chapter 2, develop a less pronounced relief. In more exposed beds wave energy focusing causes enhanced erosion of hummocks and thereby partly eliminates the relief. It might be that mussel bed areas which are less exposed to wave forcing develop a stronger relief than those at wave-exposed locations. However, under storm conditions these beds might be more prone to enhanced erosion and break up of mussel bed structure.

3.6 Summary and conclusions

The main objective of this research was to assess the effects of hummock formation on flow patterns and food availability. Two types of flow impact were observed in the field: acceleration of flow over the hummock and routing of flow around the hummock. Their relative contributions depend on water level/water depth. These processes were modeled with SWASH, of which the results were subsequently coupled to an advection-diffusion type model that describes the uptake of food by mussels. Both hydrodynamic processes have opposite effects on food availability for the hummock. The routing of flow reduces horizontal advection of food towards the bed, while flow acceleration enhances vertical mixing and increases food availability towards the bed. Model results show that food uptake is more effective on wide elevated mussel hummocks. Therefore banded patterns are most beneficial as these patterns limit flow routing. As food supplies are large this enables mussels to grow faster, and become more resistant against erosion. These findings suggest that the survival chances of mussel beds reduce as mussel cover becomes more scattered.

4 Implications of an ice action event for the long-term persistence of an intertidal mussel bed

This chapter is based on:

DONKER, J. J. A., VAN DER VEGT, M., HOEKSTRA, P. (2014), Implications of an ice action event for the long-term persistence of an intertidal mussel bed. Submitted to: Continental Shelf Research

Abstract

The persistence of intertidal mussel beds is governed by both biotic and abiotic processes. In many studies, waves and currents have been identified as the most important forcing agents, but it is demonstrated that in temperate regions ice action can be important as well. These findings result from a 27 month monitoring campaign on a mature intertidal mussel bed in the Dutch Wadden Sea. Daily camera observations revealed two periods in which substantial erosion was caused. The first event occurred in a period during which the bed was covered by ice. Ice action resulted in an initial drop of 19% in mussel covered area around the monitoring station. The losses were concentrated in three gaps of which the biggest two were located close to the beds edge. Around these gaps up to 0.3 m high ridges of piled up mussels had formed, the highest ridges were located westward of these erosion holes. The combined existence of eroded gaps and stripes and the development of mussel ridges support the view that the mechanism by which the bed was damaged was, at least partly, physical disturbance by scouring ice. Recovery was limited in the 19 months following the period during which the mussel bed was damaged. Due to sedimentation and reorganization of the mussels, initial relief was reduced again and mussels spread out over a larger area. Nevertheless, a further reduction in mussel cover was observed due to wave action during a storm period. Especially areas which became elevated as a result of ice action suffered large losses. In conclusion, while the results only concern a single observation, they suggest a twofold impact of ice action on mussel bed cover: firstly by directly eroding mussels from mussel beds; secondly by indirectly increasing the exposure of mussel beds to hydrodynamic forces. The latter suggests a synergistic relation between erosion by ice action and wave forcing.

4.1 Introduction

Intertidal mussels are considered as a key species in the ecosystem of the Dutch Wadden Sea. Therefore several programs exist to protect and increase the area covered by intertidal mussel beds in the Wadden Sea. Most often, these mussel bed restoration plans rely on habitat suitability maps. However, to be able to create these maps knowledge on the processes determining mussel bed growth and erosion is required (i.e. Brinkman et al., 2002). The most important factors that determine mussel bed persistence are predation (Zwarts and Drent, 1981; Dankers and Zuidema, 1995), erosion of mussel beds by hydrodynamic forcing (Widdows et al., 2002), food availability (Seed and Suchanek, 1992) and the presence of a suitable substrate (Mcgrorty et al., 1993). This study focuses on a less well documented and less frequent process of erosion, namely erosion by ice action. Ice action has been mentioned by Strasser et al. (2001) as a factor causing a reduction in size or even disappearance of mussel beds. However, in temperate regions, ice cover is a rather unpredictable event and therefore no direct measurements are commonly available. For monitoring purposes on a seasonal time scale a video camera was installed on a 11 m high pole to observe the evolution of a mature mussel bed in the Western Wadden Sea. Coincidentally, during a 27 month lasting experiment the direct impact of ice action was recorded and the evolution and recovery of the mussel bed after the ice action event was followed. This study provides a follow-up to Chapter 2 which focused on the impact of waves and currents on the short time-scale.

Mussel beds are considered to be long living biogenic structures. However, they slowly deteriorate and may disappear if no new spatfall occurs (Essink et al., 2005). The decay of the mussel bed is caused by predation and erosional processes. Storms have been reported as important agents (Nehls and Thiel, 1993). Waves and currents influence intertidal mussel beds on two different time-scales. On the short time-scale (hours to days) storm conditions result in increased wave heights and enhanced flow velocities. The resulting increased bed shear stresses enhance the erosion probability of the mussels (Widdows et al., 2002). On the longer time-scales (~ years), hydrodynamic processes influence the local erosion and sedimentation trends of the substrate. Both erosion and sedimentation can threaten the survival chances of mussel beds, for example by affecting the substrate characteristics. Deposition of sediment can negatively impact immersion times, thereby limiting the food intake while simultaneously increasing the predation time for birds (Brinkman et al., 2002). Furthermore, a change in local mussel bed topography influences the exposure of the bed to waves and currents. Vice versa, the impact of the physical factors partly depends on the physical and ecological conditions of the mussels, for example due to seasonal effects (Price, 1980, 1982; Carrington, 2002; Moeser et al., 2006). The attachment strength is usually lowest during fall due to reproduction. It increases slowly over winter and early spring. Reduced attachment strength reduces the bed's resistance against erosion (wa Kangeri et al., 2014).

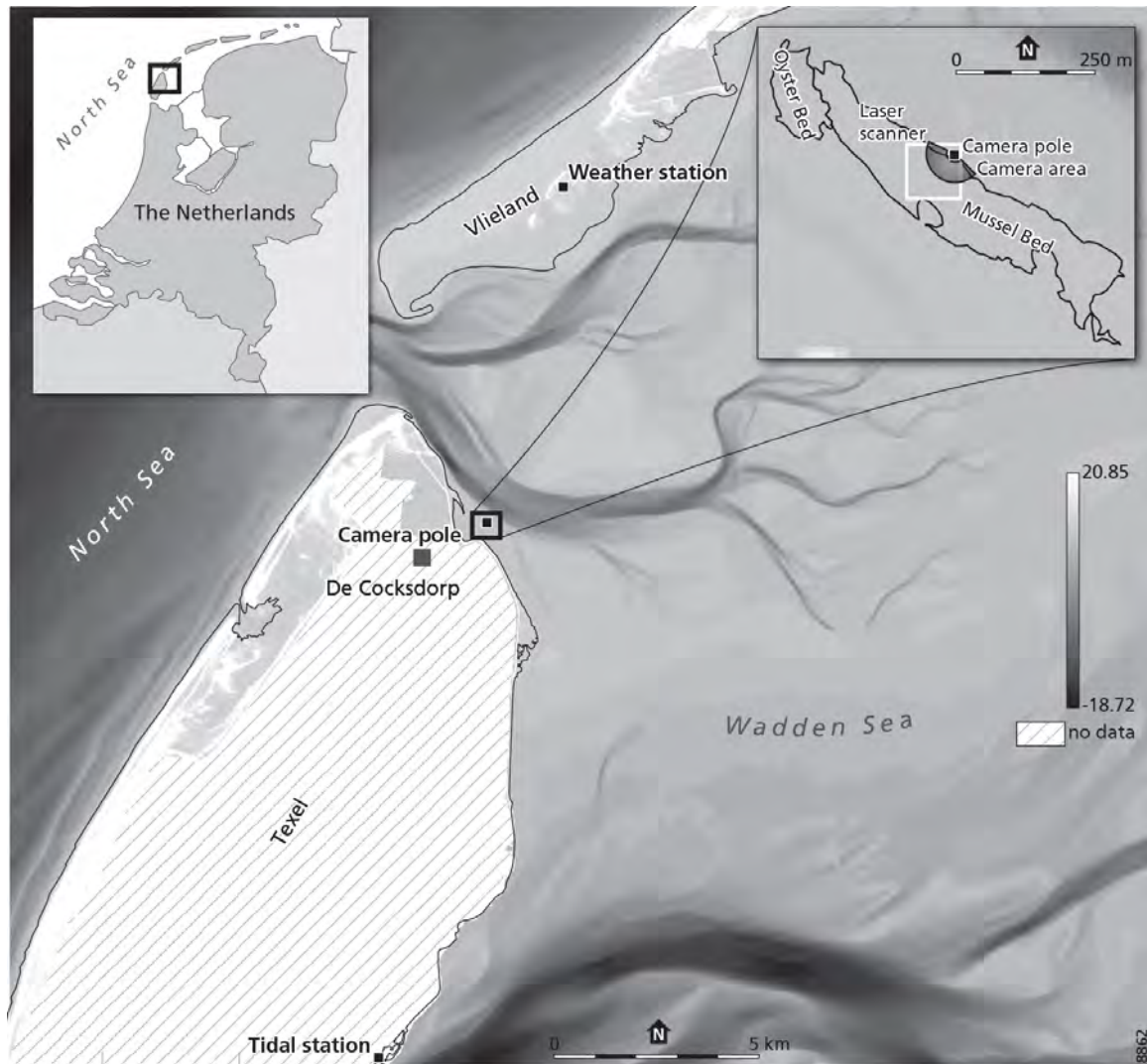


Figure 4.1 Bathymetric map of the area surrounding the measurement site, height is given with respect to the Dutch ordnance level (N.A.P.). The location of the research area, the tidal station and weather station are marked. In the top left a map of the Netherlands is shown where the area covered by the bathymetric map is outlined. In the top right corner the contour of the monitored mussel bed is shown together with the research areas covered by the camera system and the laser scanner.

On top of waves and currents, occasionally ice formation and ice action can erode mussel beds. Drifting ice is a powerful agent to move sediment in the intertidal zone (Dionne, 1984; Pejrup and Andersen, 2000). As was shown by Dionne (1988), the scouring effects of ice are largest in the temperate region (between 48° and 65° Northern latitude). Ice scour tracks on mussel beds have been observed by Conlan et al. (1998); Obert and Michaelis (1991) and Strasser et al. (2001). A second mechanism by which ice can erode mussel beds is by the development of ice in small ponds inside the mussel bed. At low tide the remaining water freezes and the ice attaches to the mussels. When the water level rises again an upward buoyant forcing arises (Denny et al., 2011), destroying the mussel bed.

This study reports and discusses the effects of ice action on mussel coverage and topography of an intertidal mussel bed. A part of an intertidal mussel bed in the Dutch Wadden Sea was monitored during a 27 month period.

4.2 Materials and Methods

4.2.1 Field location

The study site is an intertidal mussel bed located 300 meters to the north-east of the barrier island Texel near the village of De Cocksdorp, in the North of the Netherlands (53°9'N, 4°53'O) (Figure 4.1). The bed is one of the mussel beds in the Dutch Wadden Sea that are monitored in the context of the Mosselwad project (www.mosselwad.nl). A DEM (Digital Elevation Map) of the area surrounding the mussel bed is shown in Figure 4.1 together with the contour of the mussel bed. At the start of the monitoring period the mussel bed was 3 years old. A description of the mussel bed composition and population is given in van Kangeri et al. (2014). The tidal range at the study site varies between 1.20 m during neap tide and 2 m during spring tide. However, maximum water levels in the Wadden Sea are strongly affected by meteorological effects that result in a deviation of the predicted astronomical tidal water levels. Both direct wind stress and high and-low pressure areas affect the tidal water levels. Westerly winds result in a water level set-up, while easterly winds generally have the opposite effect. The study site is typically sheltered from wind and waves from the west by the islands of Texel and Vlieland and by the ebb tidal delta of the Eyerland inlet that causes severe wave dissipation. The mussel bed is mainly exposed to locally generated waves coming from easterly directions (Chapter 2), but strong easterly winds are infrequent in the Netherlands and mainly occur in winter. During storm surges the bed is also exposed to waves from the north-west coming through the tidal inlet.

4.2.2 Observations and processing

At the field site the mussel cover, the topography and water levels were monitored.

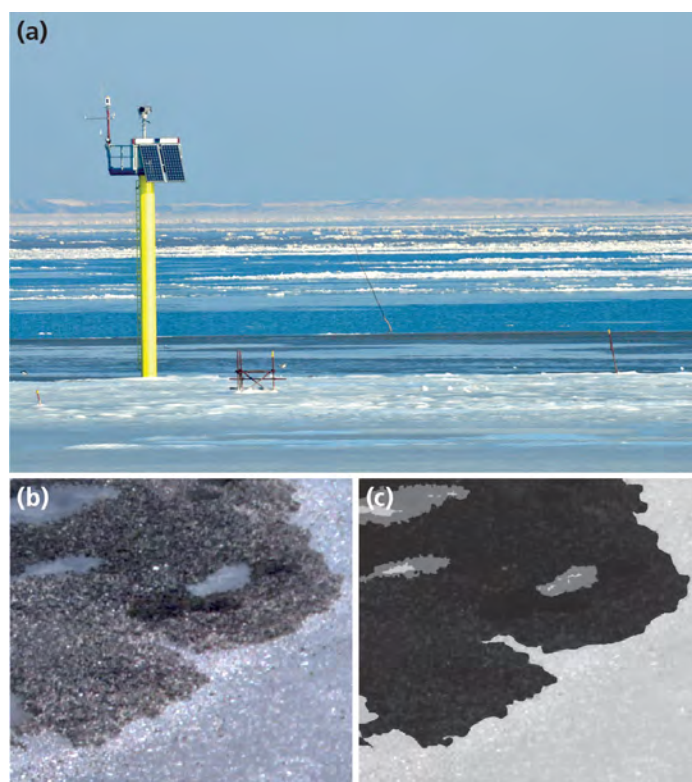


Figure 4.2 Panel a shows a photo of the camera pole on February 4 2012 taken from the coast of Texel during low water by Martin de Jong. In the image the mussel bed is fully covered with ice. Panels b and c illustrate the classification of mussel cover. In panel b, part of the mussel cover is shown, in panel c the same area is shown but with a classification overlay. The black and gray areas are classified as being covered with mussels while the white regions are classified as bare sediment. The gray color represents mussel covered areas that are covered with water.

Camera observations

Mussel coverage was monitored using photo images, taken daily by an automated digital video camera system. The camera system is located on a 11 meter high measurement pole (the system is shown in Figure 4.2a) and is able to rotate both in horizontal and vertical direction. The camera is an Arecont AV5105DN and is used with a Fujinon D32x10R4D-V41 lens. Each day during low water two panorama pictures were made: the first under an angle of -11° and the second -26° with respect to the horizontal. Each panorama consisted of 6 pictures. The quality of these observations depended both on weather and tidal conditions. Differences in lighting due to the viewing angle, water cover, droplets on the lens and variations in occurrence of other shell material, further complicate the automatic classification of mussel cover. The mussel coverage was therefore determined manually. Panorama images taken with proper light exposure and little remaining water on the mussel bed were selected. Images from the upper and lower panorama were stitched to each other using Microsoft ICE (image composition editor). These images were used to identify mussel cover using Adobe Photoshop CS6 software. To this end the images were blurred (surface blur 7 pixels with 130 threshold levels), then the fill tool was

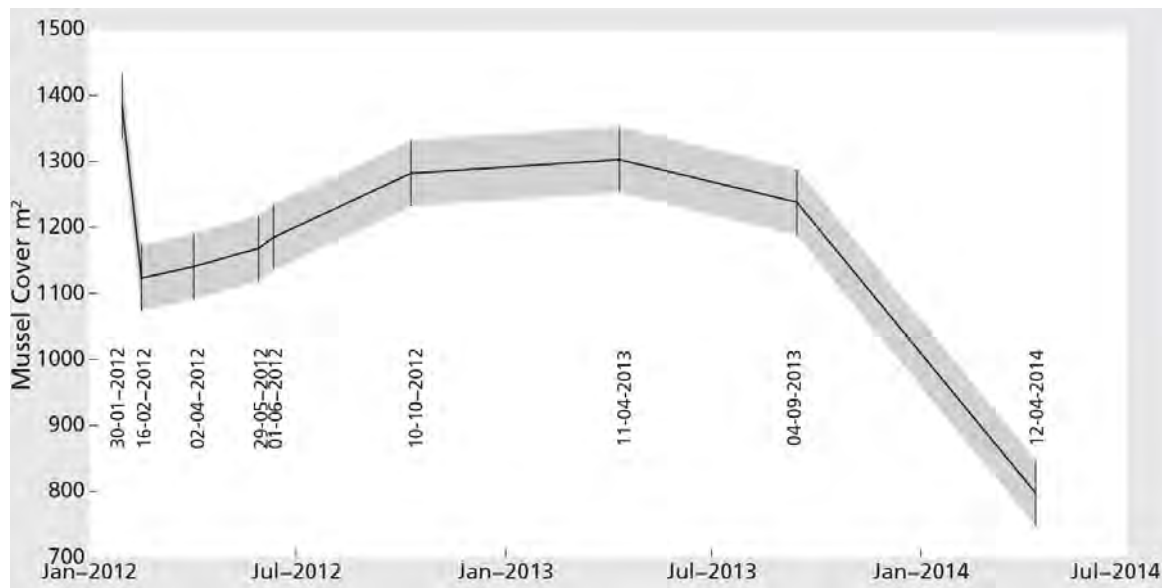


Figure 4.3 Mussel covered area during the measurement period, gray area indicates the error margin.

used to classify (tolerance 12 or 5) areas as being covered by mussels. Mussel cover could be estimated up to 40 m from the camera pole and ~3% of the mussel bed was monitored in this way. The monitored area is marked in Figure 4.1. A sample of the classification is given in Figure 4.2b and c. In the figure also drowned areas which are classified as being covered by mussels are highlighted. For submerged areas the difference in color between uncovered and mussel covered areas was small, but could be determined. In the next step the vertically stitched coverage maps were projected on a flat surface, using the camera angle. In the final part of the analysis the images were attached to each other, interpolated on a 0.02×0.02 m grid and the total area covered by mussels was determined. Based on multiple classifications of the same image by different people the error in mussel cover classification was estimated to be $\pm 50 \text{ m}^2$ which is 2% of the mussel covered surface in the monitored area.

3D Laser scans

The topography of the mussel bed is monitored using a 3D terrestrial laser scanner (type Riegl V-400). This was done four times a year on a regular basis and started in November 2011. The scans covered the area marked in Figure 4.1. During one survey a maximum of 5 scans from different positions was used to obtain an overview of the topography. One scan was taken from the camera pole at a height of ~10.8 m and four scans were taken at a height of ~1.80 m near the center of the four quadrants around the camera pole. The laser scanner was capable of obtaining a high resolution 3D map of the mussel bed, based on an angular resolution of 0.02 degrees for the scan from the camera pole and 0.03 degrees for the other scans. Six reflectors were placed as markers and were used to connect the coordinate systems of different scans from different dates and locations to each other. The exact geographical location of each reflector was determined using a dGPS. Using

the RiScan pro software the tie points were connected to world coordinates. For each scan the data was averaged on a horizontal 0.1×0.1 m grid, resulting in a digital elevation map (DEM). The area that was covered by the DEM is shown in Figure 4.1. When multiple scans had a value for a grid point, the value from the most accurate scan which had the largest angle between the point and the horizontal plane was used, this to reduce the effects of shadowing. Difference maps were created by subtracting DEMs from separate surveys. The laser scanner is unable to penetrate water; water covered areas therefore appear as missing data on the DEMs.

Hydrodynamical and meteorological data

Water levels were measured by Rijkswaterstaat (part of the Dutch Ministry of Infrastructure and the Environment) at Texel Noordzee, near the island of Texel (see Figure 4.1). Hourly averaged data of wind speed, wind direction and temperature were collected by the KNMI (Royal Dutch Meteorological Institute) station on the island of Vlieland (Figure 4.1). In addition, data of storm statistics and winter conditions were obtained from KNMI.

4.3 Results

4.3.1 Changes in mussel covered area

In Figure 4.3 the observed mussel covered area is shown as a function of time for the period between January 30, 2012 and April 12, 2014. In January 2012, $1.38 \pm 0.05 \times 10^3$ m² of the observational area was covered with mussels. During the first two weeks of February 2012 mussel cover had reduced to $1.12 \pm 0.05 \times 10^3$ m², a loss of 18.8%. A picture of the camera pole (Figure 4.2a) reveals that the mussel bed was covered with ice. Up to the fall of 2013 no significant additional reductions in mussel cover were observed. As a matter of fact after February 2012 the mussel area started to increase slowly. By September 2013 $1.23 \pm 0.05 \times 10^3$ m² was covered with mussels, resulting in a net reduction of 10.5% with respect to the initial cover in January 2012. During the following fall/winter additional losses occurred and by April 2014 $0.80 \pm 0.05 \times 10^3$ m² was left. Intermediate photographs suggest that erosion during this period progressed gradually. Two strong NW storms (windspeeds >18.0 ms⁻¹), on the 13th of October and the 5th of December; source: KNMI) were responsible for the majority of the losses and most likely triggered the gradual erosion. Unfortunately, due to a large amount of stagnant water and a malfunctioning camera system mussel cover could not be estimated during this period. A detailed study of storm damage is therefore not possible. By the end of the observation period the total reduction was $0.59 \pm 0.05 \times 10^3$ m², a total loss in mussel coverage of 39%.

4.3.2 Change in mussel bed coverage

Changes in mussel cover during the measurement period are studied using coverage change maps from three key periods: the ice action period, the recovery period and the storm period. Figure 4.4a shows the change in mussel cover over the ice action period

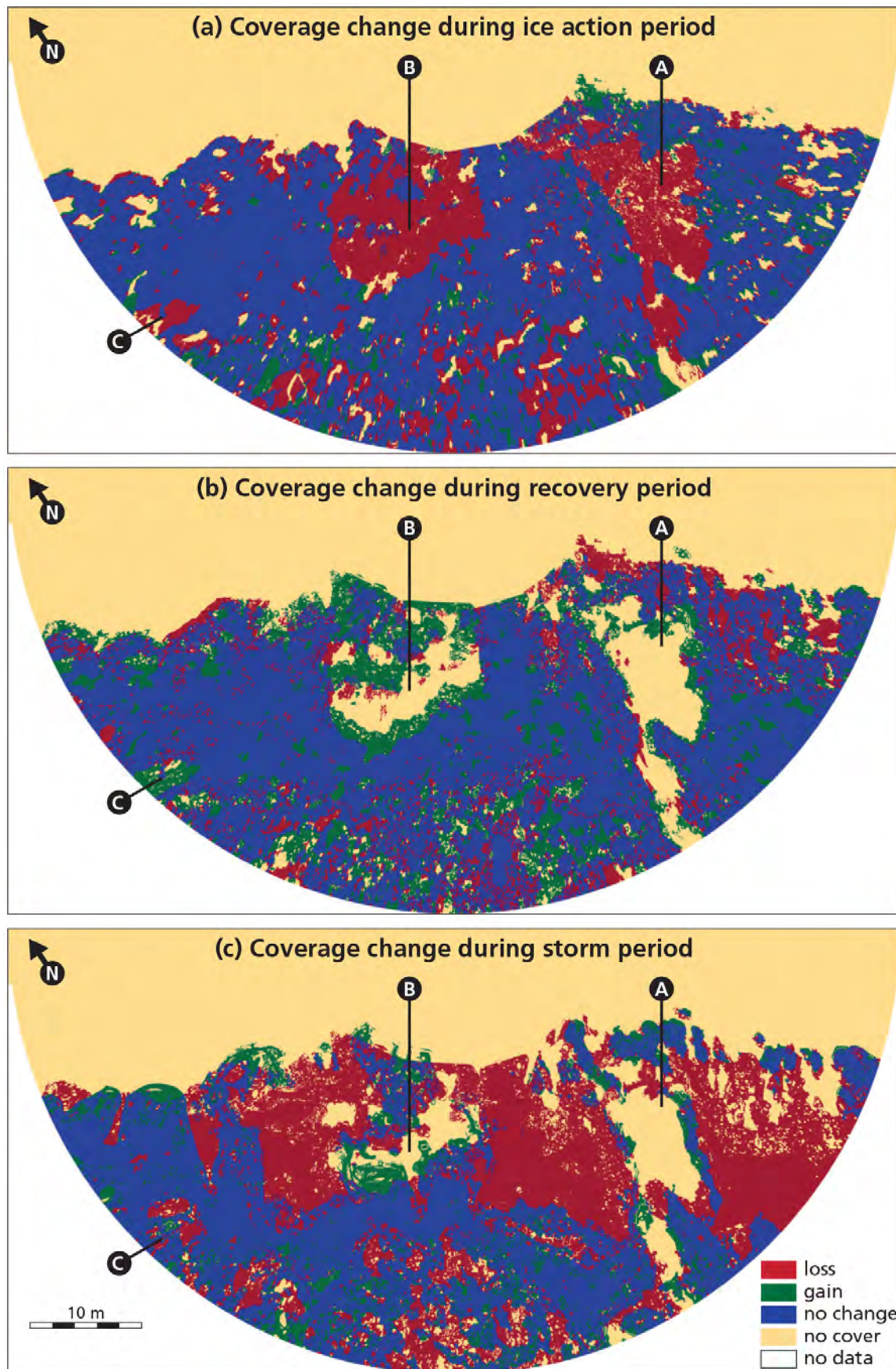


Figure 4.4 (Continued) The north is marked with an arrow in the upper left corner. Red colored areas have lost mussel cover, green colors have become covered with mussels, blue areas remained covered with mussels and yellow areas remained uncovered. Black markers indicate the location of the gaps created by ice action.

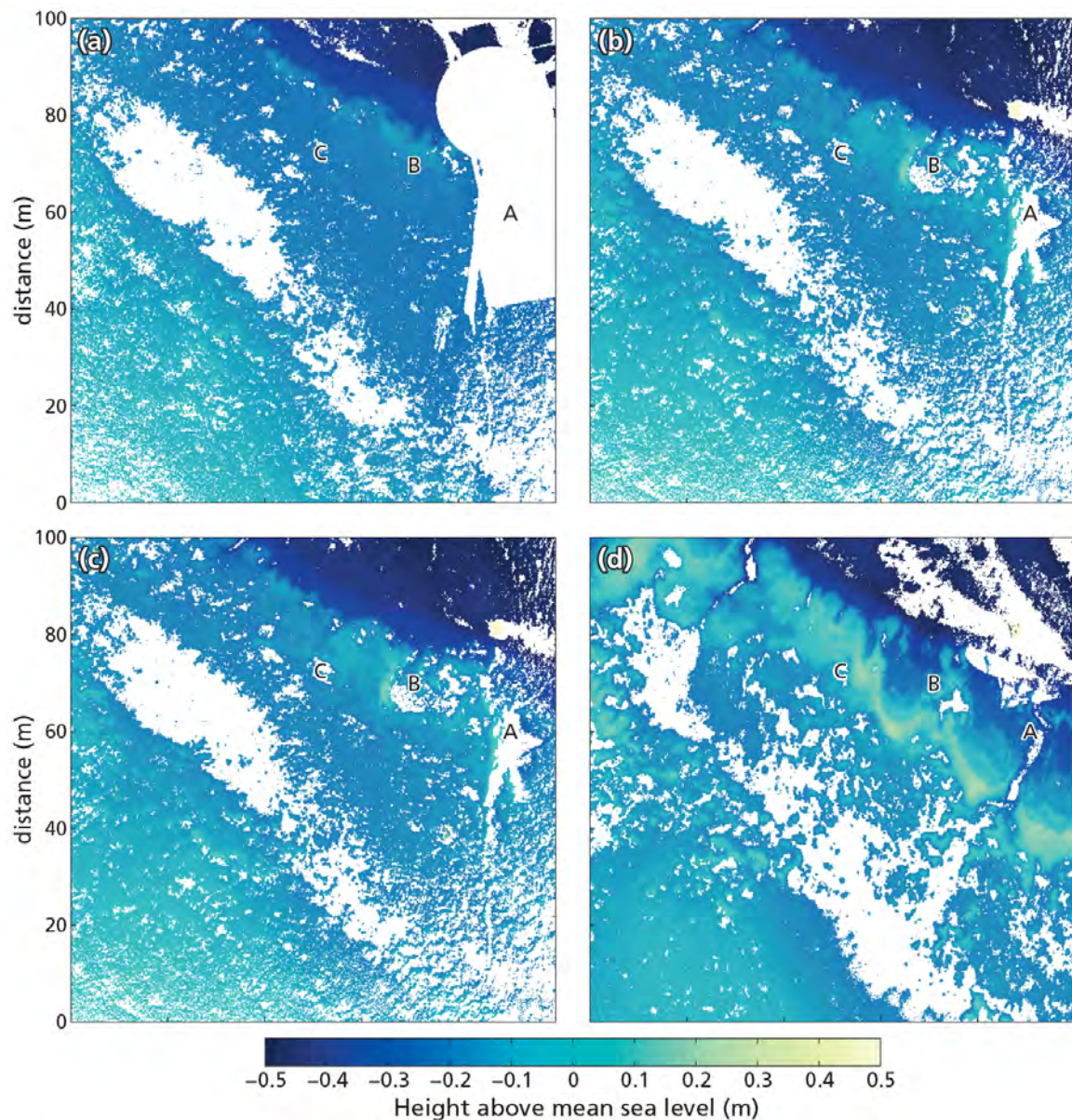
(between January 30, 2012 and February 16, 2012). In the figure the location of the three largest erosion gaps created by ice action are tagged using letters A, B and C. The two largest erosion gaps (A and B) were located close to the seaward edge of the mussel bed. Below erosion gap A an eroded track can be observed. Gap C is located more inside the mussel bed. Smaller areas deeper inside the mussel bed also suffered some erosion.

In the 19 months after the erosion by ice action the bed was able to recover. The change in mussel cover during this period (February 16, 2012 until September 4, 2013) is shown in Figure 4.4b. Results show that gap A experiences very little recovery; only close to the edges of the gap cover is increased. In gap B there is more recovery, especially at the southern edge of the gap. Gap C fully recovers during this period. Cover inside the rest of the bed also appears to have increased. This explains a large part of the observed increases in Figure 4.3.

Wave impact on the mussel bed is illustrated by the change in mussel cover during the stormy period (4 September, 2013 - 12 April, 2014) shown in Figure 4.4c. Results show that the areas just outside of the edges surrounding the gaps became strongly eroded as a result of these storms. These areas between the areas eroded by ice action suffered a retreat of the mussel bed edge of 11 to 16 m. Also, deeper inside the bed some parts have become eroded. The recovered area inside erosion gap B did not suffer substantial erosion.

4.3.3 Change in mussel bed topography

The changes in topography are investigated using the DEMs obtained from the 3D laser scans. In figure 4.5 the DEMs for November 21, 2011 (panel a), March 9, 2012 (panel b), February 27, 2013 (panel c) and April 12, 2014 (panel d) are shown. In all panels the location of the erosion gaps are indicated. Due to the limited scan positions erosion gap A was not completely covered by the scans performed on November 21, 2011. In the DEMs the seaward edge of the mussel bed is highlighted by the change in height from ~ -0.4 (dark blue) to ~ -0.2 (light blue). The bed was damaged by ice in February 2012 so the effects can be investigated by comparing the DEMs from November 2011 and March 2012 (Figure 4.5e). While in November the bed is still uniform, the DEM for March 2012 reveals ridges, with a height of 0.2 up to 0.4 m above reference level. They are located westward of the erosion gaps. The gaps themselves are filled with water and the level of these depressions is more than 0.1 m below the reference level. At the ridges the height is increased by 0.3 m. Also behind the ridges the height appears to have increased by 0.1 to 0.15 m, which is larger than the average increase which ranges between 0.05 and 0.08 m. Thus apart from the ridges, a larger area surrounding the erosion gaps increased in height. Up to February 2013 no large additional changes in topography were observed, confirming limited recovery. However, as relief around the ridges is reduced



and it appears that mussels and sediment on the ridge are spread over a larger area. Also, there is an overall increase in bed level indicating sedimentation.

Between February 27, 2013 and April 12, 2014, large topographic changes occurred in the mussel bed. On April 12, 2014 (Figure 4.5d) the edge of the mussel bed is much more pronounced. Also this edge was eroded and moved in a south-western direction, as already shown by the images. The height difference map for the period between April 12, 2014 and February 27, 2013 (Figure 4.5f) confirms this movement. At the location where the edge used to be, a relatively large drop in height can be observed (- 0.3 m). Possibly not all mussels and associated sediment were lost to the bed as a large height increase (+ 0.3 m) can be observed at the present edge. This suggests a partial redistribution of the mussels and sediment. The present seaward edge is on average 0.1 m higher than the edge

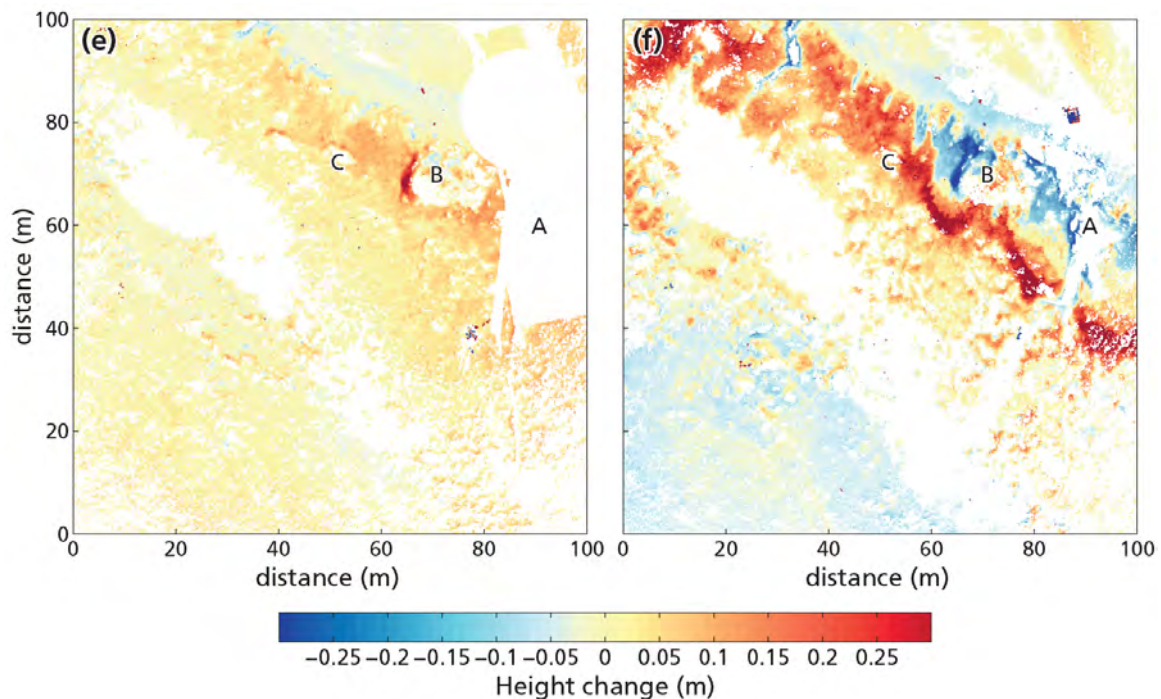


Figure 4.5 Panels a, b c and d. show the height with respect to the Dutch Ordnance level on November 8, 2011, March 9, 2012, February 27, 2013 and April 23, 2014 respectively. Panel e, shows the height difference between November 8, 2011 and March 9, 2012 (panels a and b). Panel e, shows the height difference between February 27, 2013 and April 23, 2014 (panels c and d). For all pictures, white areas show missing data points. The erosion gaps (A, B and C) are marked in all panels.

prior to the 2013 storms. A closer look at the information reveals that the ridges which became elevated by ice action suffered the largest losses during the 2013 storms. The edge at the location of the ice pushed ridges has the strongest retreat in south-western direction. In the area between scour holes B and C the mussel bed edge retreated around 15 meters. The areas further away from the scour holes showed some height increase, but no shoreward movement of the seaward edge.

4.3.4 Mechanism of ice action

Analysis of mussel cover and bed level changes revealed the presence of elevated ridges and tracks, these features are commonly associated with scour events (Dionne, 1998; Pejrup and Andersen, 2000; Konuk et al., 2005). The increased height at newly formed edges is most likely a product of the pushing of mussels and sediment by ice. During the ice period the bed became covered with a thin sheet of ice. The thickness of this sheet increased due to the freezing water remaining on the tidal flat after high water. Field observations suggest a thickness of approximately 0.1 m. The two largest erosion gaps (A and B) were located in the lower lying areas of the mussel bed. This indicates that the location of the gaps was probably not random. In lower lying areas more stagnant water could remain after high water, encouraging a further growth in thickness of the local ice

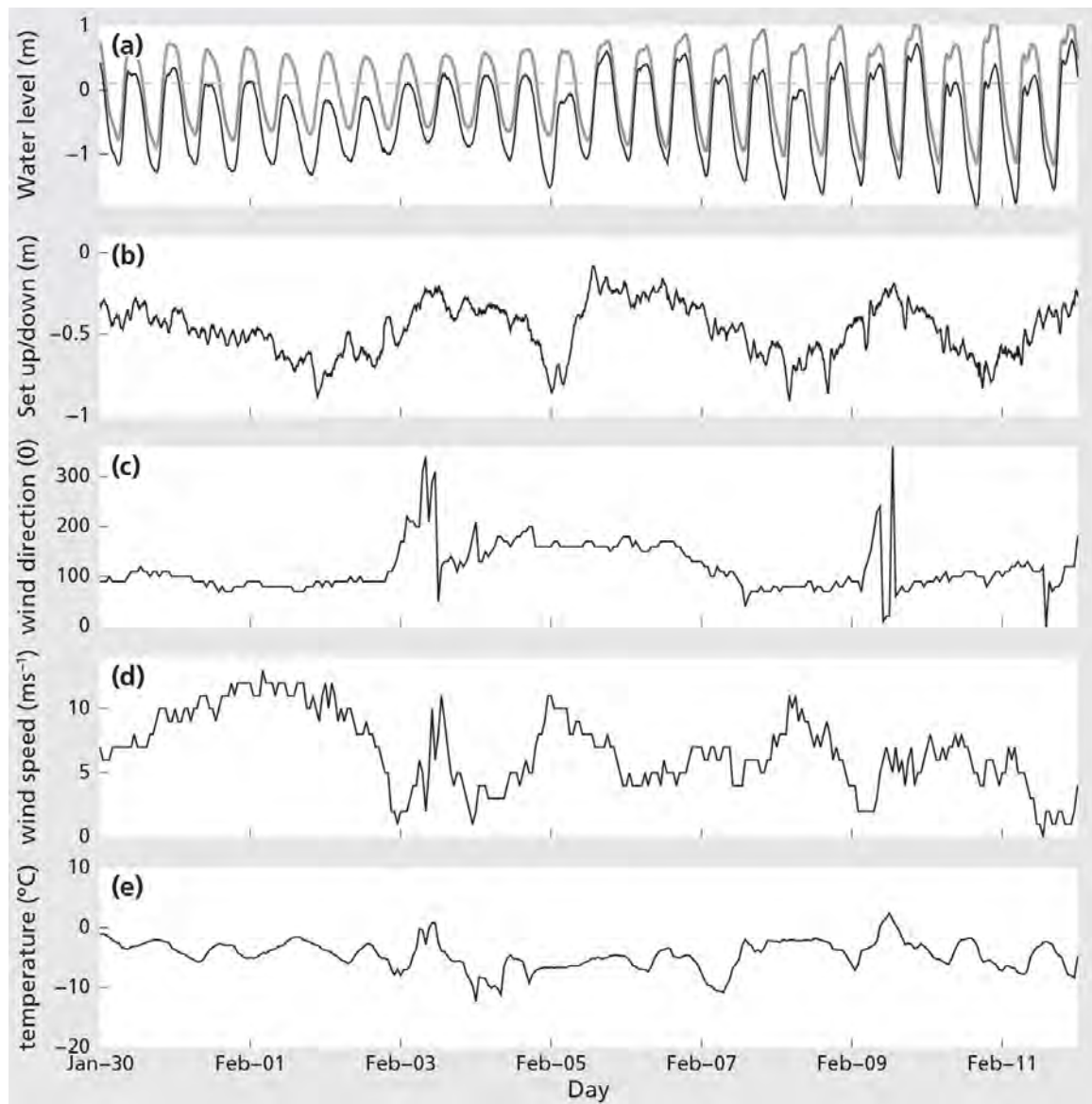


Figure 4.6 Environmental data recorded between January 30, 2012 and February 12, 2012, the period during which the bed was covered with ice. Panel a. shows the water level measured and predicted (gray) at Texel Noordzee a nearby Rijkswaterstaat tidal station. The dashed line shows the height of the seaward edge of mussel bed at 10 cm above mean sea level. Panel b features the observed set-down for the same period. Other panels show hourly weather data from the KNMI station at Vlieland, the Netherlands: panels c and d show the wind direction and speed respectively for the same period. Panel e shows the air temperature.

sheet. On the evening of February 5, 2012 the ice sheet started to move in north-western direction the thicker areas pushed against and forced over the mussel bed.

The movement of the ice sheet was forced by either wind, tidal currents, waves or a combination of the three. The environmental conditions which enabled the formation and subsequent movement of the ice sheet, are presented in Figure 4.6. Observed and

predicted water levels for the cold period are presented in Figure 4.6a. Throughout the period the measured water level was always lower than the predicted one (Figure 4.6a+b). The resulting set-down in water levels was caused by strong winds from easterly directions (Figure 4.6c and d), which push water away from the Dutch coast. The temperature variation during the cold period (Figure 4.6e) reveals that the temperatures were below zero throughout the cold period apart from two short time intervals. The average temperature was -4.5°C with a minimum temperature of -12.3°C .

The height of the mussel bed and the maximum water level reached during a tidal cycle are two important parameters for the dynamics of the ice sheet. During the first days of the cold period the mussel bed was not fully submerged because the easterly winds caused a set-down in water level. Ice formed due to stagnant water on the mussel bed. Wind and currents though were not able to move the ice sheet because it was obstructed by the mussel bed. In contrast, ice that formed on the lower lying sandy flats was carried away by the tidal flow during each high tide and therefore no thick (for the Dutch Wadden Sea) ice sheet developed. The ice scour event appears to be triggered by a drop in wind speed in the evening of February 5, taking away the effects of this set-down in water levels. As shown by Figure 4.6a this is the first time the bed is submerged since the start of the cold period.

4.4 Discussion and implications

Results show that in the period between January 24, 2012 and April 14, 2014 mussel cover reduced by 38% in the monitored area. A large portion (18%) of the losses occurred during the first weeks of February 2012, when the bed was covered with ice. The physical interaction of the bed with scouring ice was the main source of erosion during this period. The effects of ice action resulted in local topographic changes, creating a depression in the scoured region, while simultaneously elevating the surrounding area by partly redistributing the eroded mussels and associated sediment. During the next 19 months the bed recovered and the reduction was limited to 10% of the initial area. Later, during the stormy fall of 2013, the remaining 28% was eroded. Especially, areas which previously became elevated as a result of the scouring ice, suffered large erosion. Here, implications of erosion by ice for mussel bed persistence and the significance of the observations for the mussel population in the Dutch Wadden Sea are discussed.

4.4.1 Synergistic action of eroding agents

Observations revealed that during fall/winter of 2013/2014 areas which became elevated due to ice action suffered large losses, while losses in other areas along the mussel bed edge were smaller. During calm conditions the bed was able to slightly recover from the damage done by ice action. However, induced topographic changes remained intact. Under storm conditions the area surrounding the erosion gaps damaged and the eroded areas were expanded. This has led to a topographic change in which height variations became even more pronounced. The present mussel bed edge was by the end of the measurement period 0.1 m higher than before the storm period. Visual inspection of

the bed showed that after the storm, parts of the eroded patches were rolled up over the mussel bed. These observations suggest a synergistic relation between ice forcing and wave action. Mussel bed disturbance and gap formation have been extensively researched for rocky shores (Paine and Levin, 1981). For these environments a similar process has been observed, initial damage by wave erosion is found to trigger an erosion sequence in mussel beds (Denny, 1987). The suggested mechanism is a weakening mussel attachment in the area surrounding the erosion gap. This results from the removal of the byssus attachment to the eroded parts. A similar process seems to occur during the storm period where the gaps gradually increase in size. However, there is a large temporal lag between the damage by ice action and the erosion by wave forcing. During this period the byssus attachments would have recovered. This thus suggests that a different mechanism relates these eroding agents.

The enhanced wave exposure of the areas surrounding the gaps eroded by ice action could be caused by: (1) an increase in wave forcing in these areas. Wave forcing depends critically on the local topography, which was substantially altered by ice action. The increased bed levels promote wave shoaling leading to an increase in wave orbital forcing. Additionally, wave refraction could add to that by focusing of waves on the higher areas. (2) Attachment of the mussels in the ridges to the underlying substrate could be reduced. The piling-up of mussels near the ridges limits the access of mussels located at the bottom of these piles to food. This reduces the ability of the mussels to maintain their attachment to the substrate. It must be noted that since this observation only concerns a single event and that the erosion by wave action in this area could be coincidental.

4.4.2 Implications for the persistence of intertidal mussel beds in the Dutch Wadden Sea

This study followed the survival of a mature mussel bed during several years. Mature mussel beds are more resilient against forcing (Dankers et al., 2001), since their attachment strength is stronger (Price, 1981). Results also suggest that the limited submergence time and reduced water level have facilitated ice sheet development. This suggests that mussel beds located above mean sea level are most exposed to this type of ice action. Only a small portion of the mussel beds are located at these levels (Brinkman et al., 2002). However, during colder winters more thick ice sheets may develop, and especially during melt periods these can break up and form ice flows, capable of damaging intertidal mussel beds (Strasser et al., 2001). Observed wind conditions during the measurement period did not vary much from long term observations. The generation of ice sheets is not uncommon in the Wadden Sea. For example, during the winter of 2013 again ice sheets were observed, also at other intertidal mussel beds. However, the ice sheets were much thinner and no damage was reported. The winters of 2012 and 2013 were cold, but not extreme as they belong to the coldest 35% but not the coldest 25% winters in the Netherlands since 1901. The winter of 2014 was mild with a Hellmann number of 19.5. As a fourth of the winters are colder, conditions leading to an event, such as described above, are not unlikely to occur. Observations of tracks resulting from ice scour on tidal flats in the Wadden Sea (Pejrup and Andersen, 2000) and the observed damage in intertidal

mussel beds (Strasser et al., 2001) suggest that damage by ice action in mussel beds is not uncommon. The synergistic character of ice action in combination with wave events is anticipated to be a relevant factor for the long term persistence of mussel beds.

4.5 Conclusions

Results of a 27 month long monitoring campaign on a mature intertidal mussel bed revealed that physical disturbance by ice action can substantially influence the long-term persistence of an intertidal mussel bed. While directly causing a loss of 10% of the initial mussel area in the monitored region ice action also induced topographic changes. These changes might have enhanced wave-driven erosion, resulting in an additional loss of 28% of the initial area during a stormy period. The bed was damaged by means of scouring; this was determined from the presence of gaps and the formation of tracks and elevated ridges. The bed was scoured by the ice sheet which had formed on top of the bed in the days prior to the event. This ice sheet could develop due to the set-down in water level by an easterly wind which accompanied the cold period. The ice action event appears to be triggered by a change in wind direction, taking away the effects of this set-down in water levels. Ice action resulted in a scour hole (0.1 m deep), surrounded by elevated ridges (0.3 m high). These features strongly indicate that the bed was damaged by scouring ice. During the first 19 months after the ice action event, small changes in both mussel bed cover as well as elevation were observed, revealing limited recovery. In the next fall and winter though, with a number of severe storms, the bed was damaged again. Largest losses were observed in areas which became most elevated as a result of the previous ice action. In conclusion, ice action has a twofold impact on the persistence of intertidal mussel beds: (1) by directly eroding parts of the mussel bed; (2) by increasing the susceptibility of the bed to wave erosion. Observations only concern a single event, further study is required to confirm the existence of a synergistic relation between ice- and wave erosion.

5 Wave forcing in the Dutch Wadden Sea and the effects on mussel habitats

This chapter is based on:

DONKER, J. J. A., VAN DER VEGT, M., HOEKSTRA, P. (2014), Wave forcing in the Dutch Wadden Sea: effects on mussel habitats (In preparation)

Abstract

Mussel beds are important elements in the ecosystem in the Dutch Wadden Sea. Over the past decades intertidal mussel cover has declined especially in the Western Wadden Sea. Wave forcing is an important process in limiting mussel bed survival in intertidal areas. The main objectives of this chapter are therefore: (1) to determine the spatial distribution in wave forcing in the Dutch Wadden Sea; (2) to relate wave forcing to the occurrence of intertidal mussel beds; (3) to study the differences in wave forcing and mussel bed occurrence between the Western and Eastern Wadden Sea. A wave model was used to determine spatial distribution of wave forcing, in terms of the root mean squared near-bed wave orbital velocity amplitude, in the Dutch Wadden Sea for 1480 environmental scenarios. Obtained model results were, subsequently, related to frequency of occurrence of these scenarios to obtain statistically representative estimates of wave exposure. The results reveal differences in the average wave forcing between basins up to 50%. Wave forcing is largest in the Western basins and smallest in the Eastern basins. By comparing historical contours of mussel beds and average basin forcing it was established that in more wave-exposed basins a relatively smaller portion of the intertidal area is covered with mussel beds. Furthermore, the average wave forcing at all observed intertidal mussel beds is 0.20 ms^{-1} . This value is slightly larger in the West than in the East. In the West, wave exposure at mussel beds is also clearly smaller (14%) than the basin-averaged intertidal wave forcing. In the East there is little difference between average intertidal and average mussel bed exposure in terms of wave conditions. It is concluded that less intertidal area the western Wadden Sea is suitable for mussel bed settlement as the area is limited by wave forcing, and that therefore habitat suitability in the Western Wadden Sea is more sensitive to changes in the wave climate. This gives a plausible explanation for the pronounced differences in mussel cover between the Western and Eastern Wadden Sea.

5.1 Introduction

Intertidal mussel communities are important for the ecosystem of the Dutch Wadden Sea. By attenuating wave energy (Chapter 2), reducing flow velocities (Van Leeuwen et al., 2010) and by filter feeding, they promote deposition of organic rich sediments (Flemming and Delafontaine, 1994; Oost, 1995). Mussel beds and their surroundings also provide a habitat for other species, thereby increasing biodiversity in the Dutch Wadden Sea (Dittmann, 1990; van der Zee et al., 2012). However, mussel populations vary strongly over time and in space, thereby their impact on the ecosystem varies. As shown by Folmer et al. (2014) the ratio between intertidal mussel bed area and intertidal area in the Western Wadden Sea (WWS) is low compared to that in the Eastern Wadden Sea (EWS). Also, in the WWS the present mussel bed area is low compared to that in the period between 1970 and 1980. This has been attributed to overfishing in the period 1985 to 1990 and a lack of recovery in the following period (Dankers et al., 2001).

In order to increase mussel bed area several programs exist. This study is part of the Mosselwad project, which aims to increase knowledge on mussel bed survival and to produce recommendations for restoration in the Dutch Wadden Sea. In order to restore mussel beds often mussel habitat suitability maps are used. Such a habitat suitability analysis for the Dutch Wadden was performed by Brinkman et al. (2002), and it revealed that, based on model results, wave forcing induced resulting from the orbital velocity, is the dominant factor determining habitat suitability. However, they only used modeled wave forcing for one storm. A study of the full wind climate is more appropriate, as local wave conditions depend strongly on both wind speed and wind direction. Also, less energetic conditions that occur more frequent might also influence habitat suitability by limiting settlement or reducing development opportunities. The goal of this study is to investigate whether wave forcing limits early stage mussel bed development in the Wadden Sea.

Mussels can only remain attached to the sediment when the hydrodynamic forcing is low (Widdows et al., 2002). As shown by Denny (1987) mussels erode by patches rather than by individuals. The resistance of a patch to erosion is controlled by their anchorage to the substrate. In rocky environments the weakest link is failure of the byssus attachment to the substrate (Bell and Gosline, 1996). However, in unstable soft sediments also the erodability of the underlying substrate is a weak link which controls erosion (Buschbaum, 2001; van Kangeri et al., 2014). By attaching to each other and to shell material inside the sediments mussels increase their resistance against erosion. Moreover, by adopting an intelligent attachment strategy, self-organized labyrinth-like structures are formed in the first months after settlement. These have been suggested to increase the beds resilience against erosion (van de Koppel et al., 2005). While waves are known to erode mussels during major storms (Nehls and Thiel, 1993) the role of average and more energetic (e.g. 95 percentile) wind and wave conditions on settlement chances and persistence has not been investigated. It is likely that during the settlement phase wave conditions play a key role in providing the hydrodynamic boundary conditions which allow for mussel larvae to attach to the substrate. Also, in the period after settlement mussel attachment is still weak as no patterns have yet been formed. Over time, patterns

are formed and sediments accumulate and consolidate, which increases the resistance of the bed. During the first year large losses are observed in intertidal mussel beds (Dankers et al., 2001). Surviving the first period is thus a key factor for the long-term persistence of a mussel bed. Furthermore, results presented in Chapter 4 indicate that previous erosion events make the bed more susceptible to additional erosion. These findings indicate that not only storm conditions, but, also the intermediate and more energetic wind and wave conditions influence the suitability of a specific site for the settlement of a stable mussel bed.

In back barrier basins such as the Dutch Wadden Sea waves are mostly locally generated as the area is sheltered from open sea by barrier islands and ebb tidal deltas (Groeneweg et al., 2008; van Vledder et al., 2008; van der Westhuysen, 2010). Waves only grow when their relative wave height (ratio between wave height and water depth) is small. Therefore, the high waves that occur during storm and more energetic conditions are only generated in the deeper tidal channels. Waves that occur during calmer conditions will be generated in tidal channels and over the deeper parts of intertidal shoals and flats. The length (fetch) over which waves are subject to the direct influence of the wind is thus controlled by the water depth and the orientation of the tidal channels with respect to the wind direction. As the fetch depends strongly on the water depth, both tide- and wind-induced variations in water level have significant impact on wave generation, and consequently wave forcing on intertidal flats.

When waves travel into shallow water (high relative wave height), waves lose energy by bed friction and breaking. Variations in morphology have a strong impact on the spatial distribution of wave forcing. Also, variations in bottom roughness affect the rate of wave attenuation. For instance in Chapter 2 enhanced wave attenuation over an intertidal mussel bed was found.

The goal of this study is to determine if wave forcing, in terms of the near-bed orbital velocity amplitude, is a limiting factor for mussel bed occurrence in the Wadden Sea. This is investigated by: (1) studying the wind climate and water levels which control the fetch in the Dutch Wadden Sea; (2) determining the spatial distribution of wave forcing in the Dutch Wadden Sea; (3) investigating the occurrence of mussel beds in relation to wave forcing and (4) studying the differences in wave forcing and mussel bed occurrence between the EWS and WWS.

5.2 Materials and Methods

5.2.1 Study area

The Wadden Sea (WS) is located along the Northern coast of the Netherlands and extends along the German coast and the South Western coast of Denmark. The Dutch part of the WS is approximately 150 km long. The distance between islands and mainland coast vary from ± 6 km up to ± 33 km. The total area of the Dutch Wadden Sea is ± 2250 km² (see Figure 5.1). The study area is sheltered from the North Sea (NS) due to the presence of six large barrier islands, while dikes form the boundary on the mainland side. The Dutch WS is connected with the NS through six tidal inlets, which provide for the exchange of water

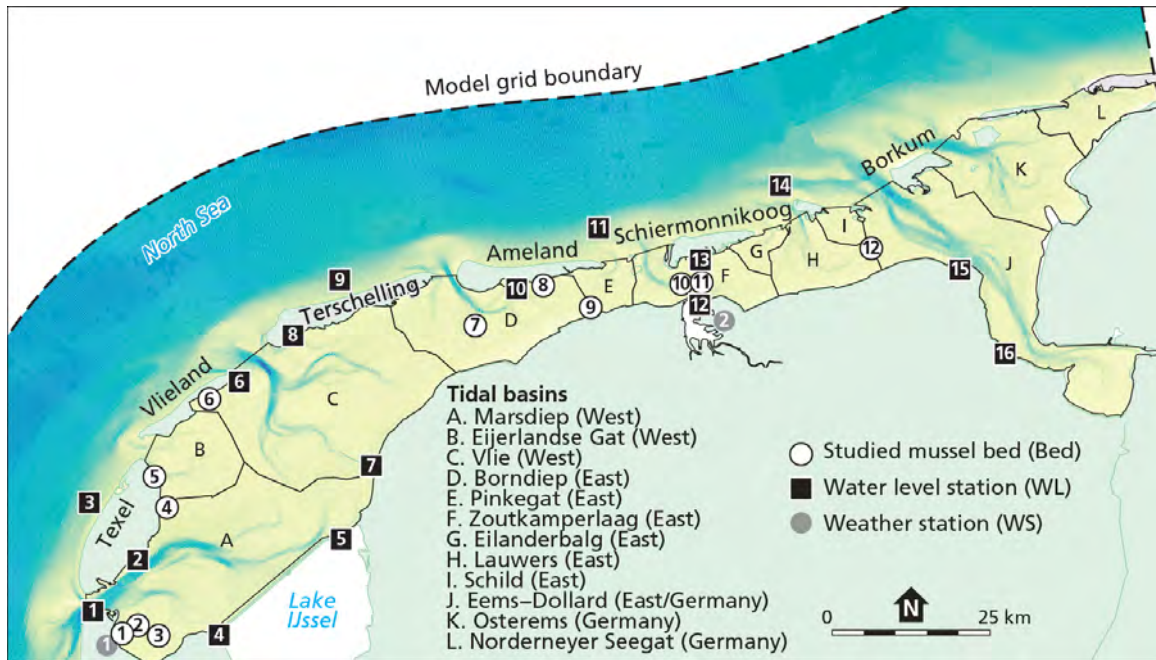


Figure 5.1 Map of the study area with the locations of the studied mussel beds (white circles), the tidal stations (black squares) and weather stations (gray circles). The background features a bathymetric map of the area, which is used as the large grid in the model study. Black lines indicate land boundaries and gray lines divide the boundaries between tidal basins (which are denoted by capitals).

between the WS and the NS. In the WS mussel beds are present on the intertidal flats of all basins and in some basins they occupy up to 6% of the intertidal area (Folmer et al., 2014).

5.2.2 Data collection

Field data was used to facilitate and to calibrate the model study. Data on wave characteristics near intertidal mussel beds were derived from near-bed pressure measurements at three locations throughout the Dutch Wadden Sea. To limit the effects of local changes in wave characteristics due to small scale morphological features, the pressure sensors (Ocean sensor systems OSSI-010-003B Wave Gauge) were located on the uncovered tidal flat adjacent to the mussel beds. The pressure sensors measured water pressure at resolution of 10 Hz. The first dataset was obtained at Bed 11 (white circle in 5.1) from April 5 to April 27 in 2012. The second dataset was obtained at Bed 5 (white circle in 5.1) from September 13 until October 31 in 2012. The third dataset was obtained at Bed 2 (white circle in 5.1) from April 29 until September 16 in 2013. Linear wave theory was applied to convert pressure to sea surface elevation. Hourly time series of sea surface elevation were used to determine the significant wave height (H_{rms}), using the method described in Chapter 2. During all measurement periods winds were relatively calm and only a few events with stronger ($>10\text{ms}^{-1}$) winds were observed.

5.2.3 Mussel bed contours

Contours of mussel beds are gathered since 1995 during annual surveys in spring by IMARES and MarinX. These contours were determined by mapping the outlines of the bed following the method described in de Vlas et al. (2004). These surveys were performed after an initial aerial inspection, during which the settlement of new beds and the disappearance of old beds was established. Beds that had suffered large losses were mapped again. Based on these observations a survey strategy was determined and between 40 and 95% of the mussel beds were visited during each survey. Also, when a bed was not measured during a specific year the contour obtained during the next survey was used to estimate the contour of the missing year. The data set and the mapping method has been extensively described in Folmer et al. (2014). In this study the contours of the spring surveys of the years 1995 up to 2011 were used.

To study the role of wave exposure in detail, this study focuses at 12 intertidal mussel beds which are spread throughout the study area. The location of the beds is shown in Figure 5.1. They are chosen because they have been extensively monitored from 2011 to 2013 in the context of project Mosselwad. Contours are determined following the same protocol as used for the annual surveys. Beds 5 and 7-12 correspond to locations 1-7 described in van Kangeri et al. (2015). The beds are distributed over East part (basins D up to J) and West part (basins A, B and C) of the Dutch Wadden Sea. Furthermore, the mussel beds vary in distance to the tidal inlet, from close to the inlet or main tidal channel (Beds 5, 7 and 10) to a location more in the interior of the back barrier basin. The studied mussel beds are located on isolated tidal shoals (Beds 1, 2, 3, 7, 10, 11 and 12), on shoals attached to the barrier islands (Beds 4, 5, 6 and 8) or are close to the mainland coast (Bed 9).

5.2.4 Model

General description

Wave forcing in the Dutch WS is modeled using SWAN (version 40.91AB). This is a 2D horizontal wave model which solves the wave action balance in a horizontal domain. No description of the model is given here as it has been described extensively in Booij et al. (1999); Holthuijsen (2007). Key features of the model are wave generation by means of local wind conditions and transfer of wave energy between frequencies through (triad and quadruplet) wave-wave interactions. Dissipation by depth-induced wave breaking, white capping and bottom friction is included. Wave shoaling as well as refraction are also incorporated in the model. As it solves the wave action balance, the model is therefore unable to model flow velocities.

Model set-up

Bathymetric maps of the Wadden Sea are publicly available on a 20×20 m grid and supplied by Rijkswaterstaat (Dutch Ministry of Infrastructure and Environment). These maps are based on soundings and LIDAR data, surveys are repeated every six years; main navigation channels are monitored more often and at a higher spatial resolution. The wave forcing in the Wadden Sea is calculated using a nested model approach. The large grid is curvilinear, and reduces from very coarse resolution in the North Sea (up to

2 by 2 km) to a very small resolution in the Dutch Wadden Sea. The extent of the model grid is shown by the bathymetric map in Figure 5.1. In the South-West it extends an additional 50 km southward. Inside the Dutch Wadden Sea the grid size varies between 300 by 300 m up to 70 by 70 m. Near the three validation sites, where pressure was measured, wave exposure was modeled at a higher spatial resolution to obtain more accurate values near the pressure sensors. For this purpose, inside the main grid a high resolution grid of the area surrounding the measurement location (4×4 km) was nested. The resolution of this grid is the same as that of the available bathymetric data (20×20 m).

Both the primary as well as the nested model simulations are performed in stationary mode. A maximum of 50 iterations was allowed. Refraction is an important feature for waves in the Dutch Wadden Sea and therefore all directions were included. Also the effects of wave-wave interactions by triads and quadruplets were taken into account. Bed friction was incorporated using the Jonswap bed friction formulation and the friction parameter for this formulation was set to 0.0038. For the nested runs the Madsen roughness formulation was used with a Nikuradse roughness of 0.02 m over uncovered flats and 0.05 m over a mussel covered area based on the results of Chapter 2. When modeling waves over the uncovered area there was little difference between using a Jonswap friction factor of 0.0038 and a Nikuradse roughness of 0.02 m. In the model set-up the effects of wave diffraction as well as wave reflection were ignored, as they are very computationally intensive and only lead to minor variations especially for peak conditions. As model runs are performed in stationary mode this results in values for saturated conditions, so no tidal cycles are modeled. This also means that the effects of tidal currents on wave propagation were not taken into account.

Model analysis

Here, an overview of the seven steps that were performed to obtain the results is given. (1) Scenarios were defined in which three of the following parameters were varied independently: wind speed (4, 8, 12, 16 and 20 ms^{-1}), wind direction (N, NE, E, SE, S, SW, W, NW) and water level (from -0.9 to 2.7 m around M.S.L. with a step size of 0.1 m). (2) SWAN was used to model wave characteristics for all scenarios at all grid points. This was done both for the primary grid as for the nested model grids. For all model runs the root mean squared wave height and near-bed wave orbital velocity were outputted. In this method no offshore wave heights were taken into account. (3) Hourly wind (source: KNMI) and water level data (source: Rijkswaterstaat) for the period 1991 - 2013 were used to create time series of wind speed, wind direction and water levels for each model grid point inside the Dutch WS. These 22 year long time series were made based on the observations of the most nearby tidal station and the most nearby meteorological station. For the wind speeds data from the meteorological stations at Den Helder (WS1) and Lauwersoog (WS2) were used. Water levels were obtained from all water level stations shown in Figure 5.1. (4) The 22 years of wind and water level data for each point were converted to their respective closest binned scenario parameter. In total 5 bins for windspeed (2-6, 6-10, 10-14, 14-18 and $18-22 \text{ ms}^{-1}$), 8 bins for wind direction (rounded to the nearest direction) and 37 bins for water level (values were rounded to the nearest decimeter)

were used. Subsequently, these binned values were linked to a model scenario and the modeled wave orbital velocity was linked to that condition. When no binned value was available the point was excluded. This occurs when a point was emerged, at very low wind speeds ($0-2 \text{ ms}^{-1}$), and for a few very rare extreme wind conditions with wind speeds ($> 22 \text{ ms}^{-1}$ which is 9 bft) or water levels larger than those modeled. (5) From the resulting time series of 22 years of modeled orbital velocities, points for which no wave forcing was modeled were removed. (6) For the remaining modeled orbital velocities the distribution was determined from which average, median and 95th percentile values were determined. The 95th percentile was chosen because this value represents wave conditions during more energetic periods which occur on average about 18 days a year. Also this value is often used in wind climate studies (e.g. Alexandersson et al., 2000), and this allowed for a comparison of the outcomes to these studies. To determine exposure direction, the orbital velocities were filtered based on their respective wind direction. From this data set for each direction the 95th percentile wave orbital velocity was calculated. Subsequently, it was determined for which direction the largest 95th percentile wave orbital velocity was modeled. (7) Using the contours of observed mussel beds in the period 1995-2011 wave forcing in areas covered by intertidal mussel beds was determined.

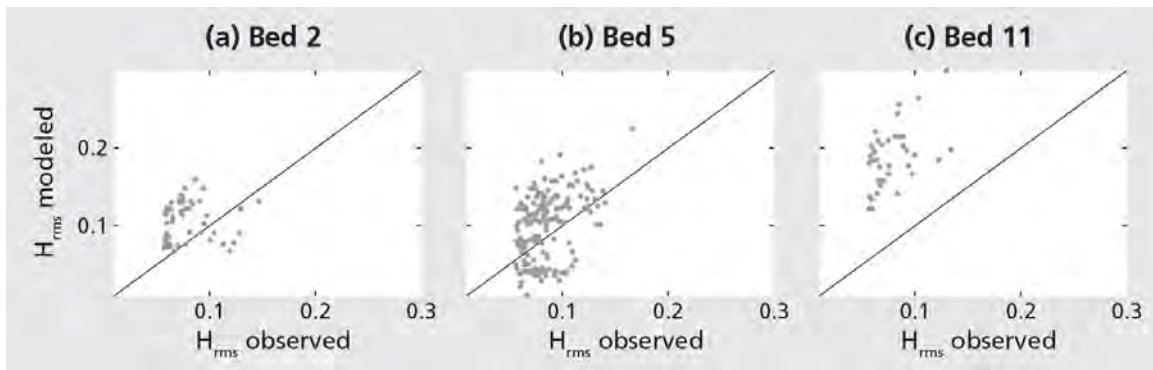


Figure 5.2 Panels a, b and c show the modeled root mean squared wave height as a function of the observed root mean squared wave height for 3 beds in the Dutch Wadden Sea.

Model validation

To validate the model, the measured wave characteristics were compared with the results of the nested model for beds 2, 5 and 11. For this comparison output of the simulations at the grid point located closest ($< 14.1 \text{ m}$) to the location of the pressure sensors was used. For each location time series of wind speed, wind direction and water level were obtained for the measurement period. These time series were, similar to the method presented above, converted to binned values and connected to their respective model scenario. To reduce the differences between model input parameters and observations the range of wind speeds per bin was halved (bins are: 3-5, 7-9, 11-13, 15-17 and 19-21 ms^{-1}). Observations that do not fall within the bin ranges were not used to validate model results. Modeled versus observed root mean squared wave height (H_{rms}) values are shown in Figure 5.2. Results show that modeled wave heights are generally in the correct range

except for bed 11, where model results systematically overestimate the observed wave forcing. Furthermore, there is clear scatter between observations and model results. This is not uncommon as other studies also show scatter between observations and modeled values of significant wave height for conditions with low energetic waves in shallow water (van der Westhuysen et al., 2012; Callaghan et al., 2010). As wind speeds during observation periods were small the validation is biased towards mild wave conditions.

5.3 Wind climate and fetch

First, the relation between wind climate and water levels in the Dutch Wadden Sea is presented, since these together strongly influence the wave climate. The wind climate was analyzed using data from two stations, Den Helder (WS1) and Lauwersoog (WS2). Hourly data of wind speed and direction from 1991 to 2013 were used for the analysis. Furthermore, by comparing the observed water levels to the predicted astronomical tidal levels set-up (or set-down) was calculated.

5.3.1 Wind climate

The wind climate of the Netherlands is dominated by South-Westerly winds. This is clearly illustrated by the wind frequency diagrams for Den Helder (WWS) and Lauwersoog (EWS) (Figure 5.3). Winds from the NW and SE are least common. At the EWS wind speeds are generally smaller than in the WWS. Especially winds from the SW are reduced, because winds from this direction travel more overland for the EWS.

5.3.2 Water level variations

Tides and wind are the two main processes that influence the water levels in the Dutch Wadden Sea. The tidal range in the Dutch Wadden Sea increases in easterly direction. During neap tide astronomical high water levels range from 0.40 m with respect to N.A.P. (Dutch Ordinance Datum) in the WWS to 0.85 m in the EWS. While during spring tide levels they increase from 0.85 m to 1.45 m from the WWS to the EWS. The wind induced set-up as a function of the local wind velocity and direction for the WWS and the EWS is shown in Figures 5.3c and d, respectively. These figures show that wind induced set-up is larger in the EWS than in the WWS. Observed water level deviations show that in general NW winds lead to an increase in water level while SE winds lead to a decrease in water level. Typical water level deviations for SE directions at 10ms^{-1} are -0.45 m in the WWS and -0.6 m in the EWS. Winds from the SSW as well as from the NNE have little effect on the water levels of the Dutch Wadden Sea. A peak in water level increase of 2.2 m occurs for NW winds (320° - 340°) with a 12 hour average wind speed of 15ms^{-1} in the EWS. In the WWS the peak occurs for winds from the West at 18ms^{-1} , generating a set-up of 1.6 m. The largest set-down in water level of 1.3 m is observed for Easterly winds (100° - 120°). Wind-induced water levels significantly modify the tidal water levels, varying from a set-up of 2 m to a set-down of 1 m. Since the Dutch Wadden Sea is a shallow tidal system, water levels strongly limit the fetch. Including the effects of wind speeds and direction on water level is thus essential when studying the wave forcing in the Dutch Wadden Sea.

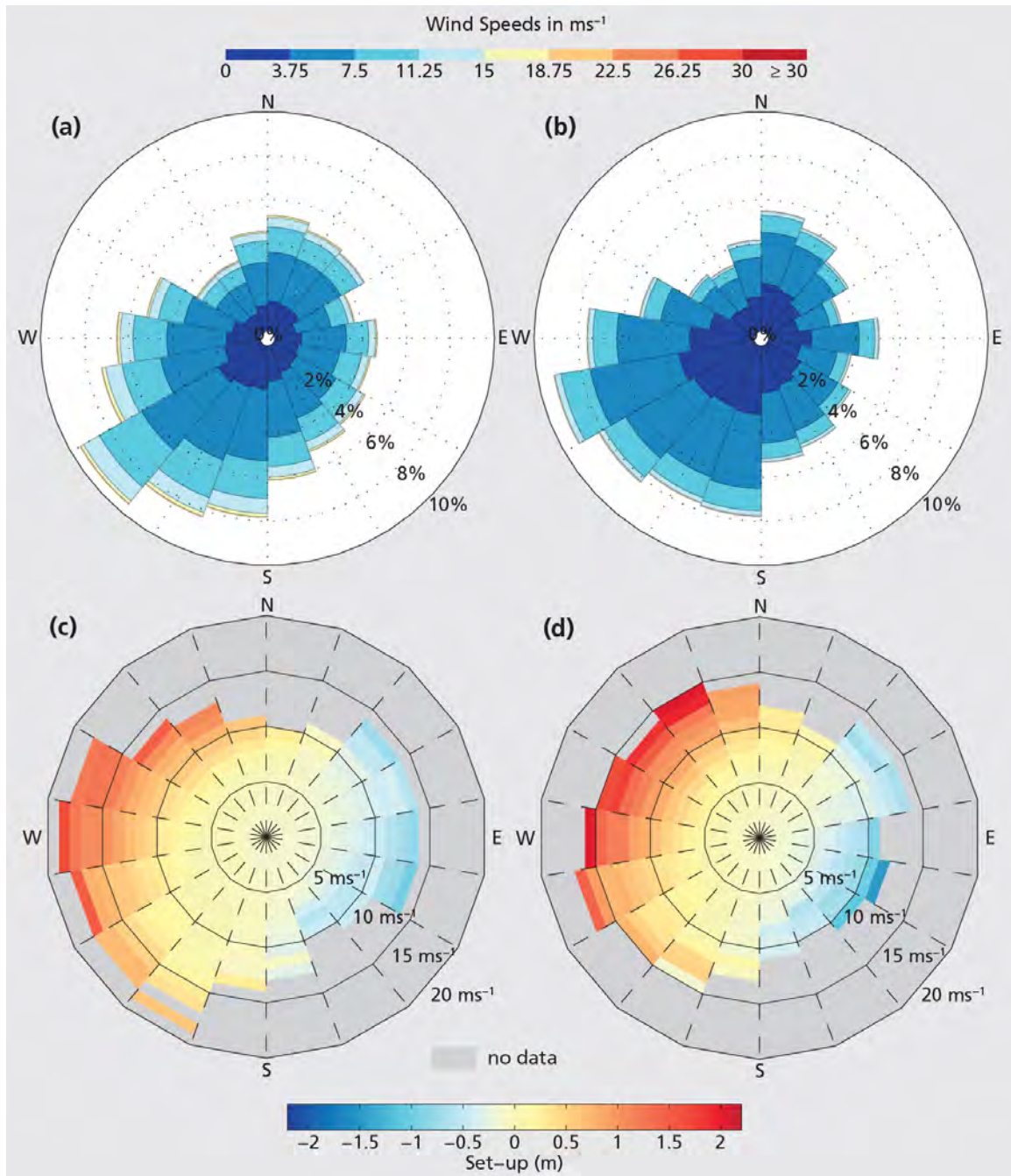


Figure 5.3 Panel a.) Frequency diagram of wind speeds and direction measured at Den Helder (WS1) representing the wind climate in the Western Wadden Sea. Panel b.) Same as Panel a but than for the station at Lauwersoog (WS3). Panel c.) Effects of 12 hour averaged wind speeds and direction on wind induced water level set-up at tidal station in Den Helder (WL1), which is representative for the effects in the Western Wadden Sea. Panel d.) same as Panel c but then for water levels measured in Lauwersoog (WL12) representative for the Eastern Wadden Sea

5.4 Results

In this section, model results are presented on the relation between mussel habitats and wave forcing. First, the spatial distribution of wave forcing (near-bed wave orbital velocity) throughout the Dutch Wadden Sea is presented. It is investigated to which directions the intertidal areas are most exposed and what the role is of wind induced water level elevations on wave forcing. The differences between the tidal basins of the Dutch WS are substantiated and related to mussel bed occurrence. Subsequently, the forcing at the 12 mussel beds is studied in detail and compared with the orbital velocities observed in their respective tidal basins. And finally, exposure of all intertidal mussel bed locations in the period 1995-2011 are compared with the exposure of the intertidal area in general and differences between the WWS and the EWS are investigated.

5.4.1 Near-bed wave orbital velocities in the Wadden Sea

Wave forcing in the Dutch Wadden Sea is investigated by studying the modeled median and 95th percentile wave orbital velocities. The median wave orbital velocities, presented in Figure 5.4a, are fairly constant throughout the intertidal areas of the Dutch Wadden Sea. Largest values occur along the Dutch mainland coast and in the higher lying intertidal areas, because these areas are only submerged when strong winds elevate the water level. The spatial distribution is similar for all basins; the highest orbital velocities are modeled around the channels near the inlet while further away from the tidal inlet wave orbital forcing is small. The largest wave orbital velocities are modeled in the Marsdiep and Vlie basin, these Western basins appear thus to be most exposed. This will be studied in more detail in Section 5.4.2.

Spatial variation in wave orbital velocities is larger at the 95th percentile (Figure 5.4b). Still the pattern of high wave orbital forcing near the sides of the tidal channels and a decreasing trend in landward direction is observed. The peaks in near-bed wave orbital forcing are located in low lying parts of the inter tidal area close to the sides of the tidal channels. Around the tidal channels the highest wave orbital forcing is generally modeled on the North-East sides of the channels. Variation in 95th percentile wave forcing between tidal basins is larger than for the median forcing. Highest wave forcing is found mainly in tidal basins with deeper, broader tidal channels and a relatively smaller amount of intertidal area. As two of these tidal basins (A and C) are located in the WWS, the 95th percentile wave forcing in the WWS appears to be on average larger than in the EWS. Next, the exposure direction at the 95th percentile is investigated. The results of this analysis are shown in Figure 5.5a. Most areas are mainly exposed to winds from the West and South-West. Easterly directions only appear at specific areas such as east of the island of Texel and West of the deeper tidal channels. The dominant exposure direction changes from South-West in the WWS to West in the EWS.

Figure 5.5b shows that taking into account wind induced set-up in water levels is a prerequisite to determine the actual wave forcing in the WS. Figure 5.5b shows the difference between 95th percentile orbital velocity taking into account only astronomical predicted water levels versus real observed water levels. Because most parts are exposed

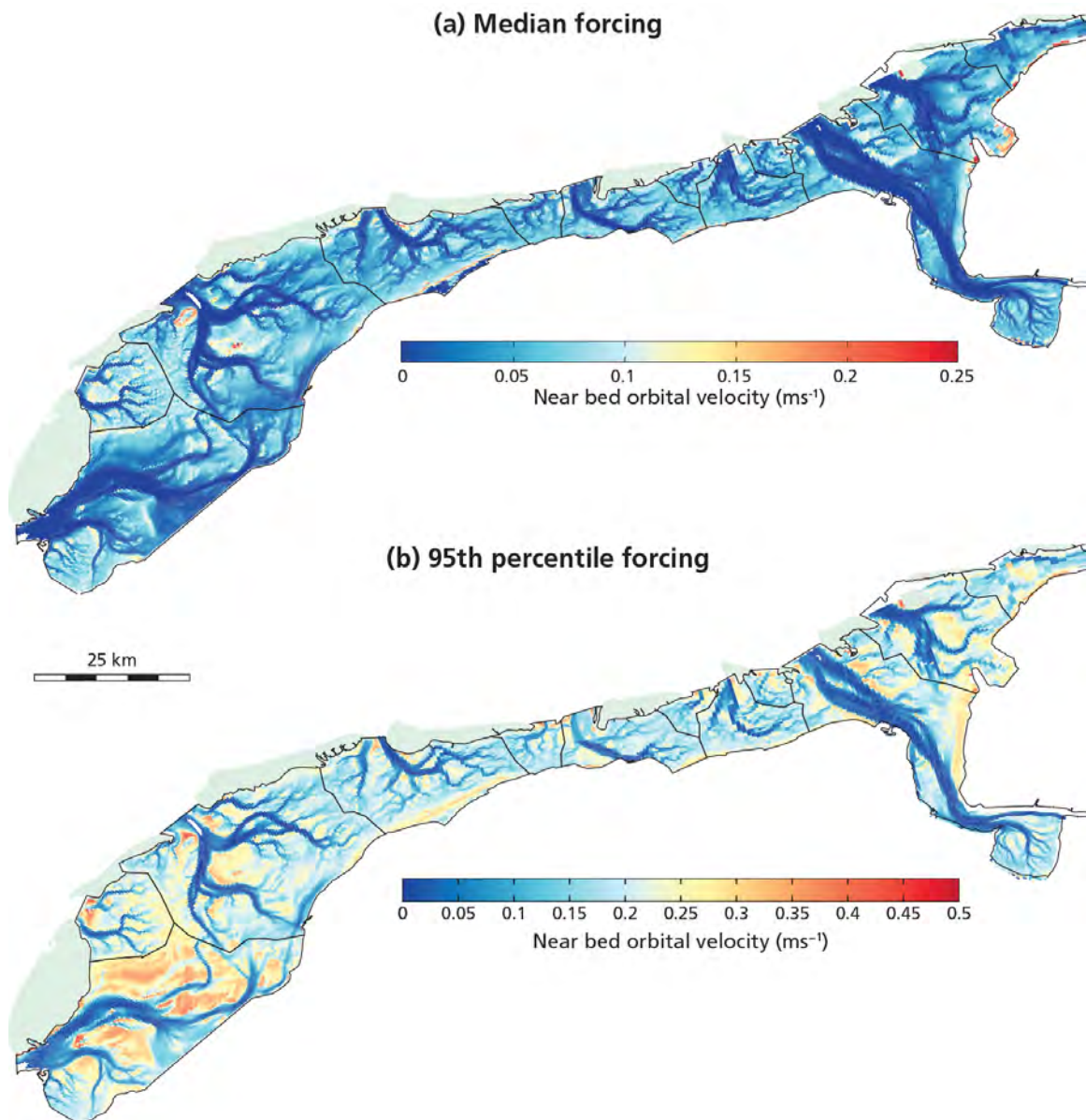


Figure 5.4 Panel a.) Median near-bed orbital velocity in the Dutch Wadden Sea for the period 1991-2013. Panel b.) Same as a, but now the 95th percentile is shown.

to winds from the West the additional set-up may enhance wave forcing in areas where wave forcing is depth-limited. For large parts of the intertidal areas of the Wadden Sea this results in an increase of 10 % with peaks of 20 % in wave orbital velocity at the 95th percentile. As bed shear stresses are related to the orbital velocity squared a 20 % increase in orbital velocity results in an increase in bed shear stresses of 44 %. Parts that are exposed to winds from the East have smaller wave orbital motions because of the wind-induced set down that limits wave generation.

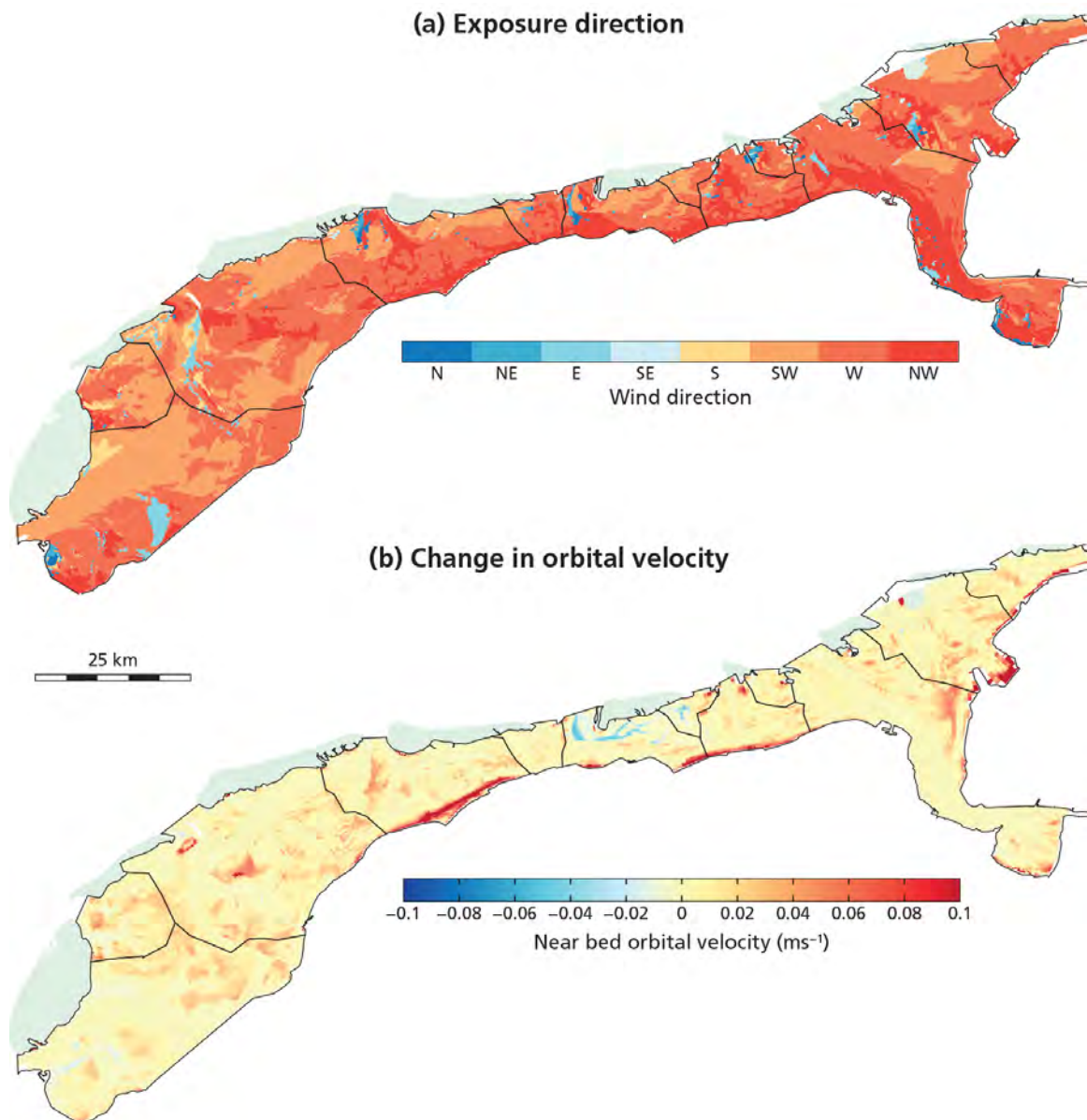


Figure 5.5 Panel a.) Direction for which the highest 95th percentile near-bed wave orbital velocity is calculated for each point. Panel b.) Change in near-bed wave orbital velocity at the 95th percentile when comparing results for astronomical tide only with results for the measured tides.

5.4.2 Wave exposure per basin

Differences between basins and between the WWS and EWS are investigated by studying the median and 95th percentile near-bed wave orbital velocity averaged (taking into account variations in grid size) over the intertidal area of each basin. The intertidal area is defined here as the area located between -1.25 m to +0.25 m with respect to N.A.P., this depth range was chosen since 90% of the intertidal mussel beds are located between these depths. The same range is used for the WWS and EWS as differences in mussel bed level are small, in the WWS on average mussel beds are located 0.1 m deeper. The median and

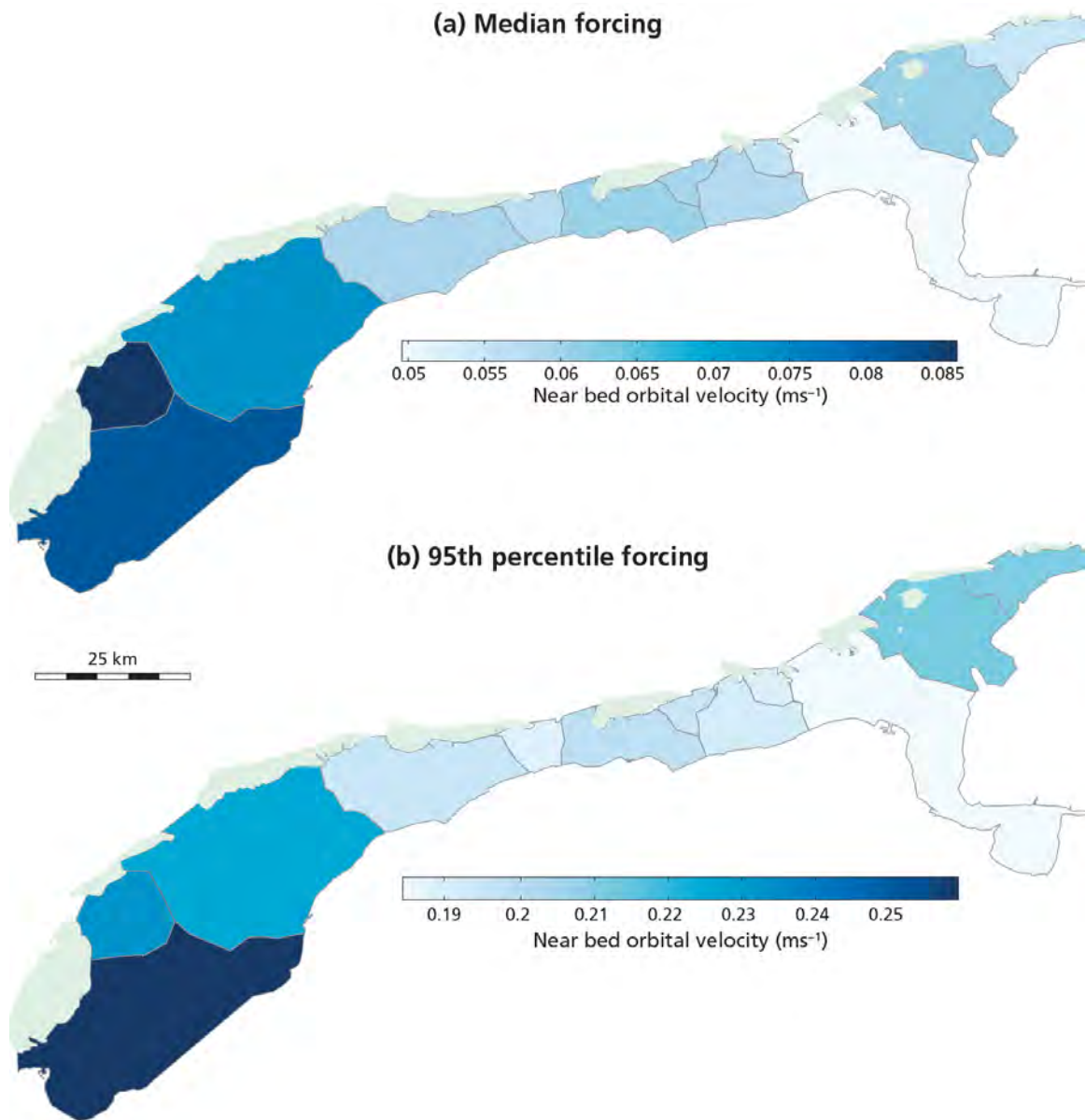


Figure 5.6 Panel a.) The median near-bed orbital velocity for the intertidal area of each basin in the Dutch Wadden Sea for the period 1991-2013. Panel b.) Same as a, but now the 95th percentile is shown.

95th percentile wave forcing for each basin are shown in Figure 5.6a and b, respectively. Results reveal that mussel beds in the West are located slightly deeper than those in the East. Basin-averaged median near-bed wave orbital velocities vary between 0.05 and 0.085 ms^{-1} . The relative differences between basins are almost 50%. Furthermore, observations show that the median wave forcing is largest in the three westerly basins. At the 95th percentile, the spatially-averaged wave forcing varies between 0.19 ms^{-1} in the EWS and 0.26 ms^{-1} in the WWS.

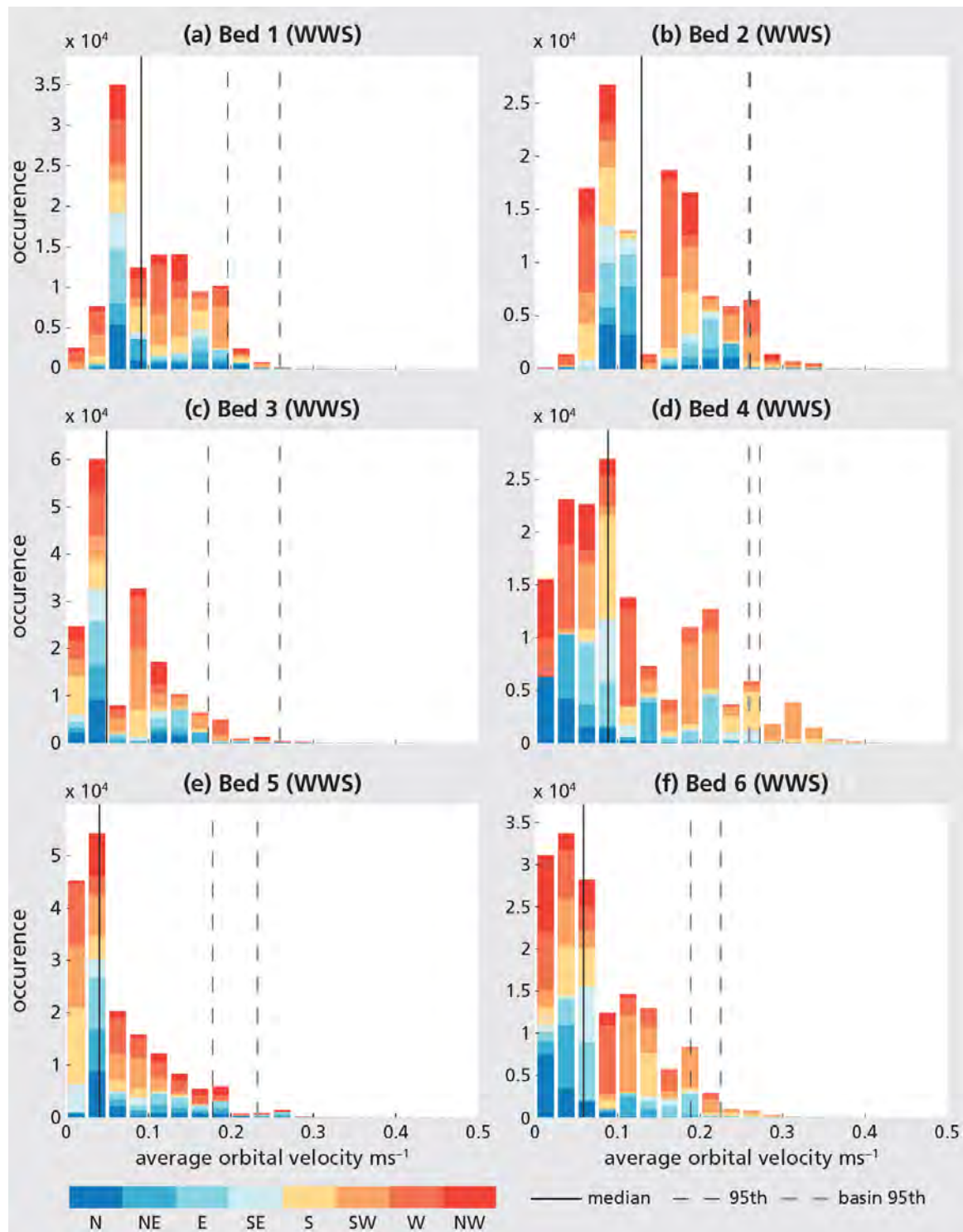


Figure 5.7 Histograms of near-bed wave-orbital velocity on the studied intertidal mussel beds in the EWS (panels a to f) and WWS (panels g to l). Colors indicate the contribution of the different wind directions to the total. (Continues on next page)

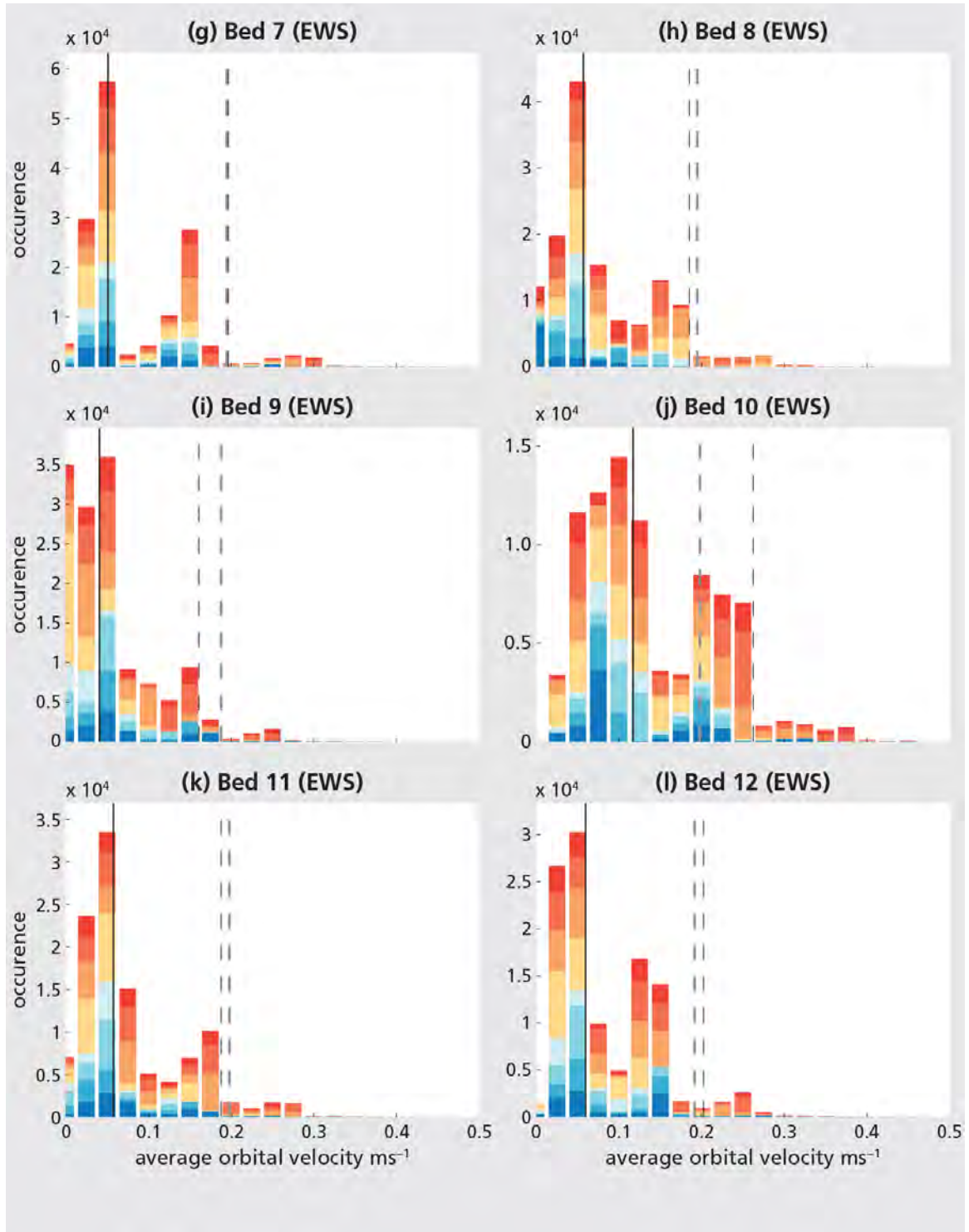


Figure 5.7 (Continued) The solid and dashed black lines indicate the median and 95th percentile near-bed wave orbital velocity, respectively. The red dashed line indicates the 95th percentile near-bed wave orbital velocity of the basin (Figure 5.6b) in which the mussel bed is located.

The absolute difference in forcing is thus about two times as large for the 95th percentile than for the median forcing. Relative differences though are smaller than for the median forcing. The differences between WWS and EWS are also clear at the 95th percentile, as wave forcing in the Westerly basins is larger than in the Easterly basins.

5.4.3 Wave exposure at the 12 focus beds

Next, the wave exposure at the 12 focus beds is studied to investigate the distributions of near-bed wave orbital velocity and the contribution of the different wind directions. For bed 10 no grid point falls within its contour, and therefore the closest grid point was chosen. In Figure 5.7 histograms of wave orbital motion are shown for the 12 beds. Each diagram also shows the contribution of each wind direction to the orbital velocity distribution. Results reveal some variation in the median orbital velocities between beds as the median values vary between 0.038 and 0.13 ms^{-1} . The average median wave forcing is slightly larger on the beds in the WWS (beds 1-6) than on the beds in the EWS (beds 7-12). Larger differences between mussel beds become apparent at the 95th percentile. At the 95th percentile, values vary between 0.16 and 0.27 ms^{-1} . For 9 of the 12 beds the orbital velocity at the 95th percentile is around 0.2 ms^{-1} . A comparison between orbital forcing per bed and average forcing per basin shows that for the beds in the WWS the near-bed orbital velocity at the 95th percentile is for 4 out of 6 beds significantly smaller than for the average forcing inside the basin. These differences are generally small. Two beds are slightly more exposed than the basin average. While for the beds in the EWS wave forcing is for 4 of the 6 beds larger than the average orbital forcing inside the basin at the 95th percentile. Furthermore, a more detailed look on the histograms reveals that some distributions are bi-modal. This is most likely the result of the differences in orbital velocity during low water and during high water under calm conditions.

Above the 95th percentile nearly all mussel beds are mainly exposed to winds from the three westerly directions. Only bed 5 deviates, as it is also exposed to the Northern and Eastern directions. A detailed study of the peak in wind direction reveals variation in dominant direction between the South West, West and North West. In general, above the 95th percentile wind conditions from the SW are dominant in the West, winds from the West winds are more important in the East. This is similar to the pattern in mean exposure direction that was observed for the tidal basins.

5.4.4 Mussel bed exposure

The relation between mussel bed occurrence and the near-bed wave orbital velocity for all mussel beds observed since 1995 in the Dutch WS is studied here. First, the relation between wave exposure for each tidal basin is analyzed and the relative intertidal mussel bed coverage (in %) in each basin. The average coverage is defined as

$$\text{coverage} = \frac{\text{area}_{\text{covered}}}{\text{area}(-1.25 < z < +0.25)}. \quad (5.1)$$

In Figure 5.8a the average spring coverage of mussel beds between 1995-2011 in each tidal basin is compared with the average wave orbital velocity at the 95th percentile. Results

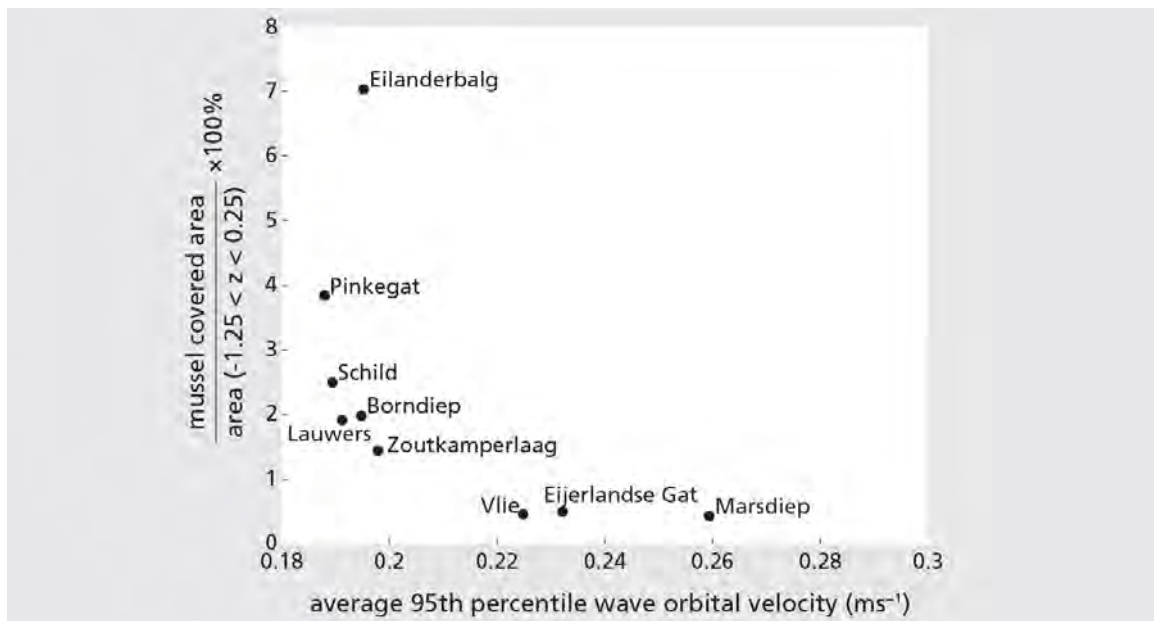


Figure 5.8 The percentage of intertidal area covered by mussels in each basin as a function of the average near-bed wave orbital velocity over the intertidal area of that basin.

show that the average intertidal mussel bed coverage drastically reduces for increasing wave forcing. However, in highly exposed basins there is little variation between mussel bed coverage and exposure, a small portion of mussel beds remains. Thus mussel beds occupy a larger portion of the intertidal area in less exposed basins.

Next, the average near-bed wave orbital velocity to which the intertidal area is exposed is compared with the average near-bed wave orbital velocity to which the mussel beds are exposed. The average 95th percentile near-bed wave orbital velocity at all mussel beds in the Dutch Wadden Sea is $0.197 \pm 0.038 \text{ ms}^{-1}$ while the average for all intertidal areas is $0.229 \pm 0.055 \text{ ms}^{-1}$. In Figure 5.9 a box-plot of the near-bed wave orbital velocity amplitude above the beds and intertidal area are shown for the WWS and EWS respectively. In the plot both the median (red line), 25 and 75 percentile (gray box), average (μ with a black cross) and standard deviation (σ with bars) are shown. All shown averages and median values differ significantly at the 95th percentile. In the WWS the near-bed wave orbital velocities above the mussel beds are significantly smaller than in the tidal basin as 75% of the mussel beds is below the median value of the intertidal area. This means that wave exposure is limiting the area suitable for mussel bed settlement in the WWS. In the EWS wave forcing is not an important limiting factor as there is little difference between median and average values.

Although, wave forcing is clearly not the only factor influencing mussel bed stability, a first estimate of suitability of the intertidal area based on wave exposure is now made. Here the obtained estimates of average wave forcing on mussel beds are compared with wave forcing on the intertidal areas of each basin. Table 5.1 shows how much of the intertidal area of each basin is located below the average wave orbital forcing on mussel beds (μ) and how much of the intertidal area is located below another threshold value

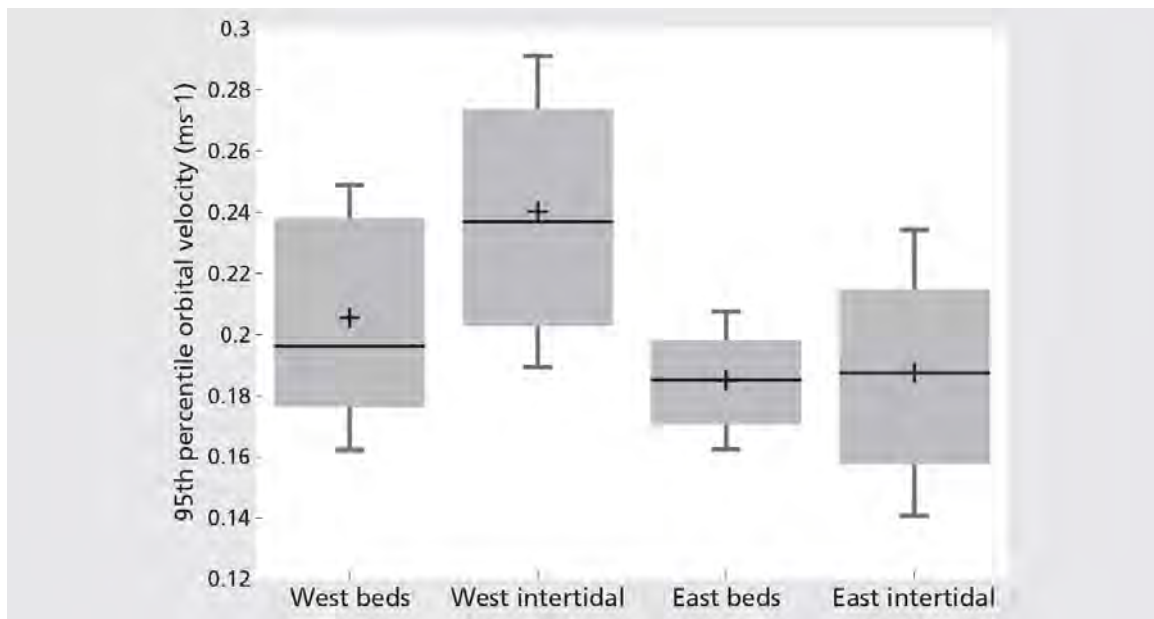


Figure 5.9 Box plots of the orbital velocity on mussel beds between 1995 and 2012 for the East and West together with box plots of orbital velocity in the intertidal area of the WWS and EWS.

($\mu + \sigma$). The latter threshold value is determined by adding the standard deviation to the average wave orbital velocity. In the basins of the WWS only around 20 % of the intertidal area is exposed to wave orbital velocities smaller than μ . While for the Eastern basins this is around 60%. The area that is below $\mu + \sigma$ is for all basins larger, for this threshold value in the Western Basins over 50% more area is available. In the EWS also the increase in area between μ and $\mu + \sigma$ is large but relative increases are smaller than in the WWS. For Eilanderbalg a very large portion of the intertidal area is located in the range $\mu - \mu + \sigma$, values are relatively high because all intertidal area is located close to the inlet, however very high values do not occur as the basin is sheltered from Schiermonnikoog.

5.5 Discussion

In this study, the hypothesis that wave forcing limits settlement of stable mussel beds in the WS was further investigated. Results show that wave forcing on the intertidal area of the WWS is much larger than in the EWS. Furthermore, they reveal that the average 95th percentile wave forcing too which mussel beds in the WWS are exposed too is significantly lower than the basin-averaged value while in the EWS these differences are smaller. Finally, the dominant exposure direction was found to be SW for the WWS and W for the EWS. Here, the results and their implications are discussed.

The SWAN wave model was used to simulate wave forcing in the Dutch Wadden Sea. Several studies have shown that the model predictions are reasonable but certainly not perfect in shallow areas such as tidal basins (Callaghan et al., 2010; van der Westhuisen et al., 2012). This was also highlighted by the validation presented in Section 5.2.4. In the model study the effects of currents through wave-current interaction and the

Tidal basin	exposure < 0.197 ms ⁻¹	exposure < 0.236 ms ⁻¹
Marsdiep (West)	18%	33%
Eijerlandse Gat (west)	18%	53%
Vlie (West)	26%	63%
Borndiep (East)	56%	90%
Pinkegat (East)	69%	90%
Zoutkamperlaag (East)	52%	83%
Eilanderbalg (East)	17%	88%
Lauwers (East)	59%	89%
Schild (East)	66%	84%
Eems-Dollard (East/Germany)	61%	86%

Table 5.1 Percentage of area that is exposed to a wave forcing with a value that is below the average and the average + the standard deviation of the wave orbital velocity.

spatial differences in water level were ignored. This was done such that wave forcing representative for a 22 year long period could be estimated from a limited amount of scenarios. This would not have been possible when taking the effects of currents and spatial differences in water level into account. The simulations were run in stationary mode and the model outcomes represent saturated wave conditions: as if the water levels and wind were static over a long period. But, especially for large fetches this will lead to an over-prediction of the wave forcing. Nevertheless, although there is potentially a difference in absolute values, the spatial patterns will be most likely similar under increased wave forcing. The spatial distribution in wave orbital velocities at the 95th percentile was compared with those at the 90th percentile and while absolute values differ, spatial patterns are very similar. There are also uncertainties in the applied input data that will influence model outcomes. Measurement stations are located at the edges of the measurement area and bathymetry data is only updated once every six years. Because the morphology in the Wadden Sea changes in time, some morphological adaptations may have occurred between the time the sounding was performed and the measurement of the mussel bed contours. This study omits the largest storms (>22 ms⁻¹ or water levels larger than 2.7 m). To stimulate the wave forcing during these storms a different model set-up is required, because wave penetration from the North Sea occurs during these conditions. To accurately model wave presentation from the North Sea, offshore wave conditions at the boundary of the model domain should be taken into account. Moreover, the relation between mussel bed occurrence and wave forcing during a storm has already been investigated by Brinkman et al. (2002). Despite all these model shortcomings these results reveal clear patterns in wave forcing.

Results of the study reveal a clear difference in wave forcing at the 95th percentile (~18 days a year) throughout the Dutch Wadden Sea, while differences in median wind forcing are small (0.02 ms⁻¹). Especially the basins which contain deeper tidal channels have on average higher near-bed orbital velocities at the 95th percentile relative to nearby shallower basins. Results show a clear distinction in wave forcing between the WWS and

EWS. The differences in wave orbital forcing also are reflected in the intertidal mussel bed coverage. More exposed basins have low mussel bed coverage while calmer basins have high intertidal mussel bed coverage. While there are large differences between the Eastern and Western tidal basins, there is little variation between the wave orbital forcing to which beds in the West and East are exposed. In the Western Basins though, average wave forcing on the intertidal zone is larger than on the mussel beds located in these basins. While in the less energetic EWS basins mussel beds are located at locations which are slightly more exposed with respect to the basin-averaged wave forcing. It suggests that wave forcing in the WWS is more a limiting factor for habitat suitability than in the EWS. This is confirmed by the estimates of intertidal area suitable for mussel bed presence, which are much smaller in the west. Consequently, mussel cover in the Western Wadden Sea will be more sensitive to changes in wind climate than in the EWS. A small increase in wave forcing would reduce the relative area suitable for settlement in the Western Wadden Sea. Apart from mussel beds also other intertidal biota are affected by these variations in wave forcing in the Wadden Sea. Species richness for example, has been reported to be reduced in more exposed intertidal areas as sediments become more coarse and stability is reduced (Gray, 2002).

The results of this study show a strong relation between wave exposure and mussel presence on intertidal areas in the Dutch Wadden Sea. This confirms the outcomes of the habitat suitability analysis performed by Brinkman et al. (2002). However, in their study, forcing during only one large storm event was used to determine the effects of wave forcing on habitat suitability. The results show that not only storms, but also median and more energetic conditions are reflected in mussel cover. They also give a more representative estimate for the degree of wave exposure locations in the Wadden Sea. The less energetic conditions might influence the settlement of stable mussel beds especially in the early stages, when they are most vulnerable. Remarkably, Folmer et al. (2014) investigated the relation between persistence of adult (> 1 yr) mussel beds and storminess and found no decrease in intertidal mussel coverage after a year with large storms. It must however be noted that they based storminess on wind speeds only. The present study shows that wind direction and set-up have a large impact (20 to 45% increase) on the spatial distribution of wave forcing, in particular for energetic (95th percentile) wind conditions.

By calculating wave forcing at different percentiles the outcomes of this study can also be related to future predictions from wind climate studies. Changes in wind climate might have contributed to the current low mussel bed coverage with respect to that the 1970ties (Dankers et al., 2001). Historical records indicate that 95th percentile as well as 99th percentile wind speeds in the North Sea basin have increased since 1960 (Alexandersson et al., 2000; Weisse et al., 2005; Feser et al., 2014). In addition, in the period 1990 to 2005 these wind speeds were larger than in the period between 1930-1980. Also an increase in grain size for the German Wadden Sea related to increased hydrodynamic forcing was observed by Bartholomä and Flemming (2007). Model studies on future (2071-2100) wind conditions in the North Sea Basin, by de Winter et al. (2012), show an increase in 99th percentile wind conditions for the W and SW, while showing a reduction for those from the N and NW. Given that the basins of the WWS are more exposed to

waves, and wave forcing is anticipated to be a more important factor limiting habitat suitability, this implies that increased winds from the W and SW limits the suitability of intertidal areas for mussel bed settlement even further. For the EWS these effects are smaller as the intertidal area is more exposed to the W and NW and the sensitivity to increased wave forcing is smaller.

5.6 Summary and conclusions

In this chapter the spatial distribution of wave forcing in the Dutch Wadden Sea was studied and related this wave forcing to the presence of intertidal mussel beds. By combining model simulations of 1480 scenarios and 22 years of observations on wind speed, wind direction and water level statistically representative estimates of wave forcing in the Dutch WS for a 22 year period could be established. The obtained maps of both median and 95th percentile wave forcing were used to study the spatial distribution of wave forcing in the Dutch WS. Spatial patterns inside tidal basins were similar: the highest near-bed wave orbital velocity amplitudes were modeled around the tidal inlet, especially eastward of the main tidal channel, and reduce further inside the basin and towards the mainland. Wave forcing in the Dutch WS is strongly influenced by the effect of winds on water levels. Wind induced set-up occurring for NW winds result in up to 40% higher bed shear stresses on the intertidal areas. A comparison of wave forcing between basins reveals that the basins of the WWS are exposed to a larger wave forcing than the basins in the EWS. This is caused by the enhanced wave generation in the deeper tidal channels in the Western Wadden Sea. Wave forcing inside the basins of the EWS is smaller because tidal channels are smaller and shallower, thereby limiting the wave growth. Besides, the WWS is more exposed to the dominant SW wind direction while the EWS is more exposed to the less frequently occurring winds from the W and NW. Differences in wave forcing between the WWS and EWS are reflected in intertidal mussel coverage. In the EWS mussel bed coverage is much larger (~ 2%) than in the WWS (< 0.3%). Moreover, in the WWS wave forcing on intertidal area is significantly larger than that on intertidal mussel beds and is therefore a limiting factor for the settlement of stable mussel beds. In the EWS, the near bed orbital velocity amplitudes over intertidal mussel beds and over the whole intertidal area are comparable. This suggest that wave forcing only limits the settlement of stable mussel beds in the WWS.

6 Conclusions and Perspectives

6.1 Introduction

The main objective of this thesis was to study the influence of hydrodynamic processes on the stability of intertidal mussel beds in the Dutch Wadden Sea (WS). This required both an understanding of the small-scale physical forcing exerted on the mussel bed by waves and currents, and also a thorough understanding of the attachment of mussels to the substrate. Mussels attach themselves to the bed by means of byssal threads; to maintain this attachment, food delivery by tidal current is needed. Furthermore, the large-scale pattern of mussel bed occurrence and physical forcing needed to be established. The general approach was to combine detailed process measurements on the small-scale, long-term monitoring of mussel cover and large-scale modeling. In Section 6.2, the methods and research results obtained in each chapter are summarized. A detailed discussion of the results is not given here as it is given in the discussion sections of the respective chapters. In Section 6.3, the main conclusions are presented and the findings of this thesis are related to the broader aim of project Mosselwad. Also, I give my perspective on how the results presented in this thesis can be used to increase the amount of mussel covered area in the Dutch WS.

6.2 Summary of main findings

6.2.1 Hydrodynamic forcing over an intertidal mussel bed (Chapter 2)

Bed shear stresses on an intertidal mussel bed were studied at a mussel bed located on a tidal flat north-east of the island Texel. Field measurements on wave, current and turbulence characteristics were performed using an Acoustic Doppler Velocimeter (ADV) on top of an intertidal mussel bed. Moreover, the spatial distribution of wave orbital velocities were determined using two perpendicular arrays of pressure sensors. The analysis of the obtained field measurements revealed that bed shear stresses exerted by wave orbital velocities are the dominant shear stress for a flat, uniformly covered intertidal mussel bed. However, bed shear stresses from currents can, especially through wave-current interaction, contribute significantly to the total bed shear stress. No evidence of wave breaking is found and waves attenuate energy by bed friction. Using both wave attenuation and dissipation of turbulent kinetic energy, the Nikuradse roughness is estimated at 0.05 m. This value was used in a subsequent model study to determine the spatial variation in wave forcing in more detail. Model results show that inner parts of the mussel bed are sheltered against wave action, since relatively large parts of the incident wave energy are dissipated at the edges and outer parts of the mussel bed. The largest forcing on the bed is observed on the edge exposed to the Dutch Wadden Sea. A model

simulation of the spatial distribution in wave forcing prior to the settlement of the mussel bed shows that this exposed edge is located in an area previously characterized by a local minimum in wave forcing. This suggests that the mussel bed is located optimal with respect to wave forcing.

6.2.2 Effects of flow patterns over high relief mussel beds on food availability (Chapter 3)

Although the shear stresses of currents in intertidal zones in the Wadden Sea are generally small, the transfer of food by currents towards the bed is important for food availability. Therefore in Chapter 3, the effect of elevations in patterned mussel beds on food availability was studied using a combination of field measurements and model simulations. Field measurements were gathered using ADVs located on top and adjacent to an elevated mussel patch (hummock) inside a mussel bed to investigate the flow difference between the locations. These measurements show that during the majority of the tidal cycle, flow velocities and turbulence intensity over the hummock were increased with respect to those next to the hummock (small channel). A peak in channel velocities is observed just before the hummock emerged, suggesting flow routing and reduced advection of food towards the hummock. Especially the latter suggests that at least part of the flow is routed around the mussel hummock, reducing advective transport of food towards the hummock. The occurrence of two flow regimes was further investigated using SWASH, a numerical model which solves the non-linear shallow water equations with the addition of a non-hydrostatic pressure term to the horizontal momentum equation and a vertical momentum equation. In this model flow behavior around an idealized mussel hummock was investigated. Obtained model results confirm the observations of flow routing around and acceleration over the mussel hummock. Using a coupled advection-diffusion model with explicit food uptake, the effects of hummock patterns on food availability were determined. Results reveal that flow routing reduces advective food transport but that this can be compensated by increased vertical mixing. However, results depend on hummock geometry; broader hummocks tend to increase the hummock acceleration type flow, while more elongated hummocks tend to promote flow routing. Banded patterns are thus optimal for food uptake.

6.2.3 Impact of erosion by ice scour on the long term development of an intertidal mussel bed (Chapter 4)

The long term effects of hydrodynamic processes on mussel bed stability were investigated in Chapter 4. A mussel bed is unstable when large hydrodynamic forcing is capable of eroding mussels from the bed, ultimately leading to a total removal of the mussel bed. To assess long term stability, mussel coverage and topography of the mussel bed near de Cocksdorp (same location as in Chapter 2) was monitored for a 27 month period. Monitoring consisted of daily observations of mussel cover using a rotating camera system on a 10 m high pole and morphological observations from a 3D terrestrial laser scanner every 3 months. Early during the measurement period the bed suffered erosion by ice action, after which a slow recovery took place. Two years later, the bed was again damaged, this

time by storms. Results of topography measurements show that ice action, in particular ice scour, results in removal of mussels from the bed at the region of impact, while bed height in the surrounding areas is increased. The bed hardly recovered, while in the surrounding areas more sediment became consolidated and height increased, resulting in increased relief. The mussel bed was damaged again 19 months later, this time by wave action. Erosion was largest in areas surrounding the location that previously suffered erosion from ice scour. These results suggest a synergy between erosion by ice action and wave forcing. Leading to the hypothesis that ice action increases the exposure of the surrounding area to erosion by; (1) increasing the relief and thereby the exposure to waves; (2) decreasing attachment strength by limiting food availability.

6.2.4 Spatial trends in wave forcing in the Dutch Wadden Sea and the implication for mussel habitat suitability (Chapter 5)

The results of Chapter 2 have shown that wave induced bed shear stresses were responsible for the largest hydrodynamic forcing on mussel beds. Therefore, in Chapter 5 the wave model SWAN was used to determine the near-bed orbital velocity amplitudes in the Dutch WS for 1480 environmental conditions. The wind speed, wind direction and water level were varied and for each condition the near-bed root mean squared orbital velocity was determined for all locations in the model domain. Subsequently, for each location a time series of near-bed root mean squared orbital velocities was determined based on 22 years of observed water levels and wind conditions. For each location the median and the 95th percentile of wave orbital forcing was determined. Subsequently, locations exposed to high and low wave orbital forcing were identified. The obtained spatial distribution of wave orbital forcing on the intertidal flats was further used to study whether wave forcing limits the settlement of stable mussel beds in the Dutch Wadden Sea. Moreover, the role of wind-induced set-up and set-down on the forcing was investigated. Wave forcing is largest in the three basins of the Western Wadden Sea (WWS) and smallest in the Eastern Wadden Sea (EWS). The WWS is predominantly exposed to waves from the south-west, the EWS to waves from the west. Wind induced water level set-up occurring for wind from the NW leads to an increase in wave forcing at the 95th percentile up to 20%, which results in a 44% increase in bed shear stress. In the exposed WWS a much smaller part of the intertidal area is covered by mussels than in the less exposed EWS. Furthermore, in the WWS mussel beds are located in areas that are exposed to much wave lower forcing than the basin average, while in the EWS the average forcing on mussel beds is close to the basin average. Differences between mussel bed averaged wave forcing between the EWS and the WWS are small, however, forcing on mussel beds in the WWS is slightly larger. Spatial patterns of wave forcing during normal and more energetic conditions show large similarities. The results show that in the WWS the near-bed wave orbital velocity amplitudes are so high that they limit the settlement of stable mussel beds.

6.3 Perspectives

Results presented in this thesis were part of the broader context of project Mosselwad: to increase both settlement as well as the persistence of mussel beds in the (Western) Dutch Wadden Sea. Results have shown that hydrodynamical conditions to which a large portion of the intertidal in the WWS is exposed are unfavorable for the settlement of stable mussel beds. Future projections for the wind climate indicate that over time these opportunities for natural increase are more likely to decrease than to increase. This means that when an increase in mussel bed area in the Dutch Wadden Sea is desired this would require active human intervention. In order to increase mussel bed area several practical approaches are available:

1. Creation of a new mussel bed at favorable locations where wave forcing is limited.
2. Restoration of an existing intertidal mussel bed.
3. Increase of natural settlement of stable mussel beds by influencing hydrodynamical boundary conditions.

The results of thesis and other research on mussel beds can be used to determine the approach and assess the feasibility of these restoration methods. First the main conclusions of this thesis are presented bullet wise followed by the practical implications of these findings.

6.3.1 Main conclusions

- Shear stress induced by wave orbital motions is the largest shear stress on a flat, uniformly covered intertidal mussel bed. (C2)
- The large roughness of mussels and the presence of an edge causes substantial protection of mussels inside the bed. (C2)
- Increased relief of an intertidal mussel bed leads to acceleration of flow over and routing of flow around mussel hummocks. (C3)
- Flow acceleration and routing result in changes in advective and turbulent food transport, influencing the uptake of food by mussels. (C3)
- Ice action is able to considerably damage an intertidal mussel bed. (C4)
- Damage by ice action exposes the mussel bed to further erosion by waves, this suggests a synergistic relation between the two eroding agents. (C4)
- Under both calm as well as more energetic conditions, near-bed wave orbital velocity amplitudes are largest in the Western Wadden Sea and smallest in the Eastern Wadden Sea. (C5)
- Shear stresses resulting from wave orbital motions limit settlement chances for mussel beds in the Western Wadden Sea. (C5)

6.3.2 Creating a new mussel bed

To create a new mussel bed, the choice of a viable location is important. Results presented in Chapter 5 show that areas with low wave orbital forcing should be chosen. Also, when selecting a location food availability must be taken into account. The detailed wave orbital forcing maps presented in Chapter 5 can be integrated with the currently used habitat suitability analysis which is an improved version of the one presented in Brinkman et al. (2002). When an intertidal area is chosen for the restoration of an intertidal mussel bed it is recommended that a detailed study on wave forcing is performed. Locally variations in local morphology affect wave forcing. Moreover, results of Chapter 2 show the edges of the bed oriented perpendicular to the gradient in hydrodynamic forcing. By nesting a high resolution grid into the large scale model of Chapter 5, high resolution results are obtained. A similar approach has been performed to obtain estimates of wave forcing over intertidal mussel beds in wa Kangeri et al. (2015). Results of Chapter 2 also show that wave attenuation reduces wave exposure inside the bed. This effect is strongest when the height increase in the direction of wave propagation is small. Thus, restoration of a mussel bed on a relatively flat part of the intertidal area allows the bed to provide shelter for its inner regions.

Recently, several experiments have been performed in which mussel beds were created; one in the context of project Mosselwad (www.mosselwad.nl/) and three in the context of the project Waddensleutels (www.waddensleutels.nl/). In the Mosselwad experiment mussels fished from the subtidal mussel beds were seeded at a low density from a ship on an intertidal flat in the Balgzand area near an existing intertidal mussel bed (Bed 2 in Chapter 5). The Waddensleutels plots were implemented on intertidal areas below the islands of Terschelling, Ameland and Schiermonnikoog. These beds were smaller and created by hand. All these restoration efforts did not result in the formation of a new stable mussel bed as all mussels were eroded away within a few months after the start of the experimental development. All four experimental locations where, according to the wave forcing maps presented in Chapter 5, located at sites which were exposed to a wave orbital forcing that exceeds the average wave orbital forcing on existing beds. In addition, the Balgzand bed was seeded at a low density.

Because the substrate in the Dutch Wadden Sea consists of soft sediment, mussels need to clump together to survive. At very low densities the mussels will be unable to clump together, resulting in high mortality (Bertness and Grosholz, 1985). Moreover, interconnectivity in self-organized spatial patterns increases at high densities (van de Koppel et al., 2008). Also, mussels protect each other and the underlying sediment from full exposure and decrease hydrodynamic forcing by attenuating wave energy (Chapter 2). Apart from creating beds at high densities, deploying mussel beds with spatial patterns could increase the chance of success. Studies by van de Koppel et al. (2005) and Liu et al. (2014b) show that large-scale (~10 m) patterns in mussel beds increase the resilience of the bed. However, little is known on the relation between pattern type (uniform, banded, patch) and local conditions because the underlying process is still not yet fully understood (Liu et al., 2012). The results presented in Chapter 3 suggest that the spatial patterns can have a strong influence on food availability but this has not been studied in the field. Mussel beds also accumulate sediment (Van Leeuwen et al., 2010), thereby

changing the characteristics and stability of the bed on the long term. Characteristics of the underlying substrate (grain size, presence of coarse shell material and degree of consolidation) influence the stability as well (wa Kangeri et al., 2014). These effects should be taken into account to increase survival chances of newly created mussel beds.

6.3.3 Mussel bed restoration

The required high density of mussels and the low chance of success make the creation of a new mussel bed unfavorable and expensive. Restoration of existing mussel beds seems to be a more viable option. The fact that locally a mussel bed exists shows that it is a viable location. By filling in the empty parts of the mussel bed, these restoration locations will be protected. However, it is important to determine why an area inside the bed is uncovered. An area might be uncovered as a result of erosion by large hydrodynamic forcing, but also due to pattern formation or a decrease in attachment strength resulting from limited food availability. The location inside the bed could thus be empty because local conditions are unfavorable for survival. Results of Chapter 3 showed that food availability changes as a result of the formation of increased relief. Also, it was suggested by Liu et al. (2014b) that resilience of uniformly covered mussel beds against food limited conditions is low compared to that of patterned mussel beds. Consequently, filling up uncovered areas in naturally formed patterns could even reduce the stability of the bed.

In order to study the feasibility of mussel bed restoration a transplantation experiment was performed in September 2012. Patches (1×1 m) of an intertidal mussel bed were extracted from the bed and placed on bare areas inside the bed. A control experiment was performed on an empty part of the tidal flat adjacent to the mussel bed, but at a similar distance from the tidal channel. The evolution of these patches was monitored in a similar way as in Chapter 4. Preliminary results show that inside the mussel bed all created patches survived and expanded, while the control plots were all eroded. This suggests that restoration of a mussel bed using intertidal mussels is, despite the above mentioned issues, a viable method to increase mussel cover inside a mussel bed. However, as mussel bed area is based on bed contours (Folmer et al., 2014) this will not lead to a direct increase in recorded mussel bed area. Further research is needed to determine whether this type of restoration has a positive effect on the long term persistence of an intertidal mussel bed survival and thereby on the total area covered by mussel beds.

Another important issue might be, that intertidal mussels were used in the transplantation experiment. For large-scale restoration efforts mainly mussels from subtidal areas are being used (from the channels). Results presented in Chapter 5 show that wave forcing in the deeper tidal channels is negligible. The periodic motion exerted by waves is different from the forcing by tidal currents to which mussels in the sub-tidal area are exposed. Mussels adapt their investment in attachment to hydrodynamic agitation (wa Kangeri et al., 2014); attachment strength of subtidal mussels is significantly smaller (personal communication: Arno wa Kangeri). The importance mussel type has been highlighted by another experiment in which small mussel patches of subtidal and intertidal mussels were placed in the intertidal area (personal communication: Hélène de Paoli). All patches with intertidal mussels survived while the patches with subtidal

mussels suffered large losses. It would thus be preferable to use intertidal mussels for restoration.

Fishing on intertidal areas is currently not allowed anymore. Also restoration using intertidal mussels will, in most cases, be ineffective as the formation of a new mussel bed will damage or remove an existing intertidal mussel bed. If such an intervention in existing mussel beds is considered in the context of existing fishery policy (e.g. testing of Jan Lauw Hypothesis (Ens et al., 2004)) or future experimental mussel bed construction, the impact of fishery should be minimized. Trawling tracks resulting from mussel fishery show a large similarity with the tracks resulting from ice scour presented in Chapter 4. Therefore, this method might have similar effects on the development as ice scour i.e. reducing the self protection and increasing the mussel bed vulnerability to additional erosion. These results suggest that fishing of mussels should occur parallel to the main flow direction and away from the exposed edge.

6.3.4 Stimulation of natural settlement

The final option, stimulation of natural settlement of mussel beds, can be done by placing structures which attenuate wave energy. Placing such structures reduces the hydrodynamic forcing on the underlying sediment, increasing the chance for spatfall and survival. Moreover, they might also serve as a substrate to which mussels can attach. Also for this method the choice of location will be also for this method crucial for success. Not only wave forcing should be limited but also mussel larvae should be able to reach the selected location. Recently, a test with two types of crates, one made from twigs the other from biological degradable plastics, has been performed (personal communication: Tjisse van der Heide). Preliminary results indicate settlement of shellfish inside the deployed structures (especially in the twig type crates). However, mussel cover around the deployed structures has not yet been observed. The placement of such structures will not only limit wave action, but also flow patterns and turbulence. This will affect both sediment dynamics and food availability. The effect on sediment dynamics might be similar as observed for sea grasses, resulting in sedimentation on the lee ward side, scour around the edges and, depending on density, also sedimentation inside the structure (Bouma et al., 2007). Changing flow patterns will also affect food availability similarly to what was modeled for elevated hummocks in Chapter 3.

Concluding remark

Chances of success for all three methods are low and projected costs are high. Current mussel populations lie around 10^8 m^2 . A mussel bed of at least 10^6 m^2 is needed to make a substantial contribution to the total mussel covered area in the Wadden Sea. A large amount of mussels is needed to create such an mussel bed at a sufficiently high density. Similarly, the application of wave attenuating structures requires a large intertidal area to be covered with such structures. Apart from the costs, this will also raise questions on the environmental impact of such an intervention.

Bibliography

- ACKERMAN, J. D., M. R. LOEWEN and P. F. HAMBLIN (2001), Benthic-pelagic coupling over a zebra mussel reef in western Lake Erie. *Limnology and Oceanography* 46(4), 892–904.
- ALBRECHT, A. and K. REISE (1994), Effects of *fucus vesiculosus* covering intertidal mussel beds in the Wadden Sea. *Helgoländer Meeresuntersuchungen* 48(2-3), 243–256.
- ALEXANDERSSON, H., H. TUOMENVIRTA, T. SCHMITH and K. IDEN (2000), Trends of storms in NW Europe derived from an updated pressure data set. *Climate Research* 14(1), 71–73.
- BARTHOLOMÄ, A. and B. FLEMMING (2007), Progressive grain-size sorting along an intertidal energy gradient. *Sedimentary Geology* 202(3), 464–472.
- BELL, E. and J. GOSLINE (1996), Mechanical design of mussel byssus: material yield enhances attachment strength. *Journal of Experimental Biology* 199(4), 1005.
- BERTNESS, M. D. and E. GROSHOLZ (1985), Population dynamics of the ribbed mussel, *geukensia demissa*: the costs and benefits of an aggregated distribution. *Oecologia* 67(2), 192–204.
- BOOIJ, N., R. C. RIS and L. H. HOLTHUIJSEN (1999), A third-generation wave model for coastal regions: 1. model description and validation. *Journal of Geophysical Research: Oceans* 104(C4), 7649–7666.
- BORSJE, B. W., B. K. VAN WESENBEECK, F. DEKKER, P. PAALVAST, T. J. BOUMA, M. M. VAN KATWIJK and M. B. DE VRIES (2011), How ecological engineering can serve in coastal protection. *Ecological Engineering* 37(2), 113–122.
- BOUMA, T. J., L. A. VAN DUREN, S. TEMMERMAN, T. CLAVERIE, A. BLANCO-GARCIA, T. YSEBAERT and P. M. J. HERMAN (2007), Spatial flow and sedimentation patterns within patches of epibenthic structures: Combining field, flume and modelling experiments. *Continental Shelf Research* 27(8), 1020–1045.
- BRINKMAN, A., N. DANKERS and M. VAN STRALEN (2002), An analysis of mussel bed habitats in the Dutch Wadden Sea. *Helgoland Marine Research* 56(1), 59–75.
- BUSCHBAUM, C. (2001), Selective settlement of the barnacle *Semibalanus balanoides* (L.) facilitates its growth and reproduction on mussel beds in the Wadden Sea. *Helgoland Marine Research* 55(2), 128–134.
- BUTMAN, C. A., M. FRECHETTE, W. R. GEYER and V. R. STARCZAK (1994), Flume experiments on food supply to the blue mussel *Mytilus edulis* L. as a function of boundary-layer flow. *Limnology and Oceanography* 39(7), 1755–1768.
- CALLAGHAN, D. P., T. J. BOUMA, P. KLAASSEN, D. VAN DER WAL, M. J. F. STIVE and P. M. J. HERMAN (2010), Hydrodynamic forcing on salt-marsh development: Distinguishing the relative importance of waves and tidal flows. *Estuarine, Coastal and Shelf Science* 89(1), 73–88.
- CARRINGTON, E. (2002), Seasonal variation in the attachment strength of blue mussels: causes and consequences. *Limnology and Oceanography* 47(6), 1723–1733.
- COMMITO, J. and N. DANKERS (2001), Dynamics of spatial and temporal complexity in European and North American soft-bottom mussel beds. In: *Ecological comparisons of sedimentary shores*, Springer, 39–59.
- CONLAN, K. E., H. S. LENIHAN, R. G. KVITEK and J. S. OLIVER (1998), Ice scour disturbance to benthic communities in the canadian high arctic. *Marine Ecology Progress Series* 166(1), 1–16.

- CÔTÉ, I. M. and E. JELNIKAR (1999), Predator-induced clumping behaviour in mussels (*Mytilus edulis Linnaeus*). *Journal of Experimental Marine Biology and Ecology* 235(2), 201–211.
- DAME, R. F. and N. DANKERS (1988), Uptake and release of materials by a Wadden Sea mussel bed. *Journal of Experimental Marine Biology and Ecology* 118(3), 207 – 216.
- DANKERS, N. and D. R. ZUIDEMA (1995), The role of the mussel (*Mytilus edulis* L.) and mussel culture in the Dutch Wadden Sea. *Estuaries* 18(1), 71–80.
- DANKERS, N., A. BRINKMAN, A. MEIJBOOM and E. DIJKMAN (2001), Recovery of intertidal mussel beds in the Wadden Sea: use of habitat maps in the management of the fishery. In: *Coastal Shellfish : A Sustainable Resource*, Springer, 21–30.
- DANKERS, N., A. MEIJBOOM, M. DE JONG, E. DIJKMAN, J. CREMER and S. VAN DER SLUIS (2004), Het ontstaan en verdwijnen van droogvallende mosselbanken in de Nederlandse Waddenzee. *Alterra*.
- DANKERS, N. M. J. A. (2014), Ervaringen met stimuleren van ontwikkeling nieuwe mosselbanken. In: *Mosselworkshop 2014*, 15–17.
- DE SWART, H. E. and J. T. F. ZIMMERMAN (2009), Morphodynamics of tidal inlet systems. *Annual review of fluid mechanics* 41, 203–229.
- DE VLAS, J., B. BRINKMAN, C. BUSCHBAUM, N. DANKERS, M. HERLYN, P. S. KRISTENSEN, G. MILLAT, G. NEHLS, M. RUTH, J. STEENBERGEN and A. WEHRMAN (2004), Intertidal blue mussel beds. In: K. Essink, C. Dettmann, H. Farke, K. Laursen, G. Lüerßen, H. Marencic and W. Wiersinga, eds., *Wadden Sea Quality Status Report 2004 (QSR)*, Trilateral Monitoring and Assessment Group, Common Wadden Sea Secretariat, Wilhelmshaven, Germany., 190–200.
- DE WINTER, R. C., A. STERL, J. W. DE VRIES, S. L. WEBER and B. G. RUESSINK (2012), The effect of climate change on extreme waves in front of the Dutch coast. *Ocean Dynamics* 62(8), 1139–1152.
- DENNY, M., K. M. DORGAN, D. EVANGELISTA, A. HETTINGER, J. LEICHTER, W. C. RUDER and I. TUVAL (2011), Anchor ice and benthic disturbance in shallow antarctic waters: Interspecific variation in initiation and propagation of ice crystals. *The Biological Bulletin* 221(2), 155–163.
- DENNY, M. W. (1987), Lift as a mechanism of patch initiation in mussel beds. *Journal of Experimental Marine Biology and Ecology* 113(3), 231–245.
- DENNY, M. W. (1995), Predicting physical disturbance: mechanistic approaches to the study of survivorship on wave-swept shores. *Ecological Monographs* 65(4), 371–418.
- DIJKEMA, K. (1991), Towards a habitat map of the Netherlands, German and Danish Wadden Sea. *Ocean and shoreline management* 16(1), 1–21.
- DIONNE, J. C. (1984), An estimate of ice-drifted sediments based on the mud content of the ice cover at Montmagny, Middle St. Lawrence estuary. *Marine geology* 57(1), 149–166.
- DIONNE, J. C. (1988), Characteristic features of modern tidal flats in cold regions. In: P. L. de Boer, A. van Gelder and S. D. Nio, eds., *Tide-influenced sedimentary environments and facies*, Reidel Publishing Company, Dordrecht, 301–332.
- DIONNE, J. C. (1998), Sedimentary structures made by shore ice in muddy tidal-flat deposits, St. Lawrence estuary, Québec. *Sedimentary Geology* 116(3), 261–274.
- DITTMANN, S. (1990), Mussel beds – amensalism or amelioration for intertidal fauna? *Helgoländer Meeresuntersuchungen* 44(3-4), 335–352.
- DOLMER, P. (2000), Algal concentration profiles above mussel beds. *Journal of Sea Research* 43(2), 113–119.

- ELGAR, S., B. RAUBENHEIMER and R. T. GUZA (2005), Quality control of acoustic Doppler velocimeter data in the surfzone. *Measurement Science and Technology* 16, 1889.
- ENS, B. J., A. C. SMAAL and J. DE VLAS (2004), The effects of shellfish fishery on the ecosystems of the Dutch Wadden Sea and Oosterschelde: final report on the second phase of the scientific evaluation of the Dutch shellfish fishery policy (EVA II). Alterra.
- ESCARTIN, J. and D. G. AUBREY (1995), Flow structure and dispersion within algal mats. *Estuarine, Coastal and Shelf Science* 40(4), 451–472.
- ESSINK, K., C. DETTMANN, H. FRAKE, K. LAURSEN, G. LÜERSSEN and W. WIERSINGA (2005), Wadden sea quality status report 2004 .
- FEDDERSEN, F. and A. WILLIAMS III (2007), Direct estimation of the reynolds stress vertical structure in the nearshore. *Journal of Atmospheric & Oceanic Technology* 24(1).
- FEDDERSEN, F., J. H. TROWBRIDGE and A. J. WILLIAMS III (2007), Vertical structure of dissipation in the nearshore. *Journal of Physical Oceanography* 37(7), 1764–1777.
- FESER, F., M. BARCIKOWSKA, O. KRUEGER, F. SCHENK, R. WEISSE and L. XIA (2014), Storminess over the North Atlantic and Northwestern Europe – a review. *Quarterly Journal of the Royal Meteorological Society* .
- FLEMMING, B. W. and M. T. DELAFONTAINE (1994), Biodeposition in a juvenile mussel bed of the East Frisian Wadden Sea (southern North Sea). *Netherland Journal of Aquatic Ecology* 28(3-4), 289–297.
- FOLKARD, A. M. and J. C. GASCOIGNE (2009), Hydrodynamics of discontinuous mussel beds: Laboratory flume simulations. *Journal of Sea Research* 62(4), 250–257.
- FOLMER, E. O., J. DRENT, K. TROOST, H. BÜTTGER, N. DANKERS, J. JANSEN, M. VAN STRALEN, G. MILLAT, M. HERLYN and C. J. M. PHILIPPART (2014), Large-scale spatial dynamics of intertidal mussel (*Mytilus Edulis* L.) bed coverage in the German and Dutch Wadden Sea. *Ecosystems* 17(3), 550–566.
- FRÉCHETTE, M. and E. BOURGET (1985), Food-limited growth of *Mytilus edulis* L. in relation to the benthic boundary layer. *Canadian Journal of Fisheries and Aquatic Sciences* 42(6), 1166–1170.
- FRÉCHETTE, M., C. A. BUTMAN and W. R. GEYER (1989), The importance of boundary-layer flows in supplying phytoplankton to the benthic suspension feeder, *Mytilus edulis* L. *Limnology and Oceanography* 34, 19–36.
- GARRATT, J. R. (1994), The atmospheric boundary layer. Cambridge Univ Pr.
- GASCOIGNE, J. C., H. A. BEADMAN, C. SAUREL and M. J. KAISER (2005), Density dependence, spatial scale and patterning in sessile biota. *Oecologia* 145(3), 371–381.
- GAYLORD, B. (1999), Detailing agents of physical disturbance: wave-induced velocities and accelerations on a rocky shore. *Journal of Experimental Marine Biology and Ecology* 239(1), 85–124.
- GERBI, G. P., J. H. TROWBRIDGE, E. A. TERRAY, A. J. PLUEDDEMANN and T. KUKULKA (2009), Observations of turbulence in the ocean surface boundary layer: energetics and transport. *Journal of Physical Oceanography* 39(5), 1077–1096.
- GORDON, L. and A. LOHRMANN (2001), Near-shore doppler current meter wave spectra. In: *Proceedings of the 4th International Symposium on Ocean Wave Measurement and Analysis, WAVES2001*, ASCE, San Francisco, CA, 33–43.
- GRABOWSKI, R. C., I. G. DROPPA and G. WHARTON (2011), Erodibility of cohesive sediment: the importance of sediment properties. *Earth-Science Reviews* 105(3), 101–120.

- GRANT, W. D. and O. S. MADSEN (1979), Combined wave and current interaction with a rough bottom. *Journal of Geophysical Research* 84(C4), 1797–1808.
- GRAY, J. S. (2002), Species richness of marine soft sediments. *Marine Ecology Progress Series* 244, 285–297.
- GREEN, M. O., J. E. HEWITT and S. F. THRUSH (1998), Seabed drag coefficient over natural beds of horse mussels (*Atrina zelandica*). *Journal of Marine Research* 56(3), 613–637.
- GROENEWEG, J., A. VAN DER WESTHUYSEN, G. P. VAN VLEDDEER, S. JACOBSE, J. LANSSEN and A. VAN DONGEREN (2008), Wave modelling in a tidal inlet: Performance of SWAN in the Wadden Sea. In: *Proc. 31th Int. Conf. Coastal Eng., ASCE, World Scientific*, 411–423.
- HAMMOND, W. and C. GRIFFITHS (2004), Influence of wave exposure on South African mussel beds and their associated infaunal communities. *Marine Biology* 144(3), 547–552.
- HELMUTH, B. and M. W. DENNY (2003), Predicting wave exposure in the rocky intertidal zone: Do bigger waves always lead to larger forces? *Limnology and Oceanography* 48(3), 1338–1345.
- HENCH, J. L. and J. H. ROSMAN (2013), Observations of spatial flow patterns at the coral colony scale on a shallow reef flat. *Journal of Geophysical Research: Oceans* 118(3), 1142–1156.
- HERLYN, M. (2005), Quantitative assessment of intertidal blue mussel (*Mytilus edulis* L.) stocks: combined methods of remote sensing, field investigation and sampling. *Journal of Sea Research* 53(4), 243–253.
- HOLTHUIJSEN, L. H. (2007), *Waves in oceanic and coastal waters*. Cambridge University Press.
- HUNT, H. L. and R. E. SCHEIBLING (2001), Predicting wave dislodgment of mussels: variation in attachment strength with body size, habitat, and season. *Marine Ecology Progress Series* 213, 157–164.
- JONES, N. L. and S. G. MONISMITH (2008), The influence of whitecapping waves on the vertical structure of turbulence in a shallow estuarine embayment. *Journal of Physical Oceanography* 38(7), 1563–1580.
- JUBB, C., R. HUGHES and T. A. RHEINALLT (1983), Behavioural mechanisms of size-selection by crabs, *Carcinus maenas* (L.) feeding on mussels, *Mytilus edulis* L. *Journal of experimental marine biology and ecology* 66(1), 81–87.
- KAISER, R., G. BRANDT, J. GARTNER, D. GLASER, J. GRUNE, F. JENSEN and H. D. NIEMEYER (1994), Wave climate study in Wadden Sea areas. In: *Proceedings of 24th Conference on Coastal Engineering, ASCE, World Scientific*, 181–191.
- KEULEGAN, G. H. and L. H. CARPENTER (1958), Forces on cylinders and plates in an oscillating fluid. *Journal of research of the National Bureau of Standards* 60(5), 423.
- KONUK, I., S. YU and R. GRACIE (2005), An ALE FEM model of ice scour. In: *11th International Conference of the International Association of Computer Models and Advances in Geomechanics, Turin, Italy*.
- LIU, Q.-X., E. J. WEERMAN, P. M. J. HERMAN, H. OLFF and J. VAN DE KOPPEL (2012), Alternative mechanisms alter the emergent properties of self-organization in mussel beds. *Proceedings of the Royal Society of London B: Biological Sciences* 279(1739), 2744–2753.
- LIU, Q.-X., P. M. J. HERMAN, W. M. MOOIJ, J. HUISMAN, H. OLFF and J. VAN DE KOPPEL (2014a), Pattern formation at multiple spatial scales drives the resilience of mussel bed ecosystems. *Nature Communications* 5:5234.
- LIU, Q.-X., E. J. WEERMAN, R. GUPTA, P. M. J. HERMAN, H. OLFF and J. VAN DE KOPPEL (2014b), Biogenic gradients in algal density affect the emergent properties of spatially self-organized

- mussel beds. *Journal of The Royal Society Interface* 11(96).
- LOWE, R. J., J. FALTER, M. BANDET, G. PAWLAK, M. J. ATKINSON, S. G. MONISMITH and J. R. KOSEFF (2005), Spectral wave dissipation over a barrier reef. *Journal of Geophysical Research* 110(C4), C04001.
- MADSEN, O. S. (1994), Spectral wave-current bottom boundary layer flows. *Proceedings of the 24th International Conference on Coastal Engineering, ASCE*, 384–397.
- MCGRORTY, S., R. T. CLARKE, C. J. READING and J. D. GOSS-CUSTARD (1990), Population dynamics of the mussel *Mytilus edulis*: density changes and regulation of the population in the Exe estuary, Devon. *Marine Ecology Progress Series* 67, 157–169.
- MCGRORTY, S., J. D. GOSS-CUSTARD and R. T. CLARKE (1993), Mussel *Mytilus edulis* (Mytilacea) dynamics in relation to environmental gradients and intraspecific interactions. *Netherlands Journal of Aquatic Ecology* 27(2-4), 163–171.
- MOESER, G. M. and E. CARRINGTON (2006), Seasonal variation in mussel byssal thread mechanics. *Journal of Experimental Biology* 209(10), 1996–2003.
- MOESER, G. M., H. LEBA and E. CARRINGTON (2006), Seasonal influence of wave action on thread production in *Mytilus edulis* L. *Journal of Experimental Biology* 209(5), 881–890.
- MÖLLER, I., T. SPENCER, J. R. FRENCH, D. J. LEGGETT and M. DIXON (1999), Wave transformation over salt marshes: a field and numerical modelling study from north Norfolk, England. *Estuarine, Coastal and Shelf Science* 49(3), 411–426.
- MORI, N., T. SUZUKI, S. KAKUNO ET AL. (2007), Noise of Acoustic Doppler Velocimeter Data in Bubbly Flows. *Journal of Engineering Mechanics* 133, 122.
- NEHLS, G. and M. THIEL (1993), Large-scale distribution patterns of the mussel *Mytilus edulis* in the Wadden Sea of Schleswig-Holstein: Do storms structure the ecosystem? *Netherlands Journal of Sea Research* 31(2), 181–187.
- NEHLS, G., I. HERTZLER and G. SCHEIFFARTH (1997), Stable mussel (*Mytilus edulis*) beds in the Wadden Sea—they're just for the birds. *Helgoländer Meeresuntersuchungen* 51(3), 361–372.
- NEPE, H. M. (1999), Drag, turbulence, and diffusion in flow through emergent vegetation. *Water Resources Research* 35(2), 479–489.
- NIELSEN, P. (1992), Coastal bottom boundary layers and sediment transport, vol. 4. World Scientific. Singapore. SG.
- NIELSEN, P. and B. VISMANN (2014), Clearance rate of *Mytilus Edulis* (L.) as a function of current velocity and mussel aggregation. *Journal of Shellfish Research* 33(2), 457–463.
- OBERT, B. and H. MICHAELIS (1991), History and ecology of the mussel beds (*Mytilus edulis* L.) in the catchment area of a wadden sea tidal inlet. *Estuaries and Coasts. Spatial and Intercomparisons*. Olsen and Olsen, Fredensborg, 185–194.
- OKAMURA, B. (1986), Group living and the effects of spatial position in aggregations of *mytilus edulis*. *Oecologia* 69(3), 341–347.
- OOST, A. (1995), Dynamics and sedimentary development of the Dutch Wadden Sea, with emphasis on the Frisian inlet: a study of the barrier islands, ebb-tidal deltas, inlets, and drainage basins. *Faculteit Aardwetenschappen, Universiteit Utrecht*.
- PAINE, R. T. and S. A. LEVIN (1981), Intertidal landscapes: disturbance and the dynamics of pattern. *Ecological monographs* 51(2), 145–178.

- PEJRUP, M. and T. J. ANDERSEN (2000), The influence of ice on sediment transport, deposition and reworking in a temperate mudflat area, the danish wadden sea. *Continental Shelf Research* 20(12), 1621–1634.
- PIAZZA, B. P., P. D. BANKS and M. K. LA PEYRE (2005), The potential for created oyster shell reefs as a sustainable shoreline protection strategy in louisiana. *Restoration Ecology* 13(3), 499–506.
- PRICE, H. A. (1980), Seasonal variation in the strength of byssal attachment of the common mussel *Mytilus edulis*. *Journal of the Marine Biological Association of the United Kingdom* 60(04), 1035–1037.
- PRICE, H. A. (1981), Byssus thread strength in the mussel, *Mytilus edulis*. *Journal of Zoology* 194(2), 245–255.
- PRICE, H. A. (1982), An Analysis of Factors Determining Seasonal Variation in the Byssal Attachment Strength of *Mytilus Edulis*. *Journal of the Marine Biological Association of the United Kingdom* 62(01), 147–155.
- PULFRICH, A. (1995), Reproduction and recruitment in Schleswig-Holstein Wadden Sea edible mussel (*Mytilus edulis* L.) populations. Ph.D. thesis, Christian-Albrechts-Universität Kiel.
- REISE, K. (1998), Pacific oysters invade mussel beds in the european wadden sea. *Senckenbergiana maritima* 28(4-6), 167–175.
- SAUREL, C., J. K. PETERSEN, P. J. WILES and M. J. KAISER (2013), Turbulent mixing limits mussel feeding: direct estimates of feeding rate and vertical diffusivity. *Marine ecology. Progress series* 485, 105–121.
- SCYPHERS, S. B., S. P. POWERS, K. L. HECK JR and D. BYRON (2011), Oyster reefs as natural breakwaters mitigate shoreline loss and facilitate fisheries. *PLoS One* 6(8), e22396.
- SEED, R. and T. SUCHANEK (1992), Population and community ecology of *Mytilus*. *The mussel Mytilus: ecology, physiology, genetics and culture* 25, 87–170.
- SIMPSON, J. H., B. BERX, J. GASCOIGNE and C. SAUREL (2007), The interaction of tidal advection, diffusion and mussel filtration in a tidal channel. *Journal of Marine Systems* 68(3), 556–568.
- SOULSBY, R. L. (1997), Dynamics of marine sands: a manual for practical applications. Thomas Telford.
- STRASSER, M., T. REINWALD and K. REISE (2001), Differential effects of the severe winter of 1995/96 on the intertidal bivalves *Mytilus edulis*, *Cerastoderma edule* and *Mya arenaria* in the northern wadden sea. *Helgoland Marine Research* 55(3), 190–197.
- SVANE, I. and M. OMPI (1993), Patch dynamics in beds of the blue mussel (*Mytilus edulis* L.): effects of site, patch size, and position within a patch. *Ophelia* 37(3), 187–202.
- TEMMERMAN, S., T. J. BOUMA, G. GOVERS, Z. B. WANG, M. B. DE VRIES and P. M. J. HERMAN (2005), Impact of vegetation on flow routing and sedimentation patterns: Three-dimensional modeling for a tidal marsh. *Journal of Geophysical Research: Earth Surface* (2003–2012) 110(F4).
- THORNTON, E. B. and R. T. GUZA (1983), Transformation of wave height distribution. *J. Geophys. Res* 88(10), 5925–5938.
- VAN DE KOPPEL, J., M. RIETKERK, N. M. J. A. DANKERS and P. M. J. HERMAN (2005), Scale-dependent feedback and regular spatial patterns in young mussel beds. *The American Naturalist* 165(3), E66–E77.
- VAN DE KOPPEL, J., J. C. GASCOIGNE, G. THERAULAZ, M. RIETKERK, W. M. MOOIJ and P. M. J. HERMAN (2008), Experimental evidence for spatial self-organization and its emergent effects in mussel bed ecosystems. *Science* 322(5902), 739–742.

- VAN DE KOPPEL, J., T. J. BOUMA and P. M. J. HERMAN (2012), The influence of local-and landscape-scale processes on spatial self-organization in estuarine ecosystems. *The Journal of experimental biology* 215(6), 962–967.
- VAN DEN ENDE, D., K. TROOST, C. VAN ZWEEDEN and M. VAN ASCH (2013), Het mosselbestand en het areaal aan mosselbanken op de droogvallende platen van de Waddenzee in het voorjaar van 2013. Tech. Rep. C167/13, IMARES Wageningen UR.
- VAN DER WESTHUYSEN, A. J. (2010), Modeling of depth-induced wave breaking under finite depth wave growth conditions. *Journal of Geophysical Research: Oceans* 115(C01008).
- VAN DER WESTHUYSEN, A. J., A. R. DONGEREN, J. GROENEWEG, G. P. VLEDDEER, H. PETERS, C. GAUTIER and J. C. C. NIEUWKOOP (2012), Improvements in spectral wave modeling in tidal inlet seas. *Journal of Geophysical Research: Oceans* 117(C00J28).
- VAN DER ZEE, E. M., T. VAN DER HEIDE, S. DONADI, J. S. EKLÖF, B. K. ERIKSSON, H. OLFF, H. W. VAN DER VEER and T. PIERSMA (2012), Spatially extended habitat modification by intertidal reef-building bivalves has implications for consumer-resource interactions. *Ecosystems* 15(4), 664–673.
- VAN DUREN, L. A., P. M. J. HERMAN, A. J. J. SANDEE and C. H. R. HEIP (2006), Effects of mussel filtering activity on boundary layer structure. *Journal of Sea Research* 55(1), 3–14.
- VAN LEEUWEN, B., D. AUGUSTIJN, B. VAN WESENBEECK, S. HULSCHER and M. DE VRIES (2010), Modeling the influence of a young mussel bed on fine sediment dynamics on an intertidal flat in the Wadden Sea. *Ecological Engineering* 36(2), 145–153.
- VAN VLEDDEER, G. P., J. GROENEWEG and A. VAN DER WESTHUYSEN (2008), Numerical and physical aspects of wave modelling in a tidal inlet. In: *Proceedings of the 31th International Conference on Coastal Engineering*, ASCE, World Scientific, 424–436.
- VIARENGO, A., M. PERTICA, L. CANESI, R. ACCOMANDO, G. MANCINELLI and M. ORUNESU (1989), Lipid peroxidation and level of antioxidant compounds (GSH, vitamin E) in the digestive glands of mussels of three different age groups exposed to anaerobic and aerobic conditions. *Marine environmental research* 28(1), 291–295.
- WA KANGERI, A. K., J. M. JANSEN, B. R. BARKMAN, J. J. A. DONKER, D. J. JOPPE and N. M. J. A. DANKERS (2014), Perturbation induced changes in substrate use by the blue mussel, *Mytilus edulis*, in sedimentary systems. *Journal of Sea Research* 85(C7), 233–240.
- WA KANGERI, A. K., S. ALVAREZ-FERNANDEZ, C. I. F. SILVA, J. J. A. DONKER, J. M. JANSEN, D. J. JOPPE and N. M. J. A. DANKERS (2015), Behavioural zonation , byssus production and adhesion strength in *Mytilus edulis* L. in sedimentary habitats; the effect of the non-native oyster, *Crassostrea gigas* (T.). in preperation .
- WEERMAN, E. J., J. VAN DE KOPPEL, M. B. EPPINGA, F. MONTSEERAT, Q. X. LIU and P. M. J. HERMAN (2010), Spatial self-organization on intertidal mudflats through biophysical stress divergence. *The American Naturalist* 176(1), E15–E32.
- WEISSE, R., H. VON STORCH and F. FESER (2005), Northeast Atlantic and North Sea storminess as simulated by a regional climate model during 1958-2001 and comparison with observations. *Journal of Climate* 18(3), 465–479.
- WIDDOWS, J. and M. BRINSLEY (2002), Impact of biotic and abiotic processes on sediment dynamics and the consequences to the structure and functioning of the intertidal zone. *Journal of Sea Research* 48(2), 143–156.

- WIDDOWS, J., J. LUCAS, M. BRINSLEY, P. SALKELD and F. STAFF (2002), Investigation of the effects of current velocity on mussel feeding and mussel bed stability using an annular flume. *Helgoland Marine Research* 56(1), 3–12.
- WILDISH, D. and M. MIYARES (1990), Filtration rate of blue mussels as a function of flow velocity: preliminary experiments. *Journal of Experimental Marine Biology and Ecology* 142(3), 213–219.
- WILDISH, D. J. and D. D. KRISTMANSON (1984), Importance to mussels of the benthic boundary layer. *Canadian Journal of Fisheries and Aquatic Sciences* 41(11), 1618–1625.
- WITMAN, J. D. and T. H. SUCHANEK (1984), Mussels in flow: drag and dislodgement by epizoans. *Marine Ecology Progress Series* 16(3), 259–268.
- WRIGHT, J. P. and C. G. JONES (2006), The concept of organisms as ecosystem engineers ten years on: progress, limitations, and challenges. *BioScience* 56(3), 203–209.
- YOUNG, G. (1985), Byssus-thread formation by the mussel (*Mytilus edulis*): Effects of environmental factors. *Marine ecology progress series*. Oldendorf 24(3), 261–271.
- ZIJLEMA, M., G. STELLING and P. SMIT (2011), Swash: An operational public domain code for simulating wave fields and rapidly varied flows in coastal waters. *Coastal Engineering* 58(10), 992–1012.
- ZONG, L. and H. NEPF (2010), Flow and deposition in and around a finite patch of vegetation. *Geomorphology* 116(3), 363–372.
- ZWARTS, L. and R. DRENT (1981), Prey depletion and the regulation of predator density: Oystercatchers (*Haematopus ostralegus*) feeding on mussels (*Mytilus edulis*). In: N. Jones and W. Wolff, eds., *Feeding and Survival Strategies of Estuarine Organisms*, vol. 15 of *Marine Science*, Springer, 193–216.

Summary

Intertidal mussel beds are important to the Dutch Wadden Sea. Not only do they serve as a food source for birds and crabs, but also provide a habitat for other species. The mussel population in the Dutch Wadden Sea is currently under pressure. Especially, in the Western Parts of the Dutch Wadden Sea mussel coverage is currently low with respect to observations made in the period 1970-1978. This has led to the start of project Mosselwad, which aims to study the factors that influence the survival of mussel beds in the Dutch Wadden Sea. This thesis is part of project Mosselwad and focuses on the role of hydrodynamic processes. Hydrodynamic process influence intertidal mussel beds in two ways: on the one hand currents are responsible for the transfer of food and sediments towards the beds, on the other hand, large shear stresses from waves and currents are capable of eroding mussels from intertidal mussel beds. A previous study suggested that wave exposure is an important factor determining the suitability of an intertidal area to sustain a stable intertidal mussel bed. However, the actual shear stresses associated with wave forcing have not been studied in soft-sediment environments; most research has focused on the role of currents.

To quantify the hydrodynamic exposure of intertidal mussel beds the shear stresses of waves and currents need to be determined. This was done in Chapter 2 using the results from a field experiment which was performed on a flat mussel bed, located at mean sea level. Shear stresses from waves are the largest and result come from the wave orbital motion. Wave breaking does not occur because of the small slope of the tidal flat. Current induced shear-stresses were small. However, they have a substantial effect on the total bed shear stress due to wave-current interaction. Waves lose energy as they propagate over an intertidal mussel bed as a result of increased bottom roughness of the mussel bed. By studying the wave attenuation the Nikuradse roughness of the mussel bed was quantified at 0.05 m. To determine the spatial variation in wave forcing the obtained value for the Nikuradse roughness was used in a subsequent wave model study. Model results show that wave exposure of the seaward edge is largest. Areas deeper inside the bed are protected from high wave induced bed shear stresses by this seaward edge.

In mussel beds located deeper (<0.4 m below the Dutch Ordnance level) currents are stronger and mussel beds have more relief. This is the result of sedimentation in patterned mussel beds. Patterns result from self-organisation; mussel organize themselves to increase their survival chance. The formation of elevated mussel hummocks influences flow patterns and mixing and thereby food availability which in turn influences survival chances. There is thus an interaction between formation of spatial patterns and the development elevations. The influence of hummock formation on food availability was studied in Chapter 3. Field measurements show that during the majority of the tidal cycle, flow velocities and turbulence intensity over the hummock were increased with respect to those next to the hummock (small channel). A peak in channel velocities is observed just before the hummock emerged, suggesting flow routing and reduced advection of food towards the hummock. Especially the latter suggests that at least part

of the flow is routed around the mussel hummock, reducing transport of food towards the hummock. A subsequent model study confirms the observations of flow routing around and acceleration over the mussel hummock. Model results confirm that flow routing reduces food transport towards the hummock but also show that this can be compensated by increased vertical mixing. The net effect on food availability depends on hummock geometry; broader hummocks tend to increase the hummock acceleration type flow, while more elongated hummocks tend to promote flow routing. The break-up of broad band structures commonly observed in intertidal mussel beds thus influences food availability and thereby the persistence of an intertidal mussel bed.

In Chapter 4, the direct impact of hydrodynamic processes on mussel bed persistence was studied using a 27 month long data set on coverage and topography of an intertidal mussel bed. Early on during this observation period the mussel bed was damaged by ice action. The resulting damage was a loss in mussel coverage concentrated in three gaps and increased elevation of the areas surrounding the gap. Evidence indicates that that scouring of moving ice sheets damaged the bed. The mussel bed coverage recovered slowly from the damage it sustained while relief at the erosion gaps increased as the result of sedimentation in mussel covered areas. Nearly two years after the bed was damaged by ice-action, the bed was damaged by wave-action during a stormy fall. The elevated areas, just away from the edges surrounding the erosion gaps, were severely damaged during this period. Waves focusing on these areas due to wave refraction might have caused the strong erosion in these areas. This observation suggests a synergy between erosion by ice- and wave-action.

The results presented in Chapter 2 showed that shear stresses induced by the wave orbital motion are responsible for the majority of the shear stresses exerted on the mussel bed. Therefore, in Chapter 5, the relation between wave exposure, in terms of the wave orbital velocity, and mussel bed occurrence in the Dutch Wadden Sea is investigated. To this end wave exposure was modeled for a range of wind and water level scenarios. By combining these scenarios with observations of wind conditions and water levels over the period 1991 to 2013 the wave climate in the Dutch Wadden Sea is determined. From this analysis median values, describing the exposure under normal conditions, and 95th percentile values, describing the exposure during energetic periods, are extracted. Results show that for both median values as well as 95th percentile values wave forcing is largest in the Western basins of the Dutch Wadden Sea. Wave forcing may not only be a factor limiting survival but the high wave exposure during normal conditions might also influence settlement chances for mussel beds in the Western Wadden Sea. A comparison between wave exposure and mussel bed occurrence per tidal basins shows that mussel coverage is smaller in more exposed tidal basins.

Samenvatting

Litorale (droogvallende) mosselbanken zijn belangrijk voor de Nederlandse Waddenzee. Niet alleen vormen ze een voornaam voedselbron voor vogels en krabben maar ook zorgen ze voor een toename van organisch materiaal in hun omgeving. De omgeving van een mosselbank is daarom een goed habitat voor andere diersoorten. De mosselpopulatie in de Nederlandse Waddenzee staat echter onder druk; vooral in de westelijke Waddenzee komen minder soorten voor dan op basis van historische waarnemingen uit de jaren 70 zou mogen worden verwacht. Dit heeft aanleiding gegeven tot het starten van het project Mosselwad dat onderzoek doet naar de factoren die van invloed zijn op de overleving van mosselbanken in de Nederlandse Waddenzee. Binnen dit kader is in deze thesis de rol van hydrodynamische processen op de overleving van litorale mosselbanken onderzocht. Hydrodynamische processen beïnvloeden mosselbanken op twee manieren, enerzijds zorgt stroming voor de aanvoer van voedsel en sediment, anderzijds kunnen hoge bodem schuifspanningen ten gevolge van stroming en golven mosselen uit een mosselbank eroderen. Uit habitat geschiktheidsstudies komt naar voren dat golfwerking de belangrijkste parameter is die de geschiktheid van een locatie voor de vorming van een stabiele intergetijdse mosselbank beïnvloed. Echter, de focus van de meeste studies naar de relatie tussen mosselbanken en hydrodynamica lag tot nu toe op de rol van stroming.

Om de rol van hydrodynamische processen bij erosie in kaart te brengen is het nodig golf schuifspanningen te kwantificeren en deze te vergelijken met schuifspanningen geïnduceerd door stroming. Met dit doel zijn de schuifspanningen die golven en stroming op een mosselbank uitoefenen op een vlakke hoog gelegen (rond N.A.P.) mosselbank gemeten. Golfgeïnduceerde schuifspanningen gerelateerd aan golf orbitaal beweging zijn het grootste; golf breking komt nauwelijks voor door de flauwe helling van de getijplaat. Hoewel de schuifspanningen geïnduceerd door stroming kleiner zijn kunnen ze, door middel van golf-stroom interactie, substantieel bijdragen aan de totale schuifspanning. De aanwezigheid van mosselen op de bodem maakt de bodem ruwer voor stroming en golven. Golven worden door deze verhoogde ruwheid versterkt uitgedoofd. Aan de hand van veldmetingen is de Nikuradse ruwheid van de mosselbank vastgesteld op 0.05 m. Deze ruwheid is vervolgens gebruikt om de resultaten ruimtelijk op te schalen met behulp van een golfmodel. Modelresultaten laten zien dat golfschuifspanningen het hoogste zijn op de zeewaardse rand van de mosselbank en afnemen dieper in de mosselbank. Deze zeewaardse rand beschermt dus de delen van de bank die verder van de getijgeul zijn verwijderd.

In dieper liggende banken (< -0.4 m onder N.A.P) zijn de stromingen sterker en vormt zich vaak meer reliëf op mosselbanken. Dit ontstaat doordat ruimtelijke patronen in mosselbedekking ontstaan ten gevolge van zelforganisatie; mosselen herlokalisieren zichzelf om hun voedsel opname te optimaliseren. De aanwezigheid van bulten beïnvloedt de ruimtelijke stromingspatronen en daarmee voedselbeschikbaarheid. Hierdoor treedt een mogelijke wisselwerking tussen bultvorming en patroonvorming op. De effecten van mosselbulten op stroming en voedselbeschikbaarheid zijn bestudeerd in hoofdstuk 3. Uit

veldmetingen komt naar voren dat stroming deels over verhogingen wordt versneld maar dat ook een deel van de stroming om een verhoging wordt heen geleid. De modelstudie die vervolgens is uitgevoerd laat zien dat deze processen tegengesteld effect hebben op het voedsel aanbod. Het omleiden van de stroming om de mosselbult zorgt voor een reductie in de laterale voedsel aanvoer. Een versnelling van stroming over de ruwe mosselbult zorgt voor een toename van verticale menging wat de voedselbeschikbaarheid in de grenslaag nabij de bodem, waaruit de mossel zich voed, verbetert. Mosselbultgeometrie bepaalt of de toename in verticale aanvoer van voedsel kan compenseren voor de reductie in lateraal voedseltransport. Voedselbeschikbaarheid is het hoogste in het geval van brede mosselbanden waarbij er alleen versnelling is en er geen stroming rond de bult kan worden geleid. Het opbreken van deze band patronen tijdens stormen kan daarmee consequenties hebben voor de langetermijn overleving van een mosselbank.

Om de impact van hydrodynamische processen op de erosie van een mosselbank te bepalen, is een mosselbank 2.5 jaar gemonitord (hoofdstuk 4). Er zijn twee type erosie events vastgesteld. Het eerste type erosie event werd veroorzaakt door ijsgang. Hierbij zijn delen van de zeewaardse rand van mosselbank verwijderd door ijs, en rond de geërodeerde gebieden zijn er delen opgehoogd. De rest van de erosie is het resultaat van golfwerking tijdens een stormachtige periode. Meerdere golfaanvallen hebben er tijdens deze periode voor gezorgd dat delen van de zeewaardse rand van de mosselbank zijn geërodeerd. Het is opmerkelijk dat de gebieden rondom de locaties geërodeerd door ijs zwaar zijn getroffen tijdens deze stormperiode. Deze observatie suggereert een synergetische relatie tussen ijs- en golf-werking.

De resultaten van hoofdstuk 2 lieten zien dat golforbitaalbewegingen verantwoordelijk zijn voor het grootste deel van de schuifspanningen die werken op mosselbanken. Daarom is in hoofdstuk 5 de relatie tussen mosselbanken en golfexpositie, in termen van de amplitude van golf orbitaal beweging, onderzocht. Voor de periode 1991-2013 is het golfklimaat in de Nederlandse Waddenzee bepaald. Dit is vervolgens gebruikt om de golf expositie tijdens energieke perioden (95 percentiel) alsmede kalmere perioden (mediaan) te bepalen. Golfwerking in het intergetijde gebied is tijdens energieke en kalme perioden hoger in de westelijke Waddenzee. Dit betekent ook dat tijdens perioden van mosselvestiging de condities in de westelijke Waddenzee slechter zijn dan in de oostelijke Waddenzee. Hoewel de westelijke Waddenzee als geheel meer golfgeëxponeerd is geldt dat in mindere mate voor de mosselbanken. Er is maar een klein verschil in golf expositie tussen mosselbanken in het westelijke en het oostelijke gedeelte van de Waddenzee. In het oosten is er geen verschil in gemiddelde expositie van mosselbanken en gemiddelde expositie van het gehele litorale gebied. Dit suggereert dat alleen in het westen golf expositie een belangrijke beperkende factor is. Studies van het historische wind klimaat laten zien dat in de jaren 70, in de periode van de eerste mosselkarteringen, het windklimaat milder was dan tegenwoordig. Dit zou een reden kunnen zijn waarom er in deze periode meer mosselbanken in de Westelijke kombergingen van de Nederlandse Waddenzee werden aangetroffen.

Dankwoord

Het zou onmogelijk zijn geweest om deze thesis te voltooien zonder hulp. Ik wil daarom iedereen die mij tijdens deze periode geholpen, gemotiveerd en/of geïnspireerd heeft dan ook enorm bedanken. Allereerst wil ik mijn begeleiders en Maarten van der Vegt en Piet Hoekstra bedanken dat ze me deze gegeven hebben. Maarten, bedankt voor je begeleiding, je enthousiasme en creative ideeën hebben me enorm gemotiveerd. Het was fijn dat je me veel vrijheid gaf om mijn eigen weg te zoeken in het mossel labrynt maar ook dat, wanneer ik de weg kwijt raakte, ik altijd bij je binnen kon lopen voor hulp. Het was fijn dat we het contact in de laatste fase konden intensiveren. Piet, bedankt voor je advies, commentaar op manuscripten en hulp bij logistieke uitdagingen. Ik heb ook je aanwezigheid tijdens de pilot in 2010 erg gewaardeerd om dat ik zelf nog geen veld ervaring had. Ik ben je erg dankbaar dat je in de laatste fase tijdens je onverwacht drukke periode als waarnemend decaan nog in zeer korte tijd mijn manuscripten van commentaar hebt kunnen voorzien.

Een groot deel van mijn thesis is gebaseerd op veldmetingen welke ik onmogelijk uit had kunnen voeren zonder ondersteuning van het technische team van het departement Fysische Geografie. Bas, Marcel, Henk en Chris enorm bedankt voor jullie ondersteuning. Ik heb grote bewondering voor jullie aanpak bij de ontwikkeling van de camera palen die zowel fysiek als softwarematig goed werkten. De ondersteuning tijdens de verschillende veldwerken was ook perfect, de apparatuur was altijd goed voorbereid. Die goede voorbereiding viel ook op tijdens het plaatsen van de camera palen, dit deden jullie alsof jullie niet anders gewend waren. De etentjes na afloop van een zware dag veldwerk vond ik ook erg gezellig.

Het onderzoek van deze thesis is gedaan in de context van het Mosselwad project. Ik heb veel hulp gehad van de andere deelnemers aan het project. Vooral Arno ben ik veel dank verschuldigd voor hulp tijdens het veldwerk. Zowel voor het vervoeren van mijzelf en mijn meetapparatuur van en naar de veldlocatie alsmede hulp tijdens het opbouwen en uitvoeren van experimenten. Ik ben Johan dankbaar voor zijn motiverende enthousiasme over mijn onderzoek en het aandragen van ideeën voor onderzoek. Aniek, enorm bedankt voor je assistentie tijdens het laserscanner en je onverzettelijke gesleep tijdens het transplantatie experiment. Norbert, je bent een onuitputtelijke bron als het op kennis over mosselen in de Waddenzee aan komt, bedankt dat ik daar gebruik van heb kunnen maken. Daarnaast wil ik Bruno, Jaap, Andreas, Jeroen, Martin, Anneke en Sander bedanken voor hun hulp in het veld en vruchtbare discussies. Erik, Jakkus en Joos van Kust en Zee bedankt voor de ondersteuning tijdens het project en de interesse in mijn onderzoek. Joos nog enorm bedankt voor je hulp tijdens het veldwerk. Met de onderzoekers van Waddensleutels heb ik ook fijn contact gehad. Ik heb veel opgestoken tijdens onze jaarlijkse gezamenlijke WSYS meetings. Hélène bedankt dat ik mee mocht denken tijdens je stroomgoot experiment, ik heb er zelf ook veel van opgestoken.

Tijdens mijn PhD heb ik meerdere studenten mogen begeleiden die een bijdrage aan mijn onderzoek hebben geleverd. Jantien, Edwin, Reinier, Evelien, Dominic en Jessica

enorm bedankt voor jullie hulp en het enthousiasme waarmee jullie je onderzoek hebben gedaan.

Wanneer ik niet in het veld was zat ik op kamer 205 van de zonneveld vleugel, samen met mijn paranimpf Nynke Vellinga. Nynke, bedankt voor de goed werksfeer, de fijne werk discussies, de lekkere koekjes en taarten, en het zorgen dat ik op tijd bij presentaties en vergaderingen kom. Verder wil ik Amanda Sancho García en Wei Zhang voor hun gezelligheid en discussies.

Ik heb ook erg genoten van de gezelligheid binnen de kustengroep. Ik wil daarom mijn (voormalige) collega's bedanken. Anouk, Frans, Joost, Anita, Florent, Pam, Ton, Thijs, Adrien, Albert, Timothy, Gerben, Leo, Yvonne, Florin, Ayi, Marion, Daan, Renske en Winnie bedankt voor jullie ideeën, discussies, Italiaanse broodjes en kusten meetings. Gerben, bedankt voor de kans die je mij hebt gegeven om verder te gaan in het wetenschappelijk onderzoek waarin ik me ga verdiepen in het stuivende zand. Ik heb er enorm veel zin in om dit samen met Yvonne, Winnie en Pam te gaan onderzoeken. Daan en Timothy bedankt voor onze squash battles. Op pad met de hele groep naar bijvoorbeeld een veldwerk, NCK dagen of BBOS was ook altijd erg gezellig. Anouk, nog enorm bedankt voor je hulp tijdens veldwerk.

Buiten de kustengroep heerst er ook een goede sfeer bij fysieke geografie. Dit wordt natuurlijk aangewakkerd door Juul Beltman die ervoor zorgt dat verjaardagen worden gevierd en voor sfeervolle aankleding tijdens feestdagen zorgt. Juul wil ik ook erg bedanken voor haar administratieve hulp bij het organiseren van meetings. Verder wil ik iedereen bedanken voor de gezelligheid in de koffiehoek tijdens uitjes, op kerst diners, en natuurlijk bij de sushi etentjes. Niko en Yoshi bedankt voor het organiseren van sushi feestjes op top locaties. Ik wil Ton Markus bedanken voor het opmaken van de figuren in mijn thesis.

Ik wil mijn paranimpf Anco Peeters bedanken voor nu al 26 jaar vriendschap. Johnny, Jorik, Michiel, Tomas, Mirjam, Mark, René, Ivo, Lianne en Femke, bedankt voor de gezellige verjaardagen, etentjes, uitjes en natuurlijk volleybal toernooien. Verder wil ik mijn voormalige teamgenoten van onvoorspelbaar Wouter, Marlien, Ellen, Jan, Katrijn, Esther, Paulien, Maartje, Hanna en Niek, en natuurlijk ook mijn huidige klimmaatjes Steffi en Anita bedanken voor de sportieve afleiding van het PhD werk.

Ik ben mijn ouders erg dankbaar voor hun stimulatie om te gaan studeren en het opwekken van interesse in wetenschap en techniek. Bedankt dat jullie mij en Maarten tijdens onze jeugd regelmatig meenamen naar musea, er is volgens mij geen museum waar we niet ben geweest. Ook voor jullie niet aflatende interesse in mijn studie, onderzoek en zelfs voor hulp tijdens veldwerk. Maarten, bedankt voor je interesse en gezelligheid tijdens het sporten. Mijn toekomstige-schoonfamilie Peter, Annelies, Gwenn en Jill wil ik bedanken voor hun interesse en steun.

Tot slot wil ik Joyce enorm bedanken, natuurlijk voor het doorlezen van teksten en luisteren naar presentaties, maar vooral omdat je er altijd voor me bent. Ik ben enorm gelukkig met je en vind het fantastisch dat we binnenkort gaan trouwen.

Curriculum Vitae

Jasper Donker was born on the 10th of September 1986 in the city of Zaltbommel. Jasper attended high school (VWO) at Scholengroep Cambium in Zaltbommel. At the age of 17, he started the bachelor program Physics and Astronomy at the University of Utrecht in September 2004. After his first university year he joined a research campaign studying sediment trapping in the Ems estuary, which would later become his MSc. graduation project. For his bachelor thesis he researched the effects of surface melt on the velocity of the Greenland ice sheet. In August 2009 Jasper finished his master Meteorology, Physical Oceanography and Climate. For his master thesis he researched the effects of bathymetry and settling of suspended sediment on sediment trapping in turbid estuaries. In early 2010, Jasper joined the coastal group at the department of Physical Geography of Utrecht University as a PhD student. The results of the PhD study form the basis of this thesis. From 15 December 2014 Jasper is working as a post-doc within the project 'Aeolus meets Poseidon' in which he studies the effect of surface moisture on aeolian transport and dune recovery.

List of publications

Peer reviewed articles

- DONKER, J. J. A., VAN DER VEGT, M., HOEKSTRA, P. , Wave forcing in the Dutch Wadden Sea: effects on mussel habitats. In preparation
- WA KANGERI, A. K., ALVAREZ-FERNANDEZ, S., SILVA, C. I. F., DONKER, J. J. A., JANSEN, J. M., JOPPE, D. J., DANKERS, M. J. A , Behavioural Zonation , Byssus Production and Adhesion Strength in *Mytilus edulis* (L.) in Sedimentary habitats; The effect of the non-native Oyster, *Crassostrea gigas* (T.). In preparation
- DONKER, J. J. A., VAN DER VEGT, M., HOEKSTRA, P. (2014), How mussel hummocks influence flow patterns and food uptake in intertidal mussel beds. Submitted to Journal of Geophysical Research: Oceans
- DONKER, J. J. A., VAN DER VEGT, M., HOEKSTRA, P. (2014), Implications of an ice scour event for the long-term survival of an intertidal mussel bed. Submitted to Continental Shelf Research
- WA KANGERI, A. K., JANSEN, J. M., BARKMAN, B. R., DONKER, J. J. A., JOPPE, D. J., DANKERS, M. J. A. (2013), Perturbation induced changes in substrate use by the blue mussel, *Mytilus edulis*, in sedimentary systems. Journal of Sea Research 85, 233–240
- DONKER, J. J. A., VAN DER VEGT, M., HOEKSTRA, P. (2013), Wave forcing over an intertidal mussel bed. Journal of Sea Research 82, 54–66
- DONKER, J. J. A., DE SWART, H. E. (2013), Effects of bottom slope, flocculation and hindered settling on the coupled dynamics of currents and suspended sediment in highly turbid estuaries, a simple model. Ocean Dynamics 63(4), 311–327.
- VAN DE WAL, R. S. W., BOOT, W., VAN DEN BROEKE M. R., SMEETS, C., REIJMER, C. H., DONKER J. J. A., OERLEMANS, J. (2008), Large and rapid melt-induced velocity changes in the ablation zone of the Greenland ice sheet. Science, 321 (5885), 111–113.

Conference abstracts

- DONKER, J. J. A., VAN DER VEGT, M., HOEKSTRA, P. (2015), Mussel hummocks affect flow patterns and food uptake in intertidal mussel beds. Poster at: Aquatic Sciences Meeting, Granada, Spain.
- VAN DER VEGT, M., DONKER, J. J. A., VAN DER DEIJL, E.C., HOEKSTRA, P. (2015), Enhanced wave attenuation by mussel beds significant for its own survival. Presentation at: Aquatic Sciences Meeting, Granada, Spain.

- DONKER, J. J. A., VAN DER VEGT, M., HOEKSTRA, P. (2014), Observed flow patterns near hummocks in intertidal mussel beds. Poster at: AGU Ocean Sciences Meeting, Honolulu, Hawaii , United States of America.
- DONKER, J. J. A., VAN DER VEGT, M., HOEKSTRA, P. (2013), The physical impact of ice on an intertidal mussel bed. Presented at: EGU General Assembly Conference, Vienna, Austria.
- DONKER, J. J. A., VAN DER VEGT, M., HOEKSTRA, P. (2013), The physical impact of ice on mussel beds. Poster at: NCK Days 2013, Kijkduin, The Netherlands.
- DONKER, J. J. A., VAN DER VEGT, M., HOEKSTRA, P. (2012), The physical impact of ice on mussel beds. Poster and Presentation at: 13th International Scientific Wadden Sea Symposium, WTC, Leeuwarden, The Netherlands.
- DONKER, J. J. A., VAN DER VEGT, M., HOEKSTRA, P. (2011), How waves influence mussel beds. Presented at: International symposium on the ecology of the Wadden Sea, NIOZ, Texel, The Netherlands.
- DONKER, J. J. A., VAN DER VEGT, M., HOEKSTRA, P. (2011), Predicting survival chances of mussel beds using hydrodynamical models calibrated by field measurements. Presented at: International Conference on Shellfish Restoration, Stirling, United Kingdom.
- DONKER, J. J. A., VAN DER VEGT, M., HOEKSTRA, P. (2011), Wave dissipation and bed shear stresses on an intertidal mussel bed. Presented at: NCK Days, Texel, The Netherlands.

Utrecht University
Faculty of Geosciences
Department of Physical Geography